AD-A168 717 INFRARED ISSUES FOR THE NUCLEAR WINTER PHENOMENON(U) 1/2
MISSION RESEARCH CORP SANTA BARBARA CA
G MCCARTOR ET AL. 03 OCT 85 MRC-R-955 DNA-TR-85-312
UNCLASSIFIED DNA001-84-C-0319 F/G 4/1 NL

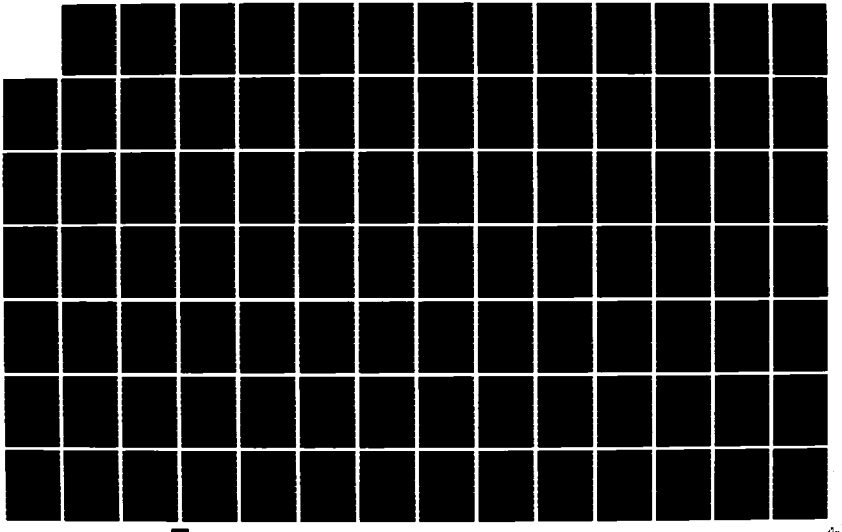

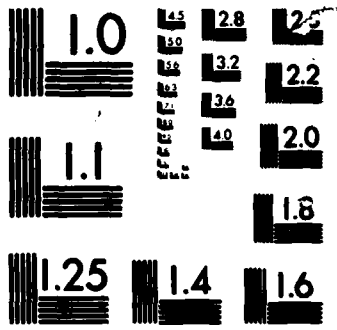

MICROCOP CHART

DNA-TR-85-312

INFRARED ISSUES FOR THE NUCLEAR WINTER PHENOMENON

G. McCartor
D. Archer
W. Wortman
T. Old
Mission Research Corporation
P. O. Drawer 719
Santa Barbara, CA 93102-0719

3 October 1985

Technical Report

CONTRACT No. DNA 001-84-C-0319

THIS WORK WAS SPONSORED BY THE DEFENSE NUCLEAR AGENCY
UNDER RDT&E RMSS CODE B322084466 S99QMXBC00134 H2590D.

Prepared for
Director
DEFENSE NUCLEAR AGENCY
Washington, DC 20305-1000

DISTRIBUTION LIST UPDATE

This mailer is provided to enable DNA to maintain current distribution lists for reports. We would appreciate your providing the requested information.

☐ Add the individual listed to your distribution list.

☐ Delete the cited organization/individual.

☐ Change of address.

NAME: _____

ORGANIZATION: _____

OLD ADDRESS	CURRENT ADDRESS
_____	_____
_____	_____
_____	_____

TELEPHONE NUMBER: ( ) _____

SUBJECT AREA(s) OF INTEREST:

_____	_____
_____	_____
_____	_____

DNA OR OTHER GOVERNMENT CONTRACT NUMBER: _____

CERTIFICATION OF NEED-TO-KNOW BY GOVERNMENT SPONSOR (if other than DNA):

SPONSORING ORGANIZATION: _____

CONTRACTING OFFICER OR REPRESENTATIVE: _____

SIGNATURE: _____

Director
Defense Nuclear Agency
ATTN: STTI
Washington, DC 20305-1000

Director
Defense Nuclear Agency
ATTN: STTI
Washington, DC 20305-1000

UNCLASSIFIED
SECURITY CLASSIFICATION OF THIS PAGE

AD-A168717

REPORT DOCUMENTATION PAGE

Form Approved
OMB No 0704-0188
Exp Date Jun 30 1986

1a REPORT SECURITY CLASSIFICATION UNCLASSIFIED	1b RESTRICTIVE MARKINGS
2a SECURITY CLASSIFICATION AUTHORITY N/A since Unclassified	3 DISTRIBUTION/AVAILABILITY OF REPORT Approved for public release; distribution is unlimited.
2b DECLASSIFICATION/DOWNGRADING SCHEDULE N/A since Unclassified	
4 PERFORMING ORGANIZATION REPORT NUMBER(S) MRC-R-955	5 MONITORING ORGANIZATION REPORT NUMBER(S) DNA-TR-85-312
6a NAME OF PERFORMING ORGANIZATION Mission Research Corporation 6b OFFICE SYMBOL (If applicable)	7a NAME OF MONITORING ORGANIZATION Director Defense Nuclear Agency
6c ADDRESS (City, State, and ZIP Code) P.O. Drawer 719 Santa Barbara, CA 93102-0719	7b ADDRESS (City, State, and ZIP Code) Washington, DC 20305-1000
8a NAME OF FUNDING/SPONSORING ORGANIZATION 8b OFFICE SYMBOL (If applicable)	9 PROCUREMENT INSTRUMENT IDENTIFICATION NUMBER DNA 001-84-C-0319
8c ADDRESS (City, State, and ZIP Code)	10 SOURCE OF FUNDING NUMBERS PROGRAM ELEMENT NO: 62715H; PROJECT NO: S99QMXB; TASK NO: C; WORK UNIT ACCESSION NO: DH008543

11 TITLE (Include Security Classification)
INFRARED ISSUES FOR THE NUCLEAR WINTER PHENOMENON

12 PERSONAL AUTHOR(S)
McCartor, G; Archer, D; Wortman, W; and Old, T.

13a TYPE OF REPORT	13b TIME COVERED	14 DATE OF REPORT (Year Month, Day)	15 PAGE COUNT
Technical Report	FROM 840717 TO 850930	851003	132

16 SUPPLEMENTARY NOTATION
This work was sponsored by the Defense Nuclear Agency under RDT&E RMSS Code B322084466 S99QMXBC00134 H2590D.

17 COSATI CODES			18 SUBJECT TERMS (Continue on reverse if necessary and identify by block number)
FIELD	GROUP	SUB-GROUP	Nuclear Winter
19	6		

19 ABSTRACT (Continue on reverse if necessary and identify by block number)

Simple models of the nuclear winter phenomenon are used to study the possibility that the infrared radiators: hydrocarbons, CO_2, NO_x, H_2O or condensed water (clouds), might have important effects. Most of these substances are found to be unimportant but water clouds, if they are present and it appears they might be, are found to be of great potential significance.

20 DISTRIBUTION/AVAILABILITY OF ABSTRACT ☐ UNCLASSIFIED/UNLIMITED ☒ SAME AS RPT ☐ DTIC USERS	21 ABSTRACT SECURITY CLASSIFICATION UNCLASSIFIED
22a NAME OF RESPONSIBLE INDIVIDUAL Betty L. Fox	22b TELEPHONE (Include Area Code) (202) 325-7042
	22c OFFICE SYMBOL DNA/STTI

DD FORM 1473, 84 MAR

SECURITY CLASSIFICATION OF THIS PAGE
UNCLASSIFIED

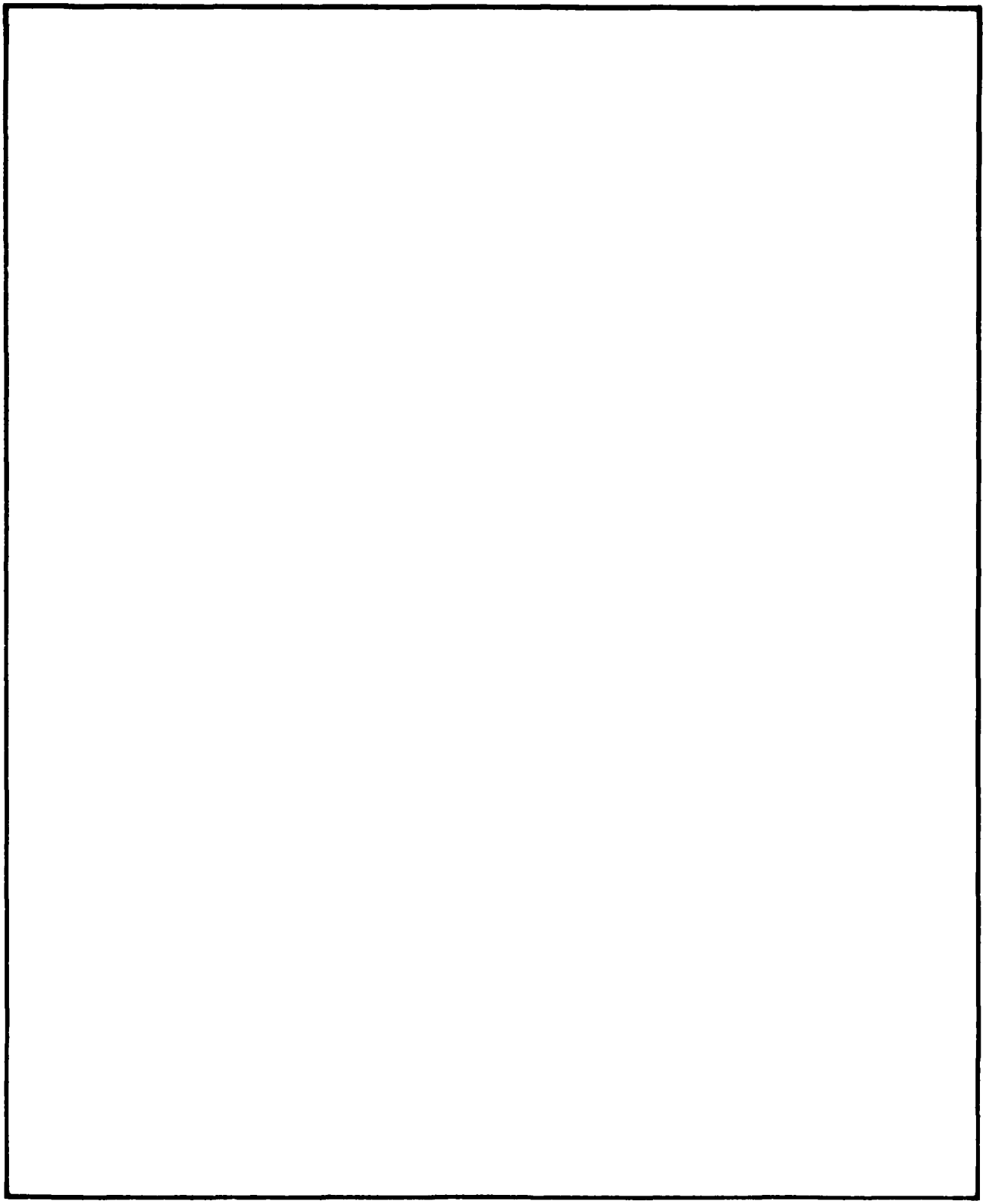

CONVERSION TABLE

Conversion factors for U.S. customary to metric (SI) units of measurement.

To Convert From	To	Multiply By
angstrom	meters (m)	1.000 000 X E -10
atmosphere (normal)	kilo pascal (kPa)	1 013 25 X E +2
bar	kilo pascal (kPa)	1.000 000 X E +2
barn	meter^2 (m^2)	1.000 000 X E -28
British thermal unit (thermochemical)	joule (J)	1.054 350 X E +3
calorie (thermochemical)	joule (J)	4.184 000
cal (thermochemical)/cm^2	mega joule/m^2 (MJ/m^2)	4.184 000 X E -2
curie	*giga becquerel (GBq)	3.700 000 X E +1
degree (angle)	radian (rad)	1.745 329 X E -2
degree Fahrenheit	degree kelvin (K)	$t_K = (t°f + 459.67)/1.8$
electron volt	joule (J)	1.602 19 X E -19
erg	joule (J)	1.000 000 X E -7
erg/second	watt (W)	1.000 000 X E -7
foot	meter (m)	3.048 000 X E -1
foot-pound-force	joule (J)	1.355 818
gallon (U.S. liquid)	meter^3 (m^3)	3.785 412 X E -3
inch	meter (m)	2.540 000 X E -2
jerk	joule (J)	1 000 000 X E +9
joule/kilogram (J/kg) (radiation dose absorbed)	Gray (Gy)	1.000 000
kilotons	terajoules	4.183
kip (1000 lbf)	newton (N)	4.448 222 X E +3
kip/inch^2 (ksi)	kilo pascal (kPa)	6.894 757 X E +3
ktap	newton-second/m^2 (N-s/m^2)	1.000 000 X E +2
micron	meter (m)	1 000 000 X E -6
mil	meter (m)	2.540 000 X E -5
mile (international)	meter (m)	1.609 344 X E +3
ounce	kilogram (kg)	2.834 952 X E -2
pound-force (lbs avoirdupois)	newton (N)	4.448 222
pound-force inch	newton-meter (N-m)	1.129 848 X E -1
pound-force/inch	newton/meter (N/m)	1.751 268 X E +2
pound-force/foot^2	kilo pascal (kPa)	4.788 026 X E -2
pound-force/inch^2 (psi)	kilo pascal (kPa)	6.894 757
pound-mass (lbm avoirdupois)	kilogram (kg)	4.535 924 X E -1
pound-mass-foot^2 (moment of inertia)	kilogram-meter^2 (kg-m^2)	4.214 011 X E -2
pound-mass/foot^3	kilogram/meter^3 (kg/m^3)	1.601 846 X E +1
rad (radiation dose absorbed)	**Gray (Gy)	1.000 000 X E -2
roentgen	coulomb/kilogram (C/kg)	2.579 760 X E -4
shake	second (s)	1.000 000 X E -8
slug	kilogram (kg)	1.459 390 X E +1
torr (mm Hg, 0°C)	kilo pascal (kPa)	1.333 22 X E -1

*The becquerel (Bq) is the SI unit of radioactivity; 1 Bq = 1 event/s.
**The Gray (Gy) is the SI unit of absorbed radiation.

TABLE OF CONTENTS

Section		Page
	CONVERSION TABLE	iii
	LIST OF ILLUSTRATIONS	v
	LIST OF TABLES	viii
1	INTRODUCTION	1
2	GASEOUS AND PARTICULATE MATTER INJECTED INTO ATMOSPHERE BY MASSIVE BURNING, AND THEIR OPTICAL PROPERTIES	4
	PRELIMINARY	4
	MOLECULAR SPECIES INJECTED	5
	BROAD-BAND IR PROPERTIES OF MOLECULAR SPECIES	8
	NO_2	9
	H_2O	10
	Hydrocarbons	12
	BROAD-BAND IR PROPERTIES OF PARTICULATE LAYERS	20
	Method	20
	Results	24
	OPTICAL PROPERTIES OF PARTICULATE LAYERS IN THE VISIBLE	31
3	MODEL CALCULATIONS	36
	THE BASIC MODEL	36
	THE EFFECTS OF CONVECTIVE INSTABILITIES	47
	NUCLEAR WINTER OVER SNOWPACK	59
4	CONCLUSIONS	63
5	LIST OF REFERENCES	65
APPENDICES		
A	BROAD-BAND EMISSIVITY FOR OPTICALLY-THIN BANDS	69

TABLE OF CONTENTS (Concluded)

Section		Page
APPENDICES		
B	BROAD-BAND EMISSIVITY FOR TWO SPECIES WITH OVERLAPPING BANDS	71
C	TABULATIONS OF OPTICAL PROPERTIES	75
D	SOLUTIONS TO THE NUCLEAR WINTER MODELS	93
	THE PROBLEM OF FIGURE 3-1	93
	THE PROBLEM OF FIGURE 3-4	94
	THE CASE OF HIGH SURFACE ALBEDO	97
E	CONVECTIVE EQUILIBRIUM WITH MULTIPLE IR GROUPS	99
	OPTICAL PROPERTIES OF THE LAYER	99
	TRANSFER EQUATIONS	101
	THREE GROUPS	103
	TWO STREAMS	104
	CONVECTIVE LIMIT	110
	REMARKS	114

LIST OF ILLUSTRATIONS

Figure		Page
2-1	Broad-band infrared emissivity of NO_2.	11
2-2	Broad-band IR emissivity for water vapor.	12
2-3	Broad-band infrared emissivity for selected hydrocarbons.	14
2-4	Particle size distributions used in calculations.	25
2-5	Broad-band IR properties of water clouds (distribution 1).	26
2-6	Broad-band IR properties of water clouds (distribution 2).	27
2-7	Broad-band IR properties of dust (basaltic glass) layers.	28
2-8	Broad-band IR properties of soot (carbon) layers.	29
2-9	Broad-band IR emissivity of sooty water clouds for selected values of the water-to-soot density ratio.	30
2-10	Optical properties in the visible (λ=0.55 μm) of water clouds (distribution 1).	32
2-11	Optical properties in the visible (λ=0.55 μm) of dust (basaltic glass) layers.	33
2-12	Optical properties in the visible (λ=0.55 μm) of soot (carbon) layers.	34
2-13	Emissivity in the visible (λ=0.55 μm) of sooty water clouds for selected values of the water-to-soot density ratio.	35
3-1	Schematic of the simple model nuclear winter which ignores convective instabilities.	40
3-2	The temperature at the earth's surface, T_E, and the temperature at the top of the soot layer, T_S, plotted vs. τ.	42

LIST OF ILLUSTRATIONS (Concluded)

Figure		Page
3-3	The temperature at the earth's surface, T_E, and the temperature at the top of the soot layer, T_s, plotted vs. α and vs. the ratio of cloud mass to soot mass.	48
3-4	Schematic of the model nuclear winter with a convection region at the top of the cloud-soot layer.	51
3-5	The temperature at the earth's surface, T_E, at the top of the cloud-soot layer, T_s, and at the bottom of the cloud-soot layer, T_L, plotted vs. α assuming convection within the cloud stabilizes, the temperature profile.	57
E-1	Broad-band IR emissivity for water-vapor (from Reference 2-10).	100
E-2	Temperature profiles for two IR groups plus solar absorption.	108
E-3	Temperature profile for two IR group approximation in a soot layer.	109
E-4	Temperature profiles for two IR group approximation in a soot layer (ORIGINAL), under convective equilibrium (UNSTRETCHED) and following a mixing with the layer above (STRETCHED).	115

LIST OF TABLES

Table		Page
2-1	Emission factors for products of combustion.	6
2-2	Assumed distribution of hydrocarbons.	6
2-3	Ambient atmospheric content and additions thereto in "baseline case".	7
2-4	Band intensities for acetylene at 300 °K.	17
2-5	Band intensities for ethylene.	19
2-6	Log-normal parameters used in the Mie calculations.	24
2-7	Input parameters to optical formulas for λ = 0.55 μm.	31
C-1	Complex index of refraction values for water.	76
C-2	Complex index of refraction values for dust (basaltic glass).	77
C-3	Complex index of refraction values for soot (carbon).	78
C-4	Broad-band IR properties of sooty water clouds.	79
C-5	Optical properties in the visible (λ=0.55 μm) of sooty water clouds.	85

SECTION 1
INTRODUCTION

In this report we shall use simple models to study the phenomenon which has come to be known as nuclear winter[1]. The models are time-independent, one-dimensional and allow solution in terms of closed form, analytic expressions. In view of the fact that time-dependent, multi-dimensional calculations of the phenomenon have been presented[1], it is perhaps appropriate to motivate the use of the much simpler models. The models have several uses: 1) they allow one to develop an understanding of the phenomenon at a more fundamental level than may be possible with the use of large, complex computer simulations; 2) they allow one to examine the parameter space of the problem or to examine the importance of including a particular type of phenomenon in the calculations. Usually a simple inspection of the formulas will reveal the sensitivity to a parameter value or type of effect, at most a simple calculation will suffice. In this way they can point to interesting regions of the parameter space where more detailed calculations should be done or to the most important additions to make in improving the more complicated calculations; 3) the models and the physical intuition they allow one to develop are useful in developing "sub-grid" models: formulas which specify in large scale simulation codes the results of processes at scales smaller than the code can resolve.

The main use we shall make of the models in this report - the purpose for which we developed them - is to study the effects of infrared radiation, IR, on the nuclear winter phenomenon. In particular we shall consider whether or not the presence of such IR radiators as hydrocarbons,

NO_2, CO_2, water vapor or condensed water (clouds) can be of importance to the phenomenon and to consider the sensitivity of the phenomenon to reasonable variation in the IR properties of soot itself. We find that hydrocarbons, NO_2 and CO_2 are not of importance; this result is in agreement with the conclusions of other workers. Water vapor is unlikely to be of more than marginal importance to the temperature structure if one ignores convective instabilities; it may be of importance in determining the stability characteristics at the top of the soot layer. Variation in the IR properties of the soot itself across the range of reasonable expectation makes a significant difference in the results. Condensed water, if it is present, can play a significant, indeed a dominant, role in the phenomenon.

A water cloud mixed with the soot will alter the entire character of the temperature profile, changing it from one in which the temperature is hot at the top of the layer and cold at the earth's surface - as shown in previous calculations of the nuclear winter phenomenon and as shown in our calculations in the absence of condensed water - to one in which the temperature is cold at the top of the cloud-soot layer and hot at the earth's surface. Furthermore the clouds can be created by the amounts of water which are likely to be present. The question of whether or not there will be clouds is complicated. There exists a strong hysteresis effect: if the cloud is there it keeps the top of the layer cold which keeps the cloud there; if the cloud is not there the top of the layer is hot which keeps a cloud from forming. Most fire plumes are initially capped with condensation clouds[2].

If the clouds persist for long periods of time they will almost certainly have a profound effect on the nuclear winter phenomenon. They will also affect the dynamics of the phenomenon at early times when the various individual plumes, some of which will probably have condensation clouds, some of which may not have condensation clouds, combine to form

the hemisphere-wide soot layer of nuclear winter. Even if the condensation clouds disappear before the late times their effects on the dynamics of the combining phase may have implications for removal rates of the soot and for the later location of the material. In turn, it is the outcome of these mixing processes, which the clouds will influence, which will determine whether or not there will be clouds at late times. Until careful calculations which include the effects of the clouds are made we do not believe that any calculation of the nuclear winter phenomenon can be completely credible: the presence of condensation clouds, which we have not been able to rule out, would alter the entire character of the event.

We also point out that the nuclear winter phenomenon is always warming over snowpack. This fact may influence global circulation patterns or may be important in other regards. The analysis of whether the warming effect over snowpack is of importance to the total phenomenon is beyond the scope of the present report.

The report is organized as follows: In Section 2 we document the data we found necessary to accumulate in order to specify the parameters or ranges for parameters in the model calculations. Much of this data was gleaned from other sources; some represent calculations we made ourselves. In Section 3 we present the model calculations - the main results of the study. The models are described in order of increasing complexity, first ignoring convective instabilities then including their effects in an approximate way. Concluding remarks are given in Section 4 and in Appendix E we make some remarks on calculating the development of the unstable interface at the top of the soot layer when no condensation cloud is present.

SECTION 2

GASEOUS AND PARTICULATE MATTER INJECTED INTO ATMOSPHERE BY MASSIVE BURNING, AND THEIR OPTICAL PROPERTIES

PRELIMINARY

One purpose of the present study is to investigate the possible amelioration of the predicted "nuclear winter" effects at the earth's surface by polyatomic molecules, injected into the atmosphere following massive burning, that might inhibit the escape to space of thermal radiation. For this purpose, we first performed a literature survey to determine the principal gaseous species produced by the burning, and to obtain estimates of the quantity of each injected. We then sought to determine, using band models and parameters from the literature where possible, the broad-band infrared (IR) emissivity and transmissivity for each of the species.

As a further aid in performing the work of this contract, we undertook calculations to estimate the broad-band IR emissivity, transmissivity, and reflectivity for particulate layers. These include water clouds, dust layers, soot (carbon) layers, and layers containing a mixture of water droplets and soot. We also performed calculations to determine the corresponding optical properties in the visible (0.55 μm) for the same particulate layers.

This section describes the methodology employed in the foregoing studies and presents the results in graphical and tabular form. The results of the literature survey of injected species and their emission

factors are given first. This is followed by the optical properties of the gaseous species and, finally, by the optical properties of the particulate layers.

MOLECULAR SPECIES INJECTED

A survey of the literature, including References 1 through 5, shows that the principal species injected into the atmosphere, as a consequence of forest and urban fires, are CO_2, CO, H_2O, $NO_x(NO_2+NO)$, and hydrocarbons. A key item for each of the species is the "emission factor," which is the number of grams of the substance emitted per gram of fuel burned. These numbers are by no means unique for each of the species, as different measurements have revealed a range of values. Table 2-1 shows values for the emission factors, the associated references, and values adopted in this report.

There are many hydrocarbons, but we have assumed that they are dominated by six species and proportioned among them as shown in Table 2-2. The corresponding emission factors adopted, based on the total hydrocarbon emission factor and the relative abundances, are also shown in Table 2-2.

In Table 2-3 we compare, data permitting, the species content in the ambient atmosphere (30°N - 70°N; 0.88 π steradians) with the additional amount added from the burning of 4500 Tg fuel (1 Tg $\equiv 10^{12}$ g). This is the "baseline case" considered in Reference 2-1 and corresponds to 3750 Tg consumed in urban fires and 750 Tg in forest fires. The amounts added from the burning are based on the emission factors given in Tables 2-1 and 2-2. In both cases the amounts are given in terms of the total number of molecules and the vertical column number in units of atm cm at NTP. For the ambient atmosphere we have used the following: CO_2 and CO mixing ratios of 3×10^{-4} and 1.9×10^{-7}, respectively, with the

Table 2-1. Emission factors for products of combustion.

Species	Emission Factor	Reference	Emission Factor Adopted
CO_2	1 — 1.75 1.9 (Ponderosa Pine)	2-2 2-4	1.75
CO	.05 .01 — .25 .01 (Ponderosa Pine)	2-1 2-2 2-4	0.18
H_2O	.25 — .75	2-2	0.75
NO_x	1.5×10^{-3} 5×10^{-4} — 4.5×10^{-3} 4×10^{-4} — 3.3×10^{-2}	2-1 2-2 2-3	5×10^{-3}
hydrocarbons (total)	.02 5×10^{-3} — 2×10^{-2} 4.5×10^{-3} — 6.5×10^{-3}	2-1 2-2 2-4	10^{-2}

Table 2-2. Assumed distribution of hydrocarbons (Reference 2-4).

Species	Relative Abundance (%)	Emission Factor Adopted
CH_4 (methane)	30.8	3.1×10^{-3}
C_2H_4 (ethylene)	25.8	2.6×10^{-3}
C_2H_2 (acetylene)	22.3	2.2×10^{-3}
C_3H_6 (propylene)	7.1	7.1×10^{-4}
C_3H_8 (propane)	7.0	7.0×10^{-4}
C_2H_6 (ethane)	7.0	7.0×10^{-4}

Table 2-3. Ambient atmospheric content and additions thereto in "baseline case".

Species	Content in Ambient Atmosphere (30°N-70°N)		Additions from 4500 Tg Fuel Burned (30°N-70°N)	
	Number of Molecules	Vertical Content (atm cm)	Number of Molecules	Vertical Content (atm cm)
CO_2	8.8×10^{39}	2.9×10^{2}	1.1×10^{38}	3.6
CO	5.3×10^{36}	1.7×10^{-1}	1.7×10^{37}	5.6×10^{-1}
H_2O	5.4×10^{40}	1.8×10^{3}	1.1×10^{38}	3.6
NO_x	4.9×10^{34}	6.3×10^{-4}	2.9×10^{35} 9.4×10^{35} *	9.7×10^{-3} 3.1×10^{-2} *
CH_4	3.3×10^{37}	1.1	5.2×10^{35}	1.7×10^{-2}
C_2H_4	-	-	2.5×10^{35}	8.2×10^{-3}
C_2H_2	-	-	2.3×10^{35}	7.4×10^{-3}
C_3H_6	-	-	4.6×10^{34}	1.5×10^{-3}
C_3H_8	-	-	4.3×10^{34}	1.4×10^{-3}
C_2H_6	-	-	6.3×10^{34}	2.1×10^{-3}

* Includes 6.5×10^{35} molecules introduced from fireballs in the baseline case (Ref. 2-1).

total concentration from Reference 2-6; the mid-latitude mean values for H_2O from Reference 2-6; NO_x and CH_4 values from References 2-7 and 2-8. The ambient atmospheric content of the hydrocarbons, other than methane, is not readily available to us and so is not included in Table 2-3.

BROAD-BAND IR PROPERTIES OF MOLECULAR SPECIES

Since thermal radiation from the earth approximates blackbody radiation, we are interested in determining the emission and absorption properties of the injected products of combustion averaged over a Planck spectrum. These average values are called "broad-band" IR properties of the molecules.

The effective radiating temperature of the earth lies between about 200 and 300 °K. At 300 °K the blackbody emission peaks at 10 μm; at 200 °K it peaks at about 15 μm. So we are interested mainly in molecules that absorb in the long-wavelength infrared (LWIR) beyond about 6 μm. All of the molecules listed in Table 2-3 satisfy this requirement except for CO whose fundamental band lies at about 4.7 μm. Thus, although Table 2-3 indicates that massive burning may inject more CO into the atmosphere than is there under ambient conditions, its presence should not alter significantly the transport of thermal radiation through it, and so we delete it from further consideration. We shall also ignore CO_2. This is because, from Table 2-3, the amount injected by burning is only about 1 percent of the ambient content. With the exception of propylene (C_3H_6), for which we could find no band-model data, estimates of the broad-band IR properties of the remaining molecules in Table 2-3 are given below. For NO_x we will include only NO_2 because very little of the fundamental band of NO at 5.3 μm extends into the LWIR region at ambient temperatures.

NO_2

The transmission of NO_2 in the ν_2 and ν_3 fundamental bands and the $\nu_1 + \nu_3$ combination band, spanning the wavenumber interval 655 to 2950 cm^{-1}, has been modeled by Pierluissi and Tomiyama (Reference 2-9) and can be written in the form

$$T = \exp\{-10^{a_1+a_2X}\} \tag{2-1}$$

where

$$X = c' + \log_{10}W \tag{2-2}$$

and

$$W = \left(\frac{P}{P_o}\right)^n \left(\frac{T_o}{T}\right)^m U \quad . \tag{2-3}$$

Here, P is the total air pressure, T is the temperature (°K), P_o and T_o (273 °K) are the corresponding STP values, U is the absorber thickness (atm cm), a_1, a_2, n, m are constants given in Reference 2-1*, and c' is tabulated in Reference 2-1 as a function of wavenumber $\tilde{\nu}$.

The spectral emissivity at wavenumber $\tilde{\nu}$ is

$$\varepsilon(\tilde{\nu}) = 1 - T(\tilde{\nu}) \tag{2-4}$$

and the broad-band emissivity, $\bar{\varepsilon}$, is

$$\bar{\varepsilon} = \frac{\int_0^\infty \varepsilon(\tilde{\nu})B(\tilde{\nu})d\tilde{\nu}}{\int_0^\infty B(\tilde{\nu})d\tilde{\nu}} \quad . \tag{2-5}$$

---

* The value of a_1 is erroneously given in Reference 2-1 as -0.25653. The correct value is 1.19711.

Here, $B(\tilde{\nu})$ is the Planck function

$$B(\tilde{\nu}) = 2hc\tilde{\nu}^3(e^{1.435\ \tilde{\nu}/T}-1)^{-1} \quad . \qquad (2\text{-}6)$$

We have evaluated $\bar{\epsilon}$ numerically from Equation 2-5 using Equations 2-1 through 2-4, in which, for the nuclear winter application, we assumed an average NO_2 layer height of 5 km with P = 540.5 mb and T = 256 °K. The calculations were performed for NO_2 layer thickness (U) ranging from 10^{-4} to 10^2 atm cm. The results are shown in Figure 2-1.

For the maximum value of U for NO_2 in Table 2-3, that incorporates contributions from fires and nuclear fireballs, the emissivity (Figure 2-1) is seen to be less than about 6×10^{-3}. This corresponds to a transmission of thermal radiation from the earth's surface of at least 99.4 percent.

H_2O

The broad-band IR emissivity for water vapor, as reported by Staley and Jurica (Reference 2-10), is shown in Figure 2-2 for two different temperatures. In this figure the path length is in units of gm cm^{-2} of water vapor (1 gm $cm^{-2} \equiv 1.2438 \times 10^3$ atm cm). For an atmospheric water-vapor content of 1.8×10^3 atm cm (Table 2-3), corresponding to 1.45 gm cm^{-2}, the emissivity is seen to be about 0.63, corresponding to a transmission of thermal radiation of 37 percent. These values are for the ambient atmosphere. However, the additional amount of water vapor injected by the fires (3.6 atm cm) contributes only insignificant increments to the ambient emissivity and transmissivity.

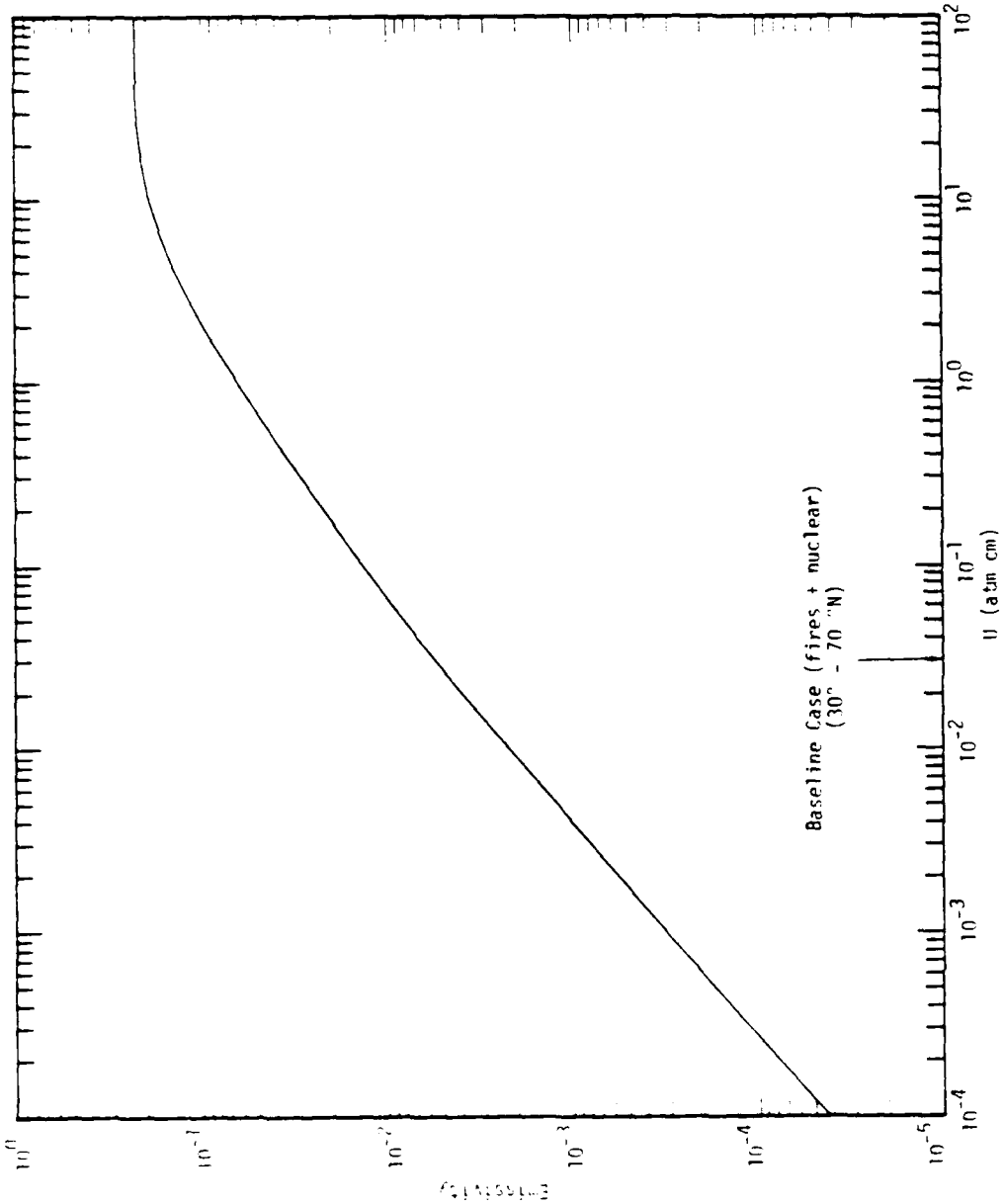

Figure 2-1. Broad-band infrared emissivity of NO_2.

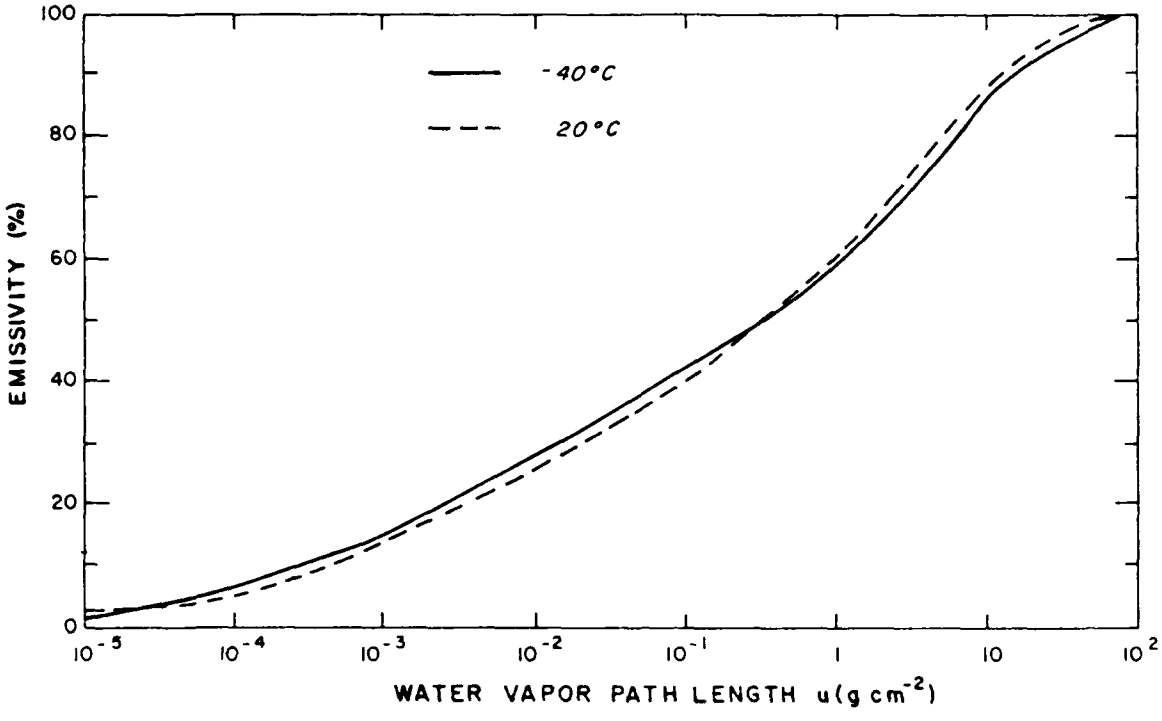

Figure 2-2. Broad-band IR emissivity for water vapor (from Reference 2-10).

Hydrocarbons

Methane (CH_4). For methane we use the band model developed by Jarem, et al. (Reference 2-11) which is formally similar to that described above for NO_2. The transmission at wavenumber $\tilde{\nu}$ is given by

$$T(\tilde{\nu}) = \exp[-10^{a(c'(\tilde{\nu})+\log_{10}W)}] \qquad (2\text{-}7)$$

where W is determined from Equation 2-3. The values of the parameters a, n, m are given in Reference 2-11 as are also the parameters $c'(\tilde{\nu})$ for $\tilde{\nu}$ ranging from 1085 to 3215 cm^{-1}. This interval spans the region of the two IR-active fundamentals ν_3(1306 cm^{-1}) and ν_4(3020 cm^{-1}). Again, the spectral emissivity is given by Equation 2-4 and the broad-band emissivity by Equation 2-5.

The broad-band emissivity, at a temperature of 256 °K and total pressure of 0.54 atm, is shown in Figure 2-3 (along with results for the other hydrocarbons described below) as a function of path length (atm cm) through the methane layer. Arrows near the bottom of Figure 2-3 show the values of U from Table 2-3 corresponding to the fire contribution in the baseline case. For methane, the ambient value for U is also shown. It corresponds to an emissivity of about 10^{-2}, which is equivalent to a transmissivity of 99 percent. The incremental amounts from the products of combustion are only about 0.1 percent.

Ethane (C_2H_6). For ethane, we have been able to find absorption-coefficient data for only the ν_9 band centered at 821.52 cm^{-1} (12.2 μm). Although this is believed to be the major band of interest to us, the results obtained below should be considered as lower limits to the broad-band emissivity.

The spectral absorption-coefficient data for the ν_9 band, obtained by Varanasi, et al. (Reference 2-12), can be represented as

$$k_{\tilde{\nu}} = S\sqrt{\frac{a}{\pi}}\exp[-a(\tilde{\nu}-\tilde{\nu}_0)^2] \quad (atm^{-1}\ cm^{-1}) \quad , \qquad (2\text{-}8)$$

where

$$S = \int_{-\infty}^{\infty} k_{\tilde{\nu}}\, d(\tilde{\nu}-\tilde{\nu}_0) = 31\ \left(\frac{300}{T}\right)\ (atm^{-1}\ cm^{-1}) \quad ,$$

$$a = 5.79 \times 10^{-4}\ cm^2 \quad ,$$

and

$$\tilde{\nu}_0 = 825\ cm^{-1} \quad .$$

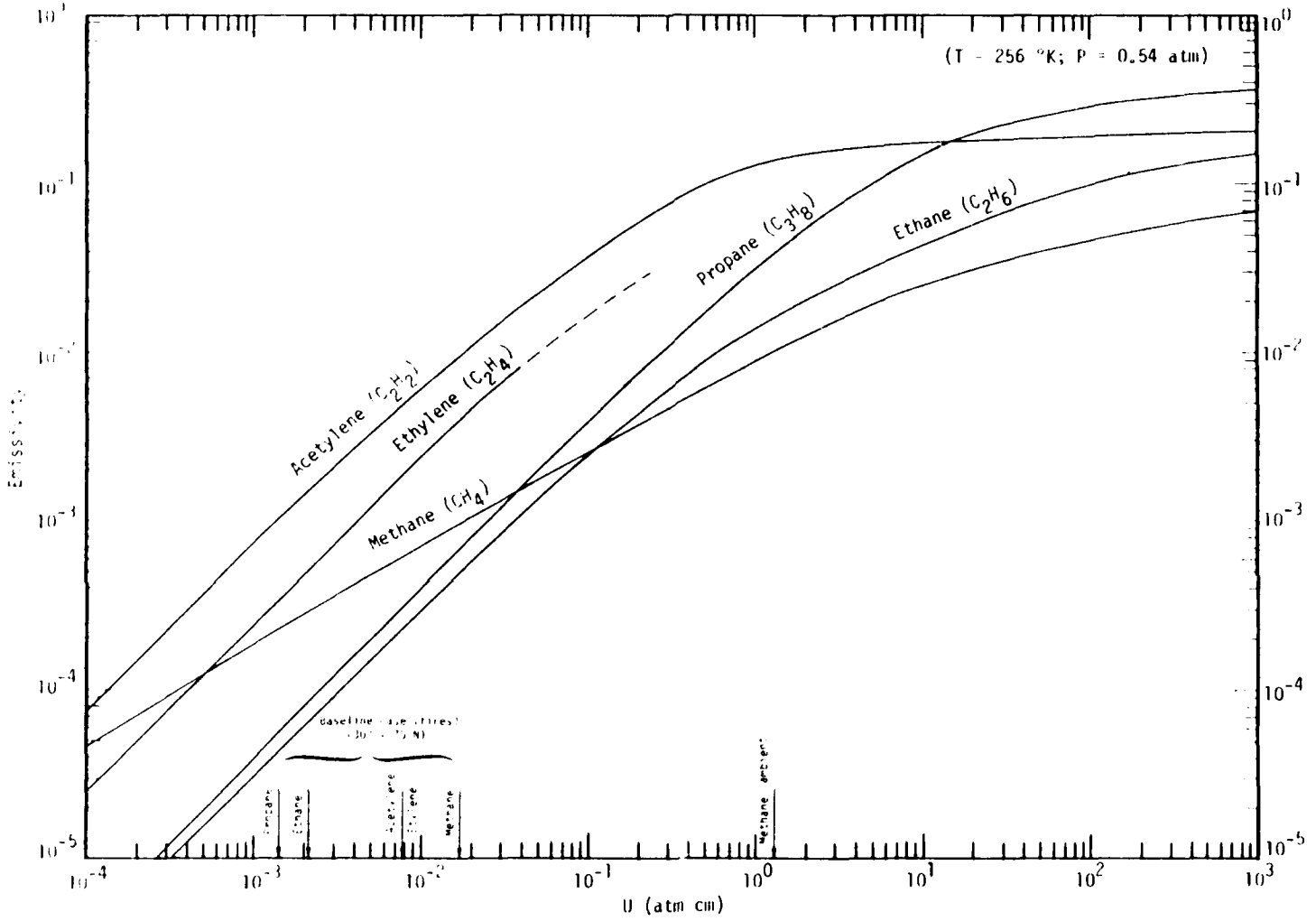

Figure 2-3. Broad-band infrared emissivity for selected hydrocarbons.

Assuming the statistical (Lorentz line) band model, the transmission is given by (Reference 2-13)

$$T(\tilde{\nu}) = \exp\left[-k_{\nu} U/\sqrt{1+k_{\nu} U/(4a_c)}\right] \qquad (2\text{-}9)$$

where, again, U (atm cm) is the absorber amount and

$$a_c = \gamma_c/d \quad . \qquad (2\text{-}10)$$

Here, γ_c and d are, respectively, the mean (collision broadened) line width and mean line spacing.

For ethane, we take (Reference 2-12)

$$\gamma_c \approx 0.102 \left(\frac{300}{T}\right)^{1/2} P_{atm} \quad ; \quad d \approx 2.6 \text{ cm}^{-1} \qquad (2\text{-}11)$$

where P_{atm} is the total pressure in atmospheres. Although a_c is generally a function of $\tilde{\nu}$, we assume it to be a constant. With the above parameter values, along with values for T and P_{atm} of 256 °K and 0.54 atm, respectively, Equations 2-4, 2-5, and 2-9 lead to the broad-band emissivity for ethane shown in Figure 2-3. For the amount of ethane injected into the atmosphere by massive burning (2.1×10^{-3} atm cm), the emissivity is seen to be very small (6×10^{-5}), corresponding to almost complete transparency of the thermal radiation. It is unlikely that this result would be significantly different had the other bands of ethane been included.

Propane (C_3H_8). For propane we use the band-model parameters of Giver, et al. (Reference 2-14). The spectral transmission can be represented by the expression

$$T(\tilde{\nu}) = \exp\left[-k_{\nu} U/\sqrt{1+k_{\tilde{\nu}} U/(\pi a_c)}\right] \qquad (2\text{-}12)$$

where

$$a_c = a_c^0(\tilde{\nu})\, P_{atm} \quad . \qquad (2\text{-}13)$$

From plots of $a_c^0(atm^{-1})$ and $k_{\tilde{\nu}}(atm^{-1}\ cm^{-1})$ as functions of $\tilde{\nu}$ given in Reference 2-14, we have computed the spectral transmissivity and emissivity from Equations 2-12 and 2-4, respectively, and the broad-band IR emissivity from Equation 2-5, as functions of U. The results are shown in Figure 2-3.

From the amount of propane injected into the atmosphere in the baseline case (1.4×10^{-3} atm cm), we see that the emissivity is nearly the same as that for ethane (6×10^{-5}) and that any decrease in the transmission of thermal radiation due to injected propane is quite negligible.

Acetylene (C_2H_2). Integrated band intensities, S, at 300 °K have been measured for several bands of acetylene by Varanasi and Bangaru (Reference 2-15). These are shown in Table 2-4. Of the four shown, two are fundamentals and two are intercombination bands. The ν_3 fundamental and the $\nu_2 + \nu_4 + \nu_5$ intercombination band severely overlap and are treated as a single band. We call this "band 3." The ν_5 fundamental and the $\nu_4 + \nu_5$ intercombination band will be referred to as bands "1" and "2," respectively. Only for band 1 are spectral absorption coefficients given in Reference 2-15. To obtain the broad-band emissivity, including contributions from bands 2 and 3, we use an approximation developed in Appendix A.

Table 2-4. Band intensities for acetylene at 300 °K (Reference 2-15).

Band	Band Center (cm^{-1})	Wavelength (μm)	S ($atm^{-1}cm^{-2}$)
(1) ν_5	729	13.7	729
(2) $\nu_4 + \nu_5$	1328	7.53	87
(3) $\begin{Bmatrix} \nu_3 \\ \nu_2 + \nu_4 + \nu_5 \end{Bmatrix}$	$\begin{Bmatrix} 3295 \\ 3282 \end{Bmatrix}$ 3290	3.04	294

Consider first "band 1." As for the case of ethane, we write the spectral transmissivity in the form

$$T(\tilde{\nu}) = \exp\left[-k_{\nu}^{\sim} u / \sqrt{1 + k_{\nu}^{\sim} u/(4a_c)}\right] \qquad (2\text{-}14)$$

where

$$a_c = \gamma_c / d = a_c^0 \, P_{atm} \quad . \qquad (2\text{-}15)$$

We have been unable to find values of a_c^0 for acetylene. However, for propane near 750 cm^{-1}, $a_c^0 \approx 1$ atm^{-1} (Reference 2-14), and we arbitrarily adopt this value here. Values for $k_{\nu}^{\sim}$ (atm^{-1} cm^{-1}) from 650 to 810 cm^{-1} are available from Reference 2-15. These, together with Equations 2-14, 2-15, 2-4, and 2-5, were used to compute the broad-band emissivity for the ν_5 band.

In Appendix A we show that if an absorbing layer is optically thin to a molecular band ($k_{\nu}^{\sim} u \ll 1$), then the broad-band emissivity for that band is given by

$$\bar{\varepsilon} \approx 1.53\ B'(\tilde{\nu}_0)SU/T^4 \qquad (2\text{-}16)$$

where

$$B'(\tilde{\nu}_0) = \tilde{\nu}_0^{\,3}(e^{1.435\ \tilde{\nu}_0/T}-1)^{-1} \quad , \qquad (2\text{-}17)$$

$\tilde{\nu}_0$ is the band-center wavenumber, S is the integrated band intensity ($atm^{-1}\ cm^{-2}$), and U(atm cm) is the layer thickness. It turns out that under nuclear-winter conditions, values of U for acetylene are sufficiently small (Table 2-3) that the layer is optically very thin and so the condition for applicability of Equation 2-16 is easily satisfied. Consequently, for bands 2 and 3, at a temperature of 256 °K, and with values for $\tilde{\nu}_0$ and S from Table 2-4, Equation 2-16 leads to the result

$$\bar{\varepsilon}_2 + \bar{\varepsilon}_3 = 1.8 \times 10^{-2}\ U \quad . \qquad (2\text{-}18)$$

Equation 2-12 for the spectral transmissivity is called the "curve of growth." For small values of $k_\nu U$, the exponent is linear in $k_\nu U$. But for large enough $k_\nu U$ the exponent varies as the square root of $k_\nu U$. In the linear region it turns out, from our detailed calculations, or from Equation 2-16, that for "band 1" we can write

$$\bar{\varepsilon}_1(k_\nu U \ll 1) = 7.3 \times 10^{-1}\ U \quad . \qquad (2\text{-}19)$$

Comparing Equations 2-18 and 2-19 we see that the contribution to the broad-band emissivity from "band 1" is about 42 times greater than that from the sum of bands 2 and 3. Consequently, bands 2 and 3 can be ignored with very little error. This permits us to plot the broad-band emissivity for acetylene as a function of U, even to large values of U.

The results are shown in Figure 2-3. For the value of U in the baseline case (7.4×10^{-3}), we see that the emissivity is about 5×10^{-3}, which corresponds to a decrease in the transmission of only 0.5 percent.

Ethylene (C_2H_4). We have found no band model nor spectral absorption coefficients in the literature for ethylene. However, Nakanaga, et al. (Reference 2-16) have measured integrated band intensities, S, for the ν_7, ν_9, ν_{10}, ν_{11}, and ν_{12} bands. The results are shown in Table 2-5. For sufficiently small values of U, we can determine the broad-band emissivity from the equation (Appendix A)

$$\bar{\varepsilon} \approx 1.53 \sum_i B'(\tilde{\nu}_i) S_i U/T^4 \qquad (2\text{-}20)$$

Table 2-5. Band intensities for ethylene (Reference 2-16).

Band	$\tilde{\nu}_i(cm^{-1})$	Wavelength (μm)	$S_i(atm^{-1}\ cm^{-2})$
ν_7	949	10.54	376.9
ν_9	3105	3.22	116.1
ν_{10}	826	12.11	0.134
ν_{11}	2989	3.35	63.9
ν_{12}	1443	6.93	46.4

where the sum in Equation 2-20 is taken over all molecular bands and $B'(\tilde{\nu}_i)$ is given by Equation 2-17. When the parameters from Table 2-5 are used in Equation 2-20, we obtain, for T = 256 °K,

$$\bar{\varepsilon}_{\substack{\text{optically thin} \\ \text{ethylene}}} \approx 0.25\ U_{atm\ cm}\ , \qquad (2\text{-}21)$$

which is plotted in Figure 2-3.

Equation 2-21 should be valid for the nuclear-winter application in which, for the baseline case, $U \approx 8.2 \times 10^{-3}$ and so $\bar{\varepsilon} \approx 2 \times 10^{-3}$. This corresponds to a decrease in the transmission of thermal radiation due to the ethylene layer of only 0.2 percent.

If we add the effects of all the hydrocarbons resulting from massive burning (baseline case), we find a total broad-band emissivity of about 8.1×10^{-3}. However, due to band overlap among the different species, the resultant emissivity will be somewhat less than this (see Appendix B). We therefore expect that the injected hydrocarbons will decrease the transmission of thermal radiation through the layer by less than 1 percent.

BROAD-BAND IR PROPERTIES OF PARTICULATE LAYERS

In this subsection we describe calculations performed to estimate the broad-band IR properties of particulate layers of interest in the nuclear-winter problem. Of special relevance are the emissivity, transmissivity, and reflectivity of water clouds, dust layers, soot (carbon) layers, and layers containing a mixture of soot particles and water droplets. We first describe the method employed and then present the results for specific particle types.

Method

We are interested in determining the broad-band IR emissivity, $\bar{\varepsilon}$, transmissivity, $\bar{T}$, and reflectivity, $\bar{R}$, for particle layers of thickness U (gm cm^{-2}). These quantities are related by the expression

$$\bar{\varepsilon} + \bar{T} + \bar{R} = 1 \quad . \tag{2-22}$$

Here, $\bar{\varepsilon}$ is defined by the relation 2-5, and $\bar{T}$ and $\bar{R}$ are defined by corresponding expressions in which the spectral emissivity, $\varepsilon(\tilde{\nu})$, is replaced by the spectral coefficients $T(\tilde{\nu})$ and $R(\tilde{\nu})$, respectively.

Initially, we attempted to calculate the spectral coefficients $\varepsilon(\tilde{\nu})$, $T(\tilde{\nu})$, and $R(\tilde{\nu})$ using a Mie-scattering code, and a radiation transport algorithm similar to one in the ROSCOE and NORSE codes. However, we ran into numerical difficulties with the method, especially when considering mixtures of particles where, for certain values of U and density ratios of particle types, the sum 2-22 exceeded unity. Subsequently, we adopted an approximate procedure, summarized by Bartky and Bauer (Reference 2-17), for calculating the spectral coefficients in terms of the Mie-scattering cross sections that we obtained from our Mie code.

The appropriate formulas for the spectral coefficients, using the parallel beam or one-dimensional approximation, are as follows:

$$\varepsilon = 2\kappa[e^{k\tau}(k+\kappa) + e^{-k\tau}(k-\kappa) - 2k]/D \qquad (2\text{-}23)$$

$$R = (k^2 - \kappa^2)(e^{k\tau} - e^{-k\tau})/D \qquad (2\text{-}24)$$

$$T = 4\kappa k/D \quad , \qquad (2\text{-}25)$$

where

$$D = (k + \kappa)^2 e^{k\tau} - (k - \kappa)^2 e^{-k\tau} \qquad (2\text{-}26)$$

$$k = \{\kappa[2(1 - \kappa)\beta + \kappa]\}^{1/2} \qquad (2\text{-}27)$$

$$\kappa = \sigma_a/(\sigma_a + \sigma_s) = q_a/(q_a + q_s) \qquad (2\text{-}28)$$

$$\alpha + \beta = 1 \qquad (2\text{-}29)$$

and

$$\beta = 0.5 \int_{\pi/2}^{\pi} P(\theta)\sin\theta d\theta = 0.5 \int_{-1}^{0} P(\mu)d\mu \quad . \qquad (2\text{-}30)$$

Here, σ_a and σ_s are, respectively, the absorption and scattering cross sections (cm^2), a_a and a_s are the related mass absorption and mass-scattering cross sections ($cm^2\ gm^{-1}$), α and β are the fractions of the radiation scattered forward and backward, respectively, at a single scattering, and $P(\theta)$ is the scattering pattern normalized such that

$$0.5 \int_{-1}^{1} P(\mu)d\mu = 1 \quad , \tag{2-31}$$

where $\mu = \cos\theta$ and θ is the scattering angle. The quantity τ is the optical depth which, for a distance z into a medium of particle number density N, is given by

$$\tau = \int_{0}^{z} (\sigma_a + \sigma_s)Ndz' \quad . \tag{2-32}$$

Alternatively,

$$\tau = (a_a + a_s)\rho = a_e\rho \quad , \tag{2-33}$$

where a_e, the sum of a_a and a_s, is the mass-extinction coefficient.

In computing the spectral coefficients ε, R, and T from Equations 2-23 to 2-25, the quantities required as input are the absorption and scattering cross sections (for determining κ) and the scattering pattern $P(\theta)$ (for determining β). We have evaluated these quantities, averaged over specified particle-size distributions, from Mie codes developed originally by Thompson at General Electric Co., TEMPO, and described in Reference 2-18. Specifically, we have performed calculations for two different size distributions of water droplets, for a distribution of dust (basaltic glass) particles, for a distribution of soot (carbon)

particles, and for a combined distribution of water droplets and soot particles. The basic ingredient in these calculations is the complex refractive index of the particles as a function of wavelength. Values used for the real and imaginary components were obtained from References 2-19 to 2-21 and are tabulated in Appendix C.

For a mixture of soot particles and water droplets, we used the following expressions for the parameters κ and β that appear in the foregoing relations:

$$\kappa = \frac{(\rho^W/\rho^S)q_a^W + q_a^S}{(\rho^W/\rho^S)q_e^W + q_e^S} \qquad (2\text{-}34)$$

$$\beta = \frac{(\rho^W/\rho^S)q_s^W\beta^W + q_s^S\beta^S}{(\rho^W/\rho^S)q_s^W + q_s^S} \qquad (2\text{-}35)$$

$$\tau = q_e^W U^W + q_e^S U^S \quad . \qquad (2\text{-}36)$$

Here, ρ^W and ρ^S are the mass density of water drops and soot particles, respectively. The other parameters have their usual meaning, with superscripts "s" and "w" referring, respectively, to soot particles and water droplets.

Particle Size Distributions. We assume the log-normal distribution of particle diameters, D:

$$f(D) = \frac{e^{-0.5[\ln(D/D_m)/\ln S]^2}}{\sqrt{2\pi}\, D \ln S} \quad , \qquad (2\text{-}37)$$

where D_m and S are the mean diameter and standard-deviation parameters, respectively. The values used for D_m and S for each particle type are shown in Table 2-6. In the case of water droplets (clouds), calculations were made for two different distributions. The first distribution approximates measurements made on altostratus clouds (see Reference 2-22); the second contains a larger fraction of larger droplets. The dust and soot distributions are those used for the baseline calculations (Reference 2-1). For calculations involving a combination of soot and water droplets, distribution 1 for water was used. These distributions are shown in Figure 2-4.

Table 2-6. Log-normal parameters used in the Mie calculations.

Particle	$D_m(\mu m)$	S
water (1)	10.477	1.6
water (2)	17.918	1.4
dust (basaltic glass)	0.5	2.0
soot (carbon)	0.2	2.0

Results

Figures 2-5 to 2-8 show the calculated broad-band IR properties for water clouds, dust layers, and soot layers as functions of the particle content (gm cm^{-2}) along the path. Figure 2-9 shows the broad-band emissivity of a layer containing a mixture of soot particles and water drops (distribution 1) for selected values of the ρ^W/ρ^S ratio. More complete results for this case, including the transmissivities and reflectivities, are given in Table C-4 of Appendix C.

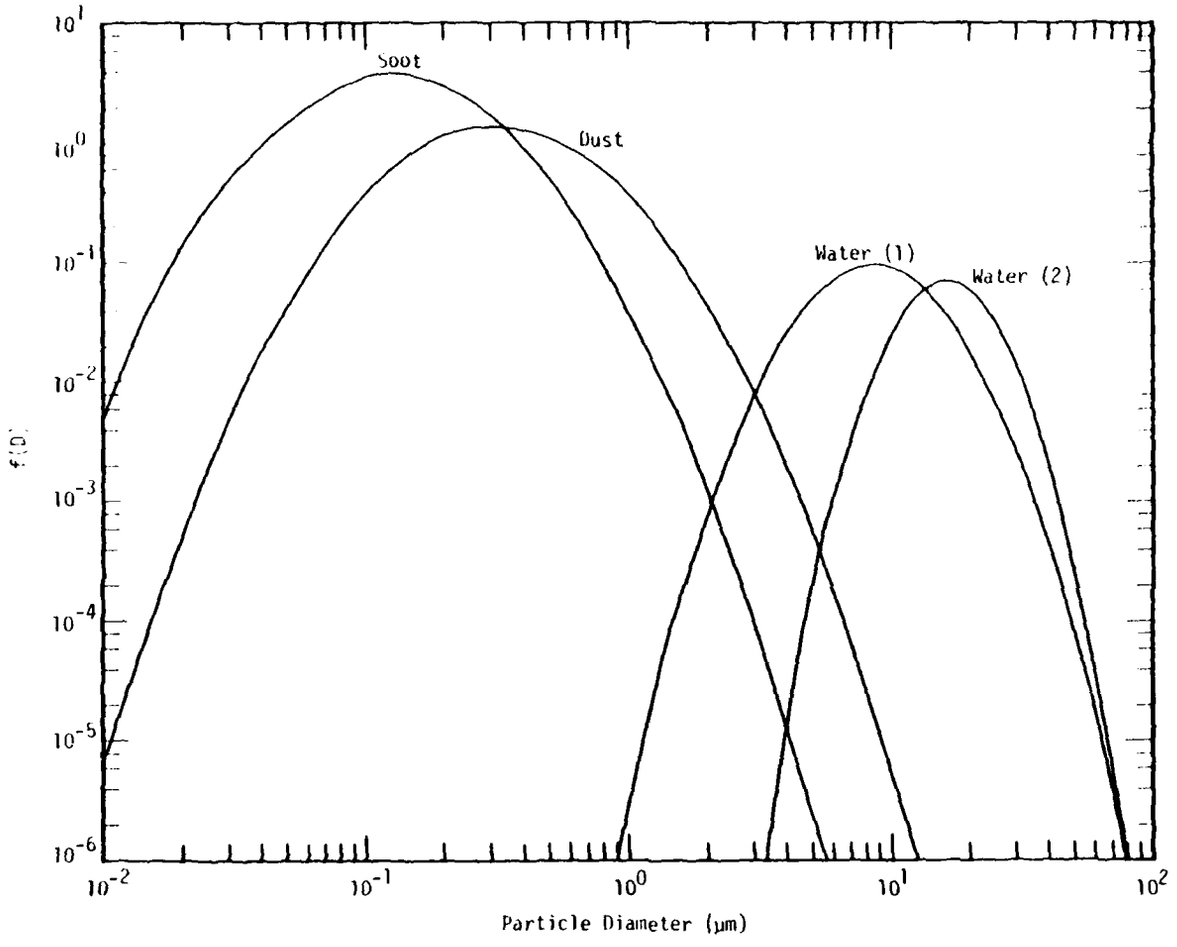

Figure 2-4. Particle size distributions used in calculations.

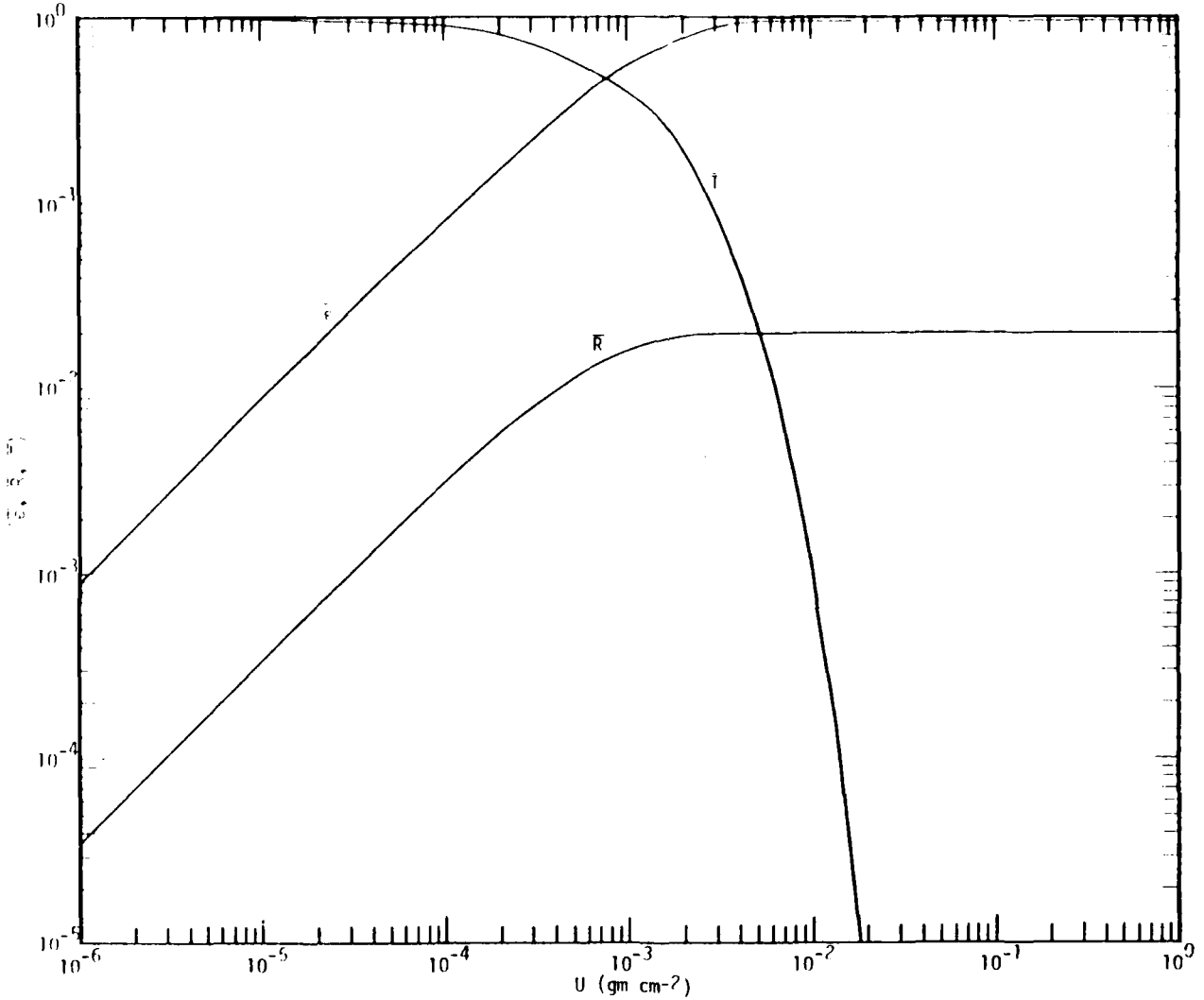

Figure 2-5. Broad-band IR properties of water clouds (distribution 1).

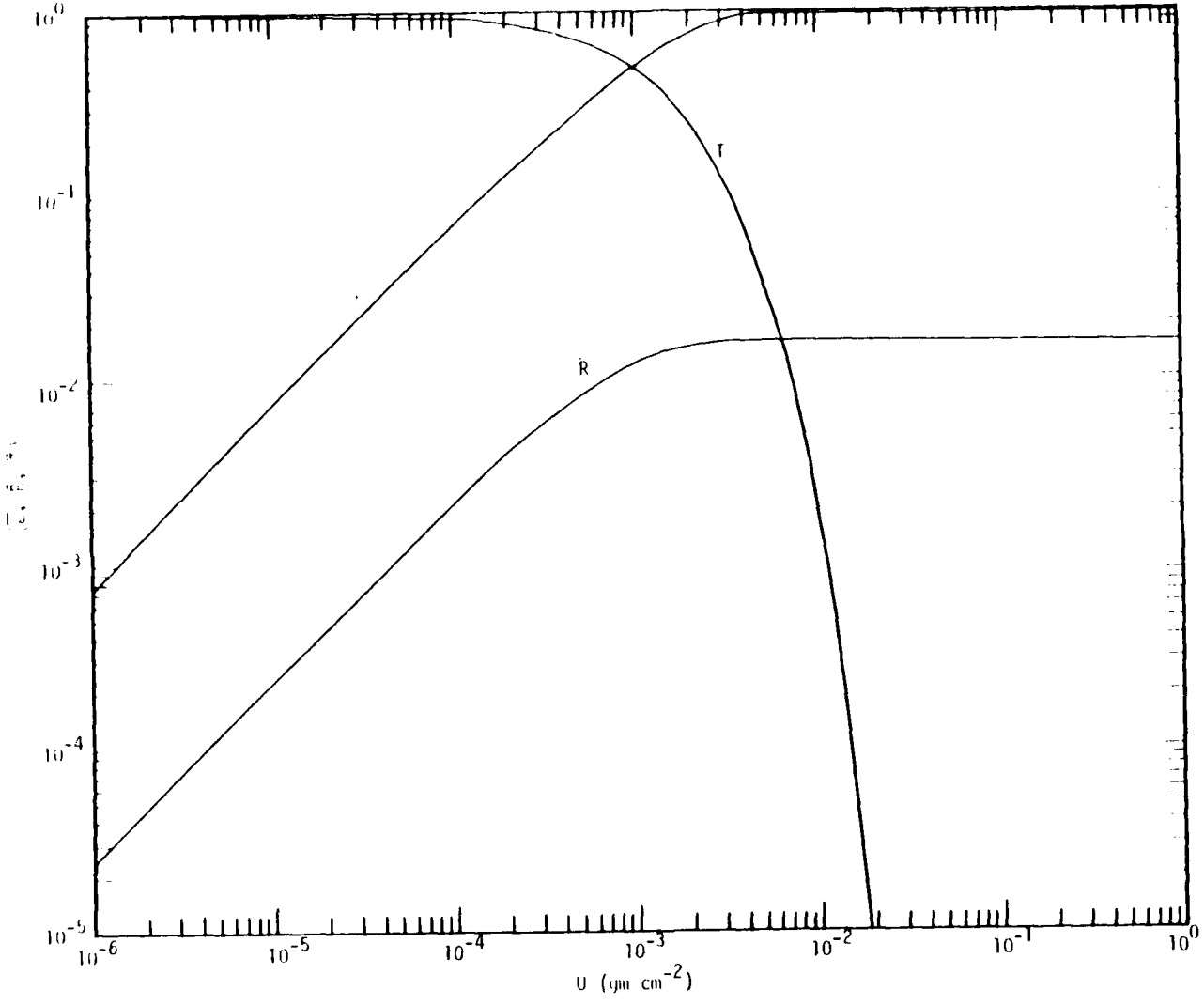

Figure 2-6. Broad-band IR properties of water clouds (distribution 2).

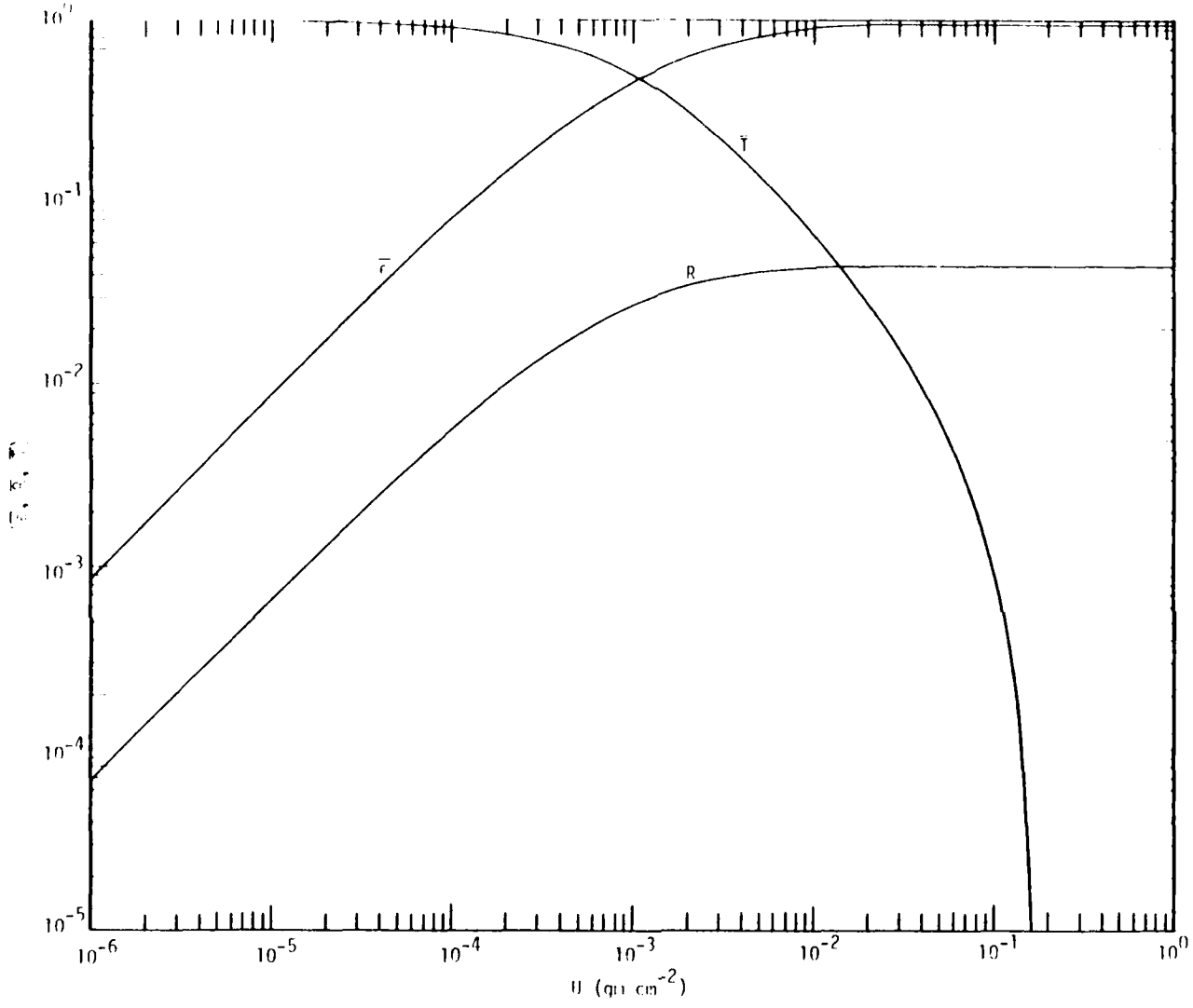

Figure 2-7. Broad-band IR properties of dust (basaltic glass) layers.

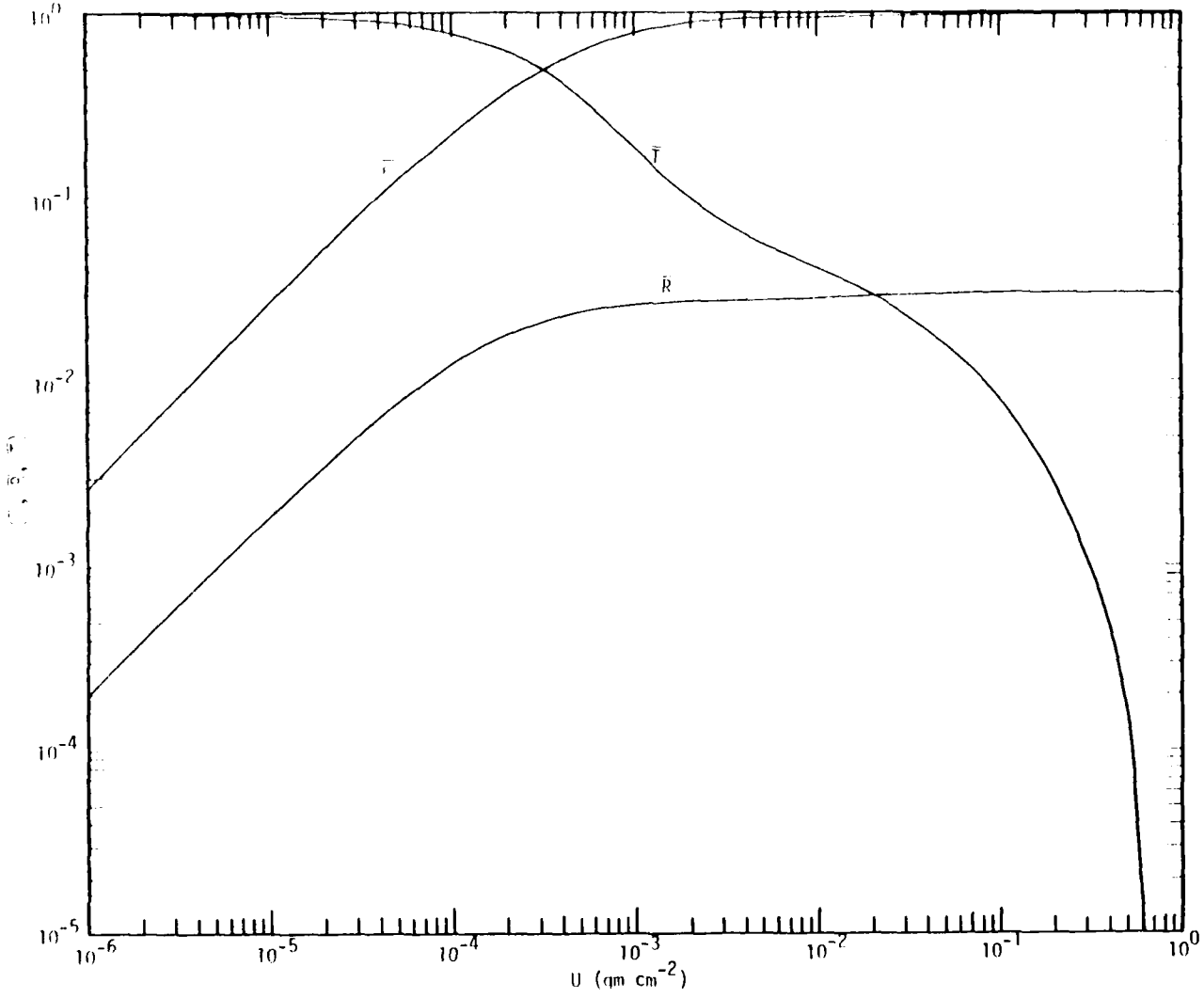

Figure 2-8. Broad-band IR properties of soot (carbon) layers.

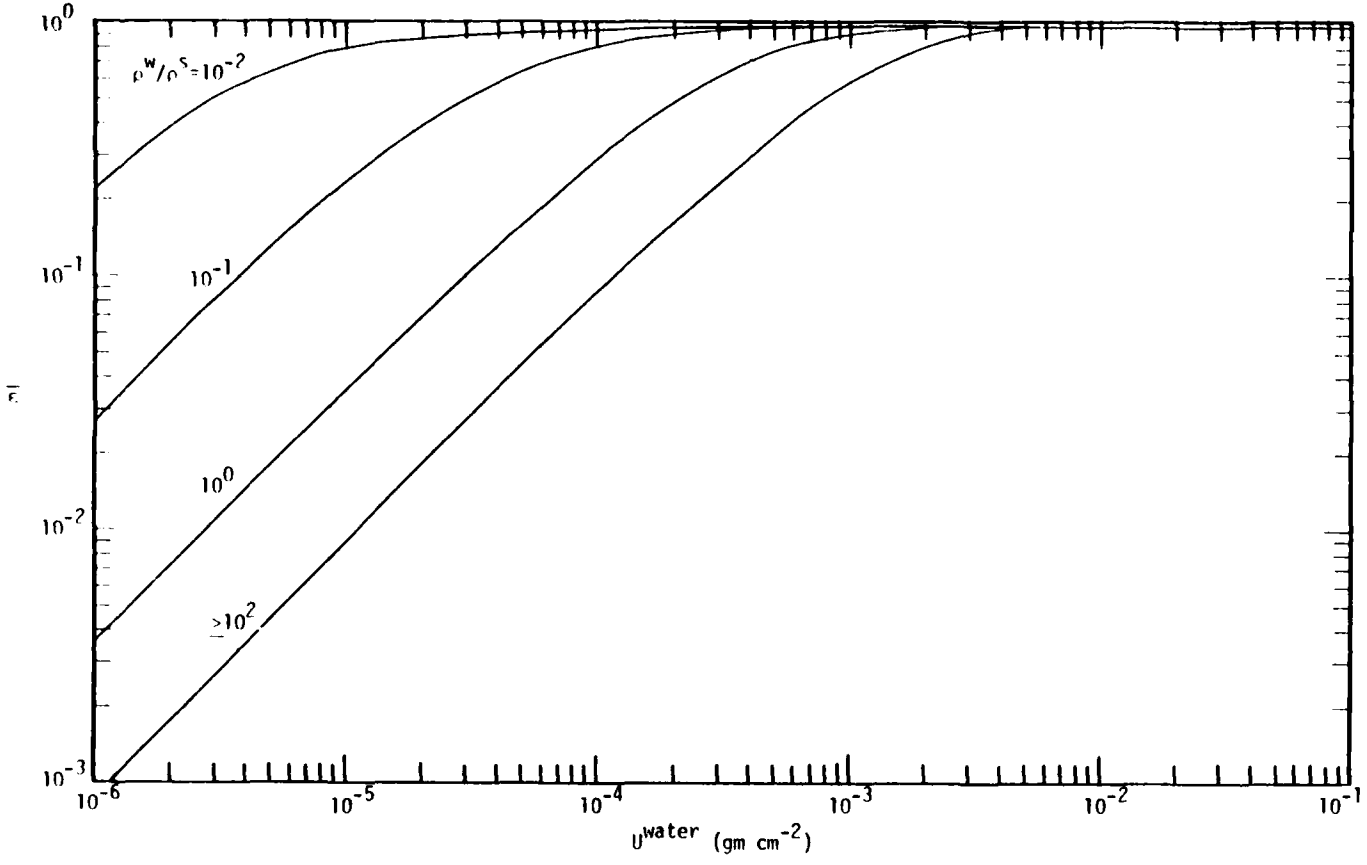

Figure 2-9. Broad-band IR emissivity of sooty water clouds for selected values of the water-to-soot density ratio.

OPTICAL PROPERTIES OF PARTICULATE LAYERS IN THE VISIBLE

The formulas 2-23 to 2-36 have been applied to the calculation of the optical properties of particulate layers at a wavelength of 0.55 μm in the visible. The calculations were done for a water cloud (size distribution 1) a dust (basaltic glass) layer, a soot (carbon)-particle layer, and a layer consisting of a mixture of water droplets (distribution 1) and soot particles. For the size-distribution parameters shown in Table 2-6, the values obtained from our Mie-code calculations for the parameters a_a, a_s, a_e, κ, and β, required for input to the formulas, are shown in Table 2-7. Also shown in Table 2-7 are the values for the real and imaginary components of the refractive index ($n = n_R - in_I$) used in the Mie calculations. For water, dust (basaltic glass), and soot, the index values were obtained from References 2-20, 2-21, and 2-1, respectively.

Table 2-7. Input parameters to optical formulas for $\lambda = 0.55$ μm.

Particle	n_R	n_I	a_a(cm^2 gm^{-1})	a_s(cm^2 gm^{-1})	a_e(cm^2 gm^{-1})	κ	β
water (1)	1.335	1.0×10^{-9}	2.568×10^{1}	1.715×10^{3}	1.741×10^{3}	1.475×10^{-7}	4.603×10^{-2}
dust	1.57	4.6×10^{-4}	8.010×10^{1}	9.228×10^{3}	9.308×10^{3}	8.605×10^{-3}	1.090×10^{-1}
soot	1.55	0.1	1.770×10^{4}	2.652×10^{4}	4.422×10^{4}	4.003×10^{-1}	6.464×10^{-2}

Figures 2-10, 2-11, and 2-12 show the resulting values of the emissivity, transmissivity, and reflectivity as functions of the layer thickness (gm cm^{-2}) through the water, dust, and soot layers, respectively. For the layer consisting of a mixture of soot particles and water droplets, results have been obtained for parametric values of the ρ^W/ρ^S ratio and the optical depth. These are shown in Table C-5 of Appendix C. The emissivity results in this case, for selected values of the ρ^W/ρ^S ratio, are shown in Figure 2-13.

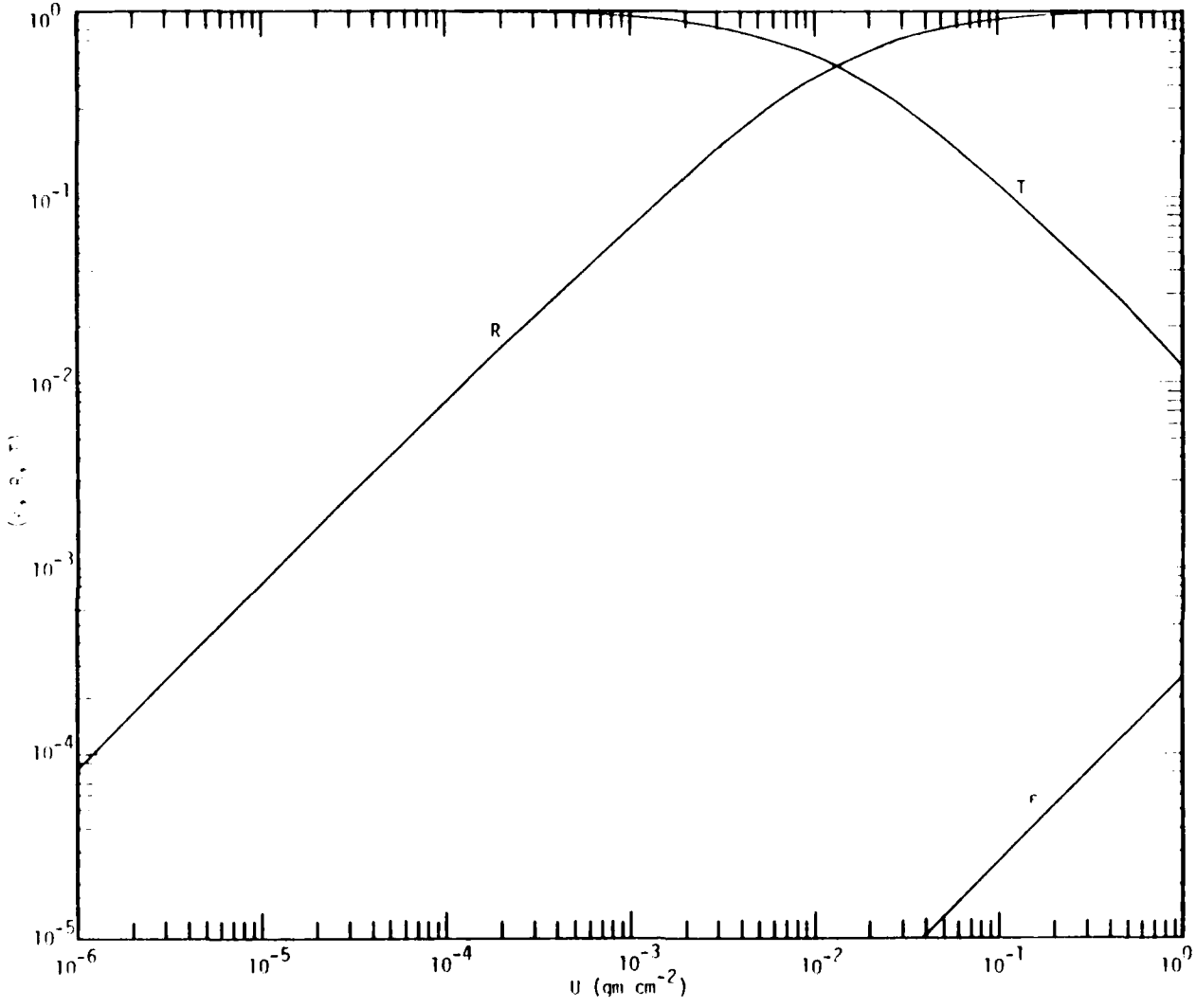

Figure 2-10. Optical properties in the visible (λ=0.55 μm) of water clouds (distribution 1).

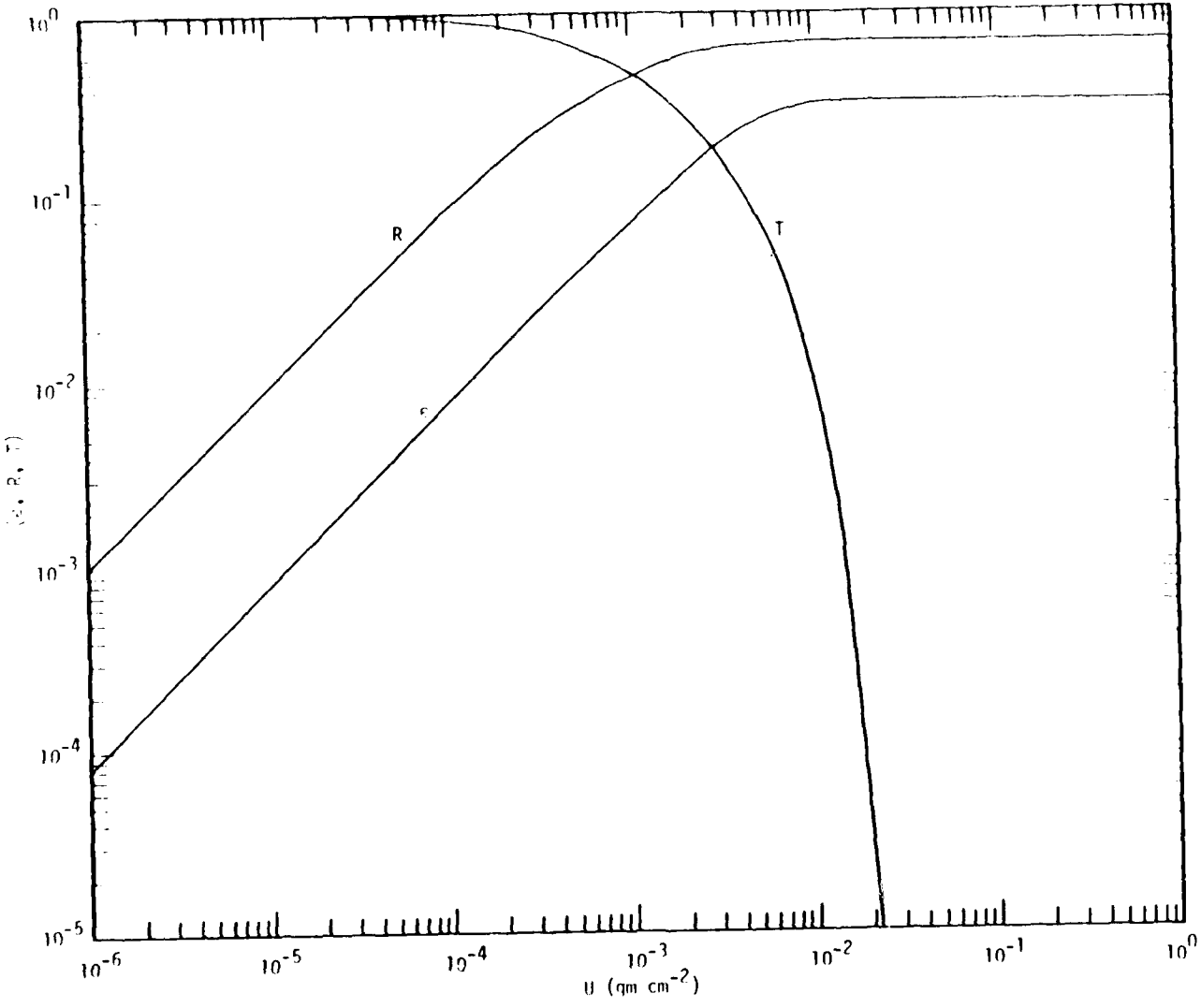

Figure 2-11. Optical properties in the visible (λ=0.55 μm) of dust (basaltic glass) layers.

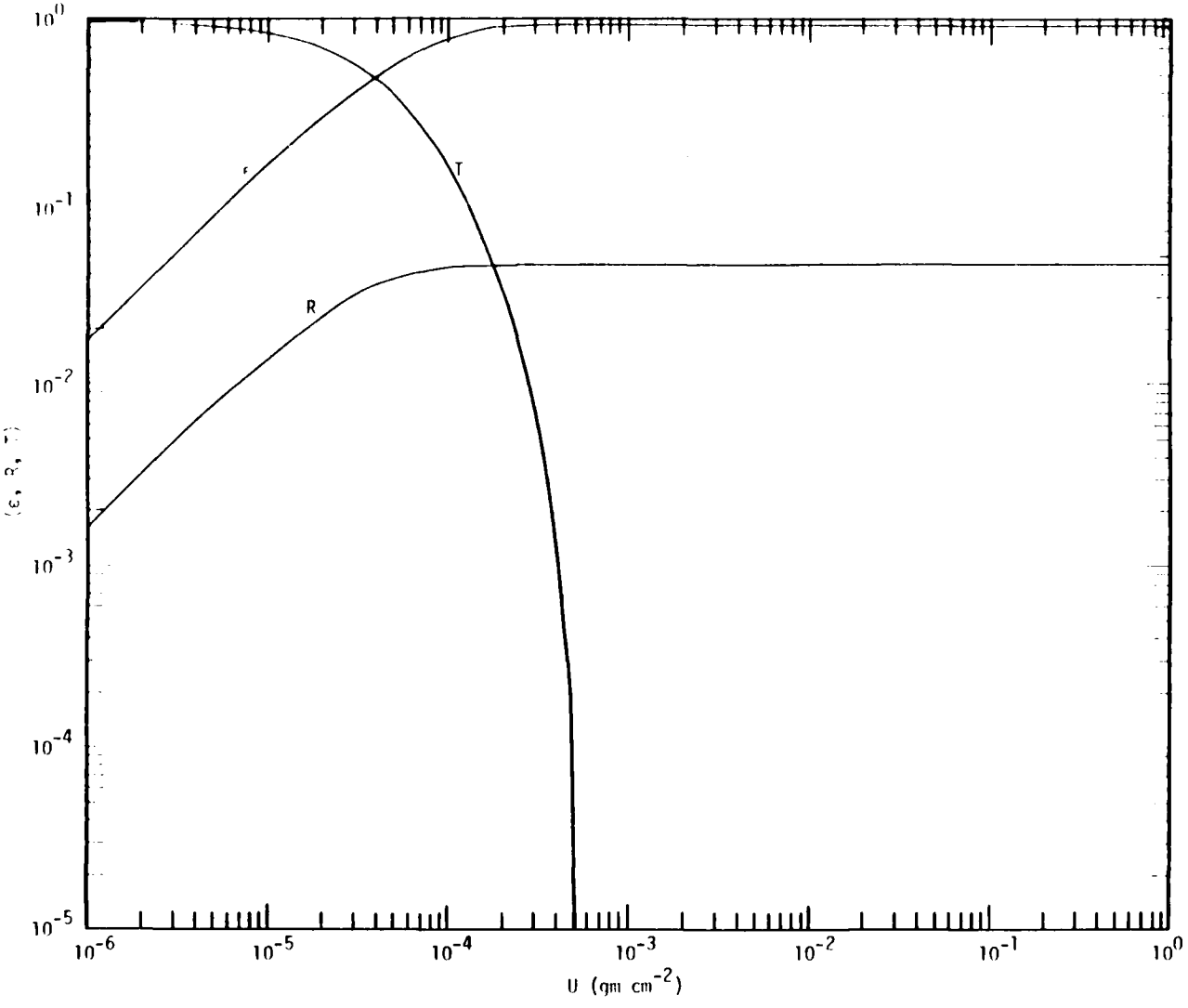

Figure 2-12. Optical properties in the visible (λ=0.55 μm) of soot (carbon) layers.

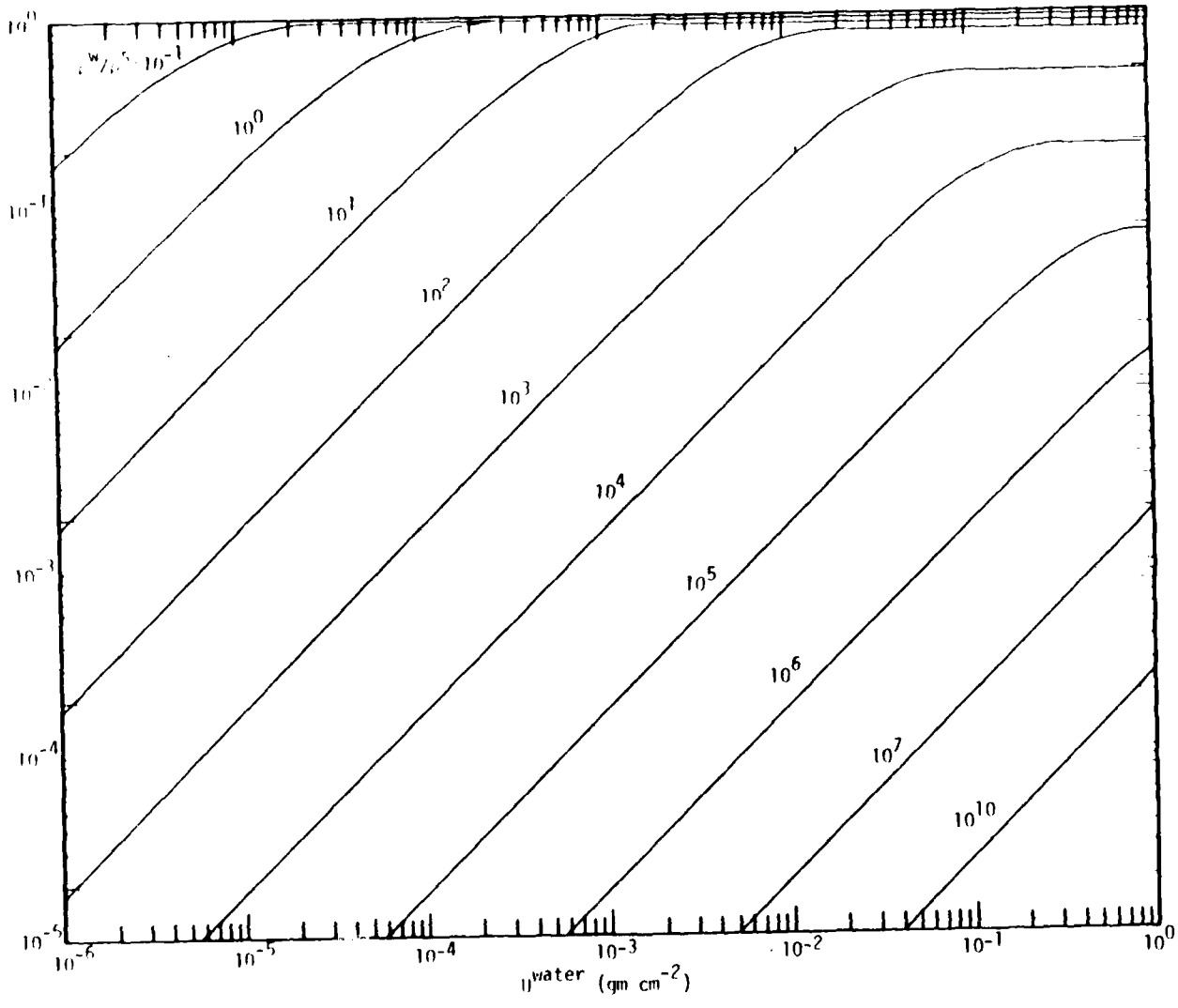

Figure 2-13. Emissivity in the visible (λ=0.55 μm) of sooty water clouds for selected values of the water-to-soot density ratio.

SECTION 3
MODEL CALCULATIONS

THE BASIC MODEL

Most of the models we shall discuss in this report will consist of two or three atmospheric layers over an earth which is assumed either to be black or to have some significant albedo (the last case is for study of the effect over snowpack). It is important to understand that within a given layer only the optical properties of the medium are taken as constant; the radiative fluxes and the temperature vary continuously throughout a given layer. Before discussing these models let us consider the case of a single layer which we shall take to be infinitely deep. We shall assume that a flux of solar energy of intensity Σ is incident on the surface of the layer which we take to be z=0. If such a flux is incident on a blackbody the body will reach an equilibrium temperature, T_{BB}, given by

$$T_{BB} = \left(\frac{\Sigma}{\sigma}\right)^{1/4} \tag{3-1}$$

where σ is the Stefan-Boltzmann constant. We shall assume that the medium in the layer is characterized by a visible opacity ε_S but that the medium does not emit in the visible. We shall also assume that the medium possesses an opacity ε_I in the infrared and that the infrared radiation consists of an upward flux, U, and a downward flux, D, since the medium does not emit in the visible the solar flux is downward and we shall call it S. The equations for the fluxes are

$$\frac{dS}{dz} = -\varepsilon_S S \tag{3-2}$$

$$\frac{dU}{dz} = \varepsilon_I U - \varepsilon_I \sigma T^4$$

$$\frac{dD}{dz} = -\varepsilon_I D + \varepsilon_I \sigma T^4$$

$$2\varepsilon_I \sigma T^4 = \varepsilon_I (U+D) + \varepsilon_s S$$

In order to produce transport equations of this form, it is necessary to assume local thermodynamic equilibrium, ignore scattering and provide an ansatz for the angular distribution of the radiation. If the radiation fields are taken to be uniform in angle over each hemisphere (up and down) but possibly of a different amplitude (Eddington's approximation), the above equations result provided that ε is interpreted as twice the absorption opacity. The general solution to these equations (which we shall need later) is

$$\begin{aligned}
S &= \Sigma e^{-\varepsilon_s z} \\
U &= \frac{1}{2}\left\{A\left(1 - \frac{\varepsilon_I}{\varepsilon_s}\right) e^{-\varepsilon_s z} + B(\varepsilon_I z + 1) + C\right\} \\
D &= \frac{1}{2}\left\{-A\left(1 + \frac{\varepsilon_I}{\varepsilon_s}\right) e^{-\varepsilon_s z} + B(\varepsilon_I z - 1) + C\right\} \\
\tau \equiv \sigma T^4 &= \frac{1}{2}\left\{A\left(\frac{\varepsilon_s}{\varepsilon_I} - \frac{\varepsilon_I}{\varepsilon_s}\right) e^{-\varepsilon_s z} + B\,\varepsilon_I z + C\right\}
\end{aligned} \tag{3-3}$$

where we have defined τ to be σT^4 in order to simplify the notation. The boundary conditions for the problem at hand are

$$\begin{aligned}
S\big|_{z=0} &= \Sigma \\
D\big|_{z=0} &= 0 \\
U\big|_{z=0} &= S\big|_{z=0}
\end{aligned} \tag{3-4}$$

For the temperature we get

$$\tau = \frac{\Sigma}{2}\left[1 + \frac{\varepsilon_I}{\varepsilon_s} + \left(\frac{\varepsilon_s}{\varepsilon_I} - \frac{\varepsilon_I}{\varepsilon_s}\right)e^{-\varepsilon_s z}\right] \tag{3-5}$$

Many of the IR effects on the nuclear winter phenomenon can be understood in terms of this equation. If $\varepsilon_I = \varepsilon_s$ we find that

$$\tau = \sigma T_{BB}^4 \tag{3-6}$$

independent of z. If $\varepsilon_s > \varepsilon_I$ we find that at the top of the layer the temperature is hotter than T_{BB}:

$$\tau\Big|_{z=0} = \sigma T_{BB}^4 \frac{1}{2}\left(1 + \frac{\varepsilon_s}{\varepsilon_I}\right) \tag{3-7}$$

The temperature decreases from this value as one proceeds into the layer asymptotically approaching a value less than T_{BB}:

$$\tau\Big|_{z=\infty} = \sigma T_{BB}^4 \frac{1}{2}\left(1 + \frac{\varepsilon_I}{\varepsilon_s}\right) \tag{3-8}$$

If $\varepsilon_s < \varepsilon_I$ the situation is reversed: Equations (3-7) and (3-8) are still valid but they now predict that the temperature at the top of the layer is less than T_{BB} while the temperature deep within the layer is greater than T_{BB}.

In the normal atmosphere the solar absorption is small but there is appreciable IR absorption due mostly to water vapor; thus ε_I is larger than ε_s and the stratosphere is colder than T_{BB} while the earth's surface

is warmer than T_{BB}. The essence of the nuclear winter phenomenon as it has been previously reported is that a layer of soot is injected into the atmosphere whereupon ε_s becomes greater than ε_I; therefore the top of the layer, which is at several kilometers altitude, becomes hotter than T_{BB} while the surface temperature may cool to near T_{BB} or below (the reason it is usually not below T_{BB} is that the layer is not infinitely thick).

Before considering numerical examples we need a slightly more complicated model so that the effects of the finite thickness of the layers may be considered. We shall study the model shown in Figure 3-1. Layer 1 is composed primarily of dust and water vapor and we shall assume that it has a solar albedo, A_1, an IR opacity of ε_{I_1} with a total optical depth in the IR of μ_{I_1}, and no solar absorption; such a layer is probably there in realistic cases but its optional depth is probably not very great. Layer 2 is the soot layer - the main component of the nuclear winter phenomenon; we shall assume that it has a solar albedo of A_2, a solar opacity of ε_{S_2} with a total optical depth in the solar of μ_{S_2} and a ratio of $\varepsilon_{I_2}/\varepsilon_{S_2}$ of α. Layer 3 is included in the model to represent a possible rain-out layer which may or may not be present in realistic cases. We assume it has no solar absorption but has an IR opacity of ε_{I_3} with a total depth μ_{I_3} due mostly to water vapor. Under the third layer is the surface of the earth which is taken to be a black body.

Within any layer the temperature and the fluxes satisfy Equations (3-2) and so have the general solution (3-3). A complete solution is easily written down but the collection of formulae is somewhat tedious. Here we shall study the behavior of the temperature at two points: T_S, the temperature at the top of the soot layer and T_E, the temperature of the earth; the complete solution can be found in Appendix D. We have:

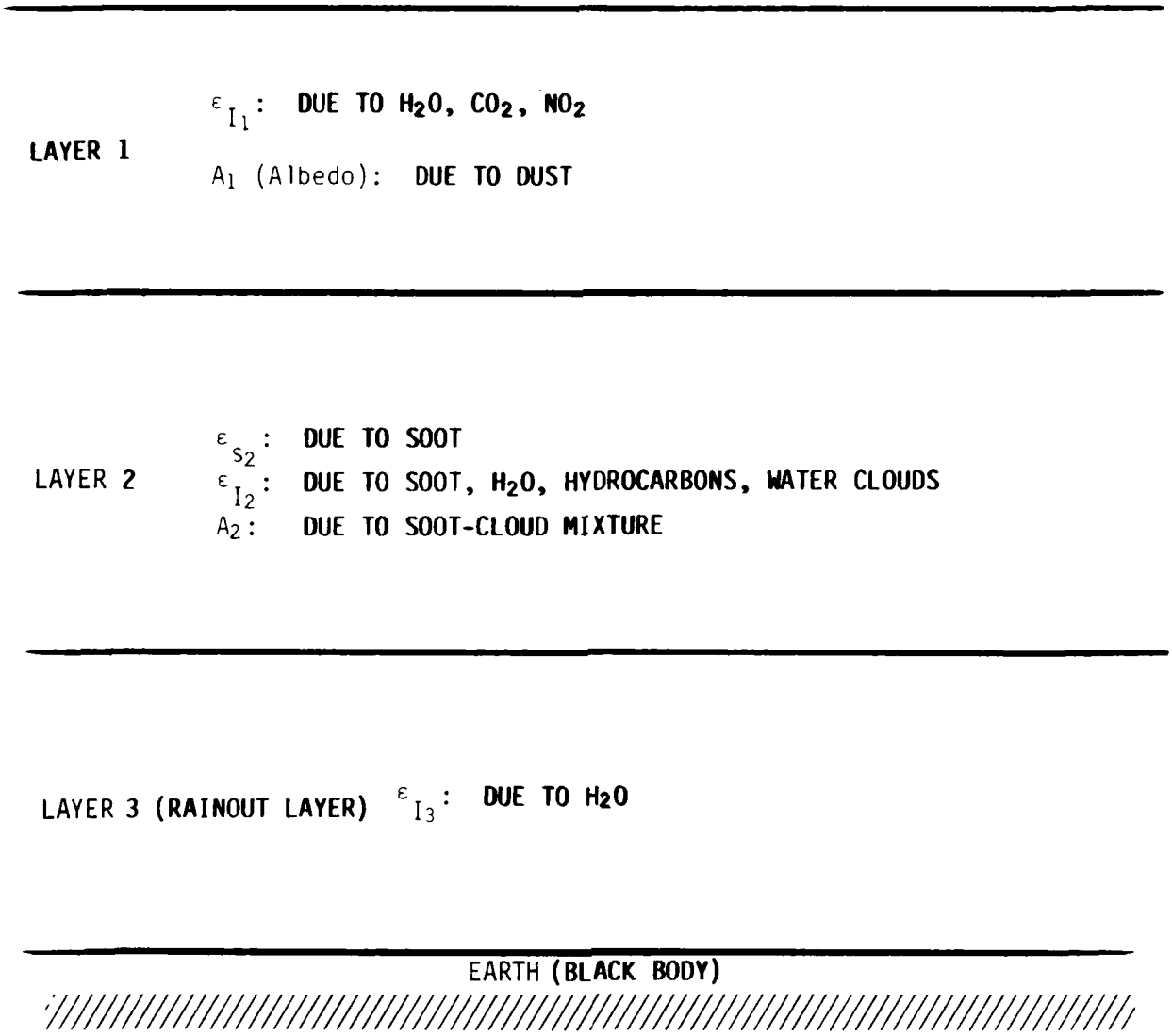

Figure 3-1. Schematic of the simple model nuclear winter which ignores convective instabilities.

$$\tau_S = \frac{1}{2} \Sigma (1-A_1)(1-A_2) \left[1 + \frac{1}{\alpha} + \mu_{I_1}\right] \quad (3\text{-}9)$$

$$\tau_E = \frac{1}{2} \Sigma (1-A_1)(1-A_2) \left[1 + \mu_{I_1} + \alpha(1 - e^{-\mu_{S_2}}) + (1 + \mu_{I_3}) e^{-\mu_{S_2}}\right] \quad (3\text{-}10)$$

Let us now look at some examples of using equations (3-9) and (3-10). We shall assume that Σ is equal to the solar constant divided by 4: $\Sigma = 3.5 \times 10^5$ ergs/cm^{2}sec. If we assume that layers 1 and 2 are missing, that $\mu_{I_3} = 1.3$ and that the total albedo is .2 we obtain a temperature for T_E of 300K. This temperature represents approximately ambient conditions in our model and should be used as a standard of comparison for other temperatures we shall calculate later. Let us now consider a case which closely resembles the NRC baseline scenario: we shall choose α to be .25, the NRC baseline value for pure soot[1], μ_{S_2} to be 2, the value attained in the NRC baseline scenario for the time of the minimum surface temperature; μ_{I_1} we shall choose to be .2 based on the assumption that there will be a few times 10^{-3}g/cm^2 of water vapor above the soot layer and shall choose the albedos to be: $A_1 = .1$ based on $\approx 10^{-4}$ g/cm^2 of dust and Fig. 2-11; and $A_2 = .04$ based on Fig. 2-12. Equations (3-9) and (3-10) give $T_S = 340$K and $T_E = 255$K. We thus get a temperature for the earth which is 45K below the ambient value and a temperature for the top of the soot layer (which would have been at 237K under ambient conditions) 103K hotter than ambient; these results are in good agreement with the NRC study.

Of principal interest to the present study is the variation of these results with changes in the parameter α. In Figure 3-2 we show a plot of T_S and T_E as functions of α with all other parameters fixed at the values we have just used. The values of α shown in the graph range from .1 to 5; according to the NRC the likely range of values for α due to soot alone is .03 to 1[2]. We believe that there will always be enough water

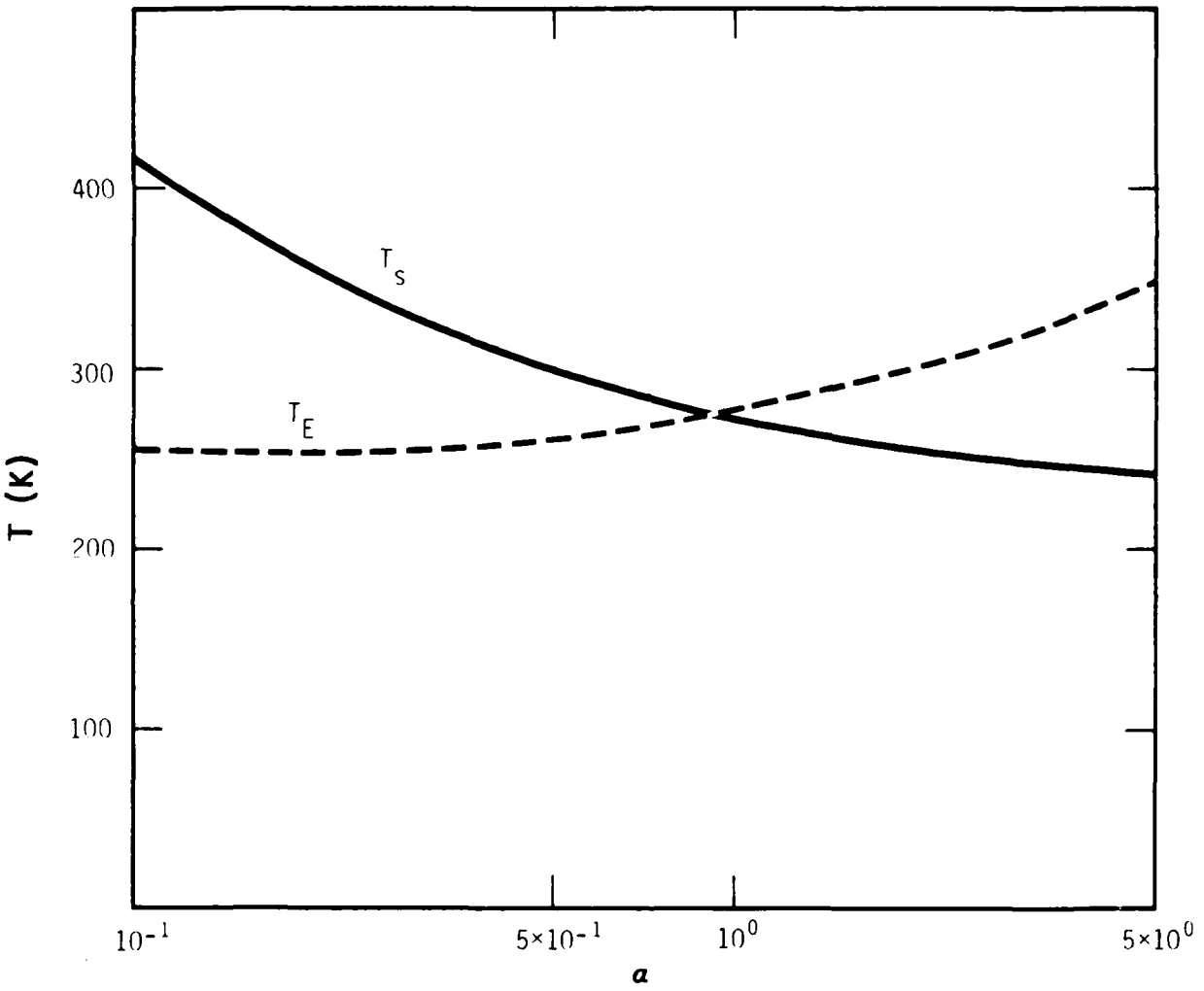

Figure 3-2. The temperature at the earth's surface, T_E, and the temperature at the top of the soot layer, T_S, plotted vs. α. Convective instabilities are ignored in these calculations.

vapor present such that the value of α for the mixture will not fall below .1; to raise the value of α to something greater than one would require the presence of absorbers which are more effective in the IR than they are in the solar. The likely candidates for such absorbers are hydrocarbon vapors, water vapor and condensed water (clouds).

By looking at Fig. 3-2 we can see that to make an appreciable change in the temperature structure we must change α by at least .1 or more; at the NRC value of .25 a change of .1 in α would lead to a 3K change in T_E and a 17K change in T_s. For the NRC range of values for pure soot ($.1<\alpha<1$) we see that the temperature of the earth ranges from 251K to 278K while the temperature at the top of the layer ranges from 413K to 272K. While convective instabilities, discussed below, will alter these ranges, particularly the range for the top of the layer, somewhat, the variation implied by the uncertainties in the properties of the soot alone is substantial and studies to determine these properties with less uncertainty are clearly warranted.

The information on hydrocarbon emissions given in section 2 along with the information on the IR properties of the hydrocarbons, especially Fig. 2-3 makes it clear that hydrocarbon emission cannot change α by an amount nearly as large as .1. The most important hydrocarbon is probably the ethylene although the acetylene appears to be stronger in Figure 2-3. The reason for the enhanced importance of ethylene is that most of its emission lies in the window where water vapor is transparent while the overlap between water vapor and acetylene will partly cancel the importance of the acetylene. Even if we ignore any questions of overlap we see that the total of all the additional hydrocarbons is only about equal in IR emissivity to the ambient methane. To estimate the effects of these gases on the temperature structure we recall that the optical depth of the visible is taken to be 2. Since the soot and the additional hydrocarbons came from the same source (the fires) they must be approximately uniformly mixed. Thus we find that α is given by

$$\alpha = \frac{\text{optical depth in the IR}}{2}$$

The IR optical depth of the soot is .5; the change in α due to the hydrocarbons is

$$\Delta\alpha = \frac{\text{IR optical depth of the hydrocarbons}}{2}$$

The IR optical depth of the hydrocarbons assuming no overlap is about 2×10^{-2} which gives

$$\Delta\alpha_{\text{hydrocarbons}} = .01$$

The specific optical depths we have been using assume a particular distribution of the soot and hydrocarbons over the earth's surface. α and $\Delta\alpha$ will, however, be approximately independent of this assumption since if the hydrocarbons are concentrated due to patchiness the soot will be also. Even if there were to exist some mechanism whereby the hydrocarbons were ten times as concentrated as the soot the effect of the hydrocarbons would have only a marginal effect on the temperature structure. We conclude that the "greenhouse" effect of the hydrocarbons cannot significantly counteract the "anti-greenhouse" effect of the soot.

Much the same situation is encountered in the case of CO_2 as was found in the case of the hydrocarbons. According to the discussion which can be found in Chapter 2 the amount of CO_2 added to the atmosphere by the fires is small compared with the amount in the ambient atmosphere. Furthermore the ambient CO_2 is mixed nearly uniformly over the portion of the atmosphere which is affected by the soot so the blasts and fires will not cause an appreciable redistribution of the CO_2. Thus the IR optical depth of the CO_2 will be the ambient value of about .004 which is not enough to change α by an appreciable amount.

In the case of NO_2 it is the value of μ_{I_1}, rather than α, which is most likely to be affected. Much of the NO_2 created by the blasts will be carried to altitudes where it will remain above the soot. Figure 2-1 shows that if the high altitude NO_2 is distributed more or less uniformly its contribution to μ_{I_1} will be less than the contribution we have assumed for water vapor by a factor of twenty; thus, even for relatively concentrated patches the NO_2 will not have a major effect on the temperature.

The question of the effects of water vapor is much more complicated. One reason is that the water vapor has a much greater chance of being important so we cannot perform a quick calculation and dismiss it. Another reason is that the ambient water vapor is not uniformly distributed over the part of the atmosphere where the soot is found (it is concentrated at the lower altitudes) so the redistribution of the ambient water vapor in addition to the addition of new water vapor must be considered. A final complication is that the absorption coefficient of water vapor has a complicated behavior as a function of frequency across the IR band whereas our simple calculations treat it as constant. To correct this last problem we should keep more IR groups (the absorption coefficient of water vapor can be well approximated by four IR groups) which would considerably complicate our formalism. We shall instead observe that optical depths on the order of one are the ones important to us and water vapor has an effective absorption coefficient of about 1 cm^2/g in this range. More complicated calculations using more than one IR group have confirmed that this procedure is sufficient to our needs.

Estimating the amount of water vapor which will be mixed with the smoke is a difficult problem. We first consider the water released by the combustion process. According to the NRC most combustable materials generate about 1 g-H_2O/g-burned; the emission factor for the soot is about .02g/g. However, the absorption coefficient for the soot in the visible

($2\times10^4 cm^2/g$) is 2×10^4 larger than the one we are assuming for water vapor in the IR. Thus the increment in α due to the water of combustion is only .0025.

While the water of combustion is not sufficient to significantly change the value of α the atmospheric water vapor redistributed by the fire plumes is much greater. The NRC estimates that a total of 40,000Tg of water would probably be drawn into the fire plumes with an upper-limit estimate of 500,000 Tg. Since the estimate for the total soot content is 180 Tg these numbers correspond to changes in α of .011 and .14 respectively. The latter number is just at the borderline where significant changes in the phenomenon might be observed. Even if the smaller number for the total entrained water is correct, which is likely the case, the water vapor will undoubtedly be distributed very unevenly depending on the particular location and also depending on the time of year of the event. In spite of these reservations we believe that water vapor will not make a significant impact on the nuclear winter phenomenon by causing an appreciable change in α. Even the extreme amounts of water vapor seem to fall just short of being enough.

We thus come finally to the question of the possible effect on α of condensed water. For condensed water one problem we had for water-vapor is removed: the strong dependence of the IR absorption coefficient on frequency; the absorption coefficient of water clouds is quite constant as a function of frequency. It does depend on the drop size distribution. For the size distribution of Figure 2-5 we find an absorption coefficient of 890 cm^2/g; for that of Figure 2-6 we find 730 cm^2/g; we have seen values as high as 2.2×10^3 cm^2/g for naturally occurring clouds quoted in the literature. We shall adopt a value of 800 cm^2/g for the moment. If we take the NRC's estimate for the most likely amount of entrained water, 40,000 Tg, we find a ratio of water mass to soot mass of 220. If all the water condensed out we would find a value of α of 9.

We thus see that if any appreciable portion of the water condenses out it will have a dominant effect on α. It will also have a significant effect on A_2 the albedo of the cloud-soot layer. From Table C-5 we see that if the ratio of water to soot is 200 to 1 the albedo will be about .26 while if it is 100 to 1 the albedo will be about .18; if the ratio is 50 to 1 which would correspond to a value of α of about 2.5 the albedo is about .12. (Note that the optical depth shown in the table is for scattering and absorption; we are interested in an absorption optical depth of 2 which requires about 10^{-4} g/cm^2 of soot.) In Figure 3-3 we plot T_S and T_E as given by Equations (3-9) and (3-10) using the value of A_2 given in Table C-5 (recall that convective instabilities were ignored in deriving these equations).

Water clouds, if they are present, have the potential to play a dominant role in the nuclear winter phenomenon. Furthermore clouds typically do form in fire plumes and once the cloud forms its presence keeps the top of the cloud cold which keeps the cloud there. We believe that the calculations just presented indicate that water clouds cannot be ignored and warrant further study; their temperatures given in Figure 3-3 cannot be considered realistic due to the fact we have ignored the effects of convective instabilities. Convective instabilities will be triggered once α becomes greater than 1 by any appreciable amount (something less than 1.2 for typical conditions). Having convinced ourselves that α might be raised to such values by the presence of clouds we shall now proceed to incorporate convection instabilities into our calculations.

THE EFFECTS OF CONVECTIVE INSTABILITIES

Up to this point we have been ignoring the fact that if the derivative of the atmospheric temperature with respect to z (recall that we are taking the direction of positive z to be downward) exceeds some value the lower hotter air will rise spontaneously and convection will set in. We shall take the critical value for the derivative to be 7K/Km, the

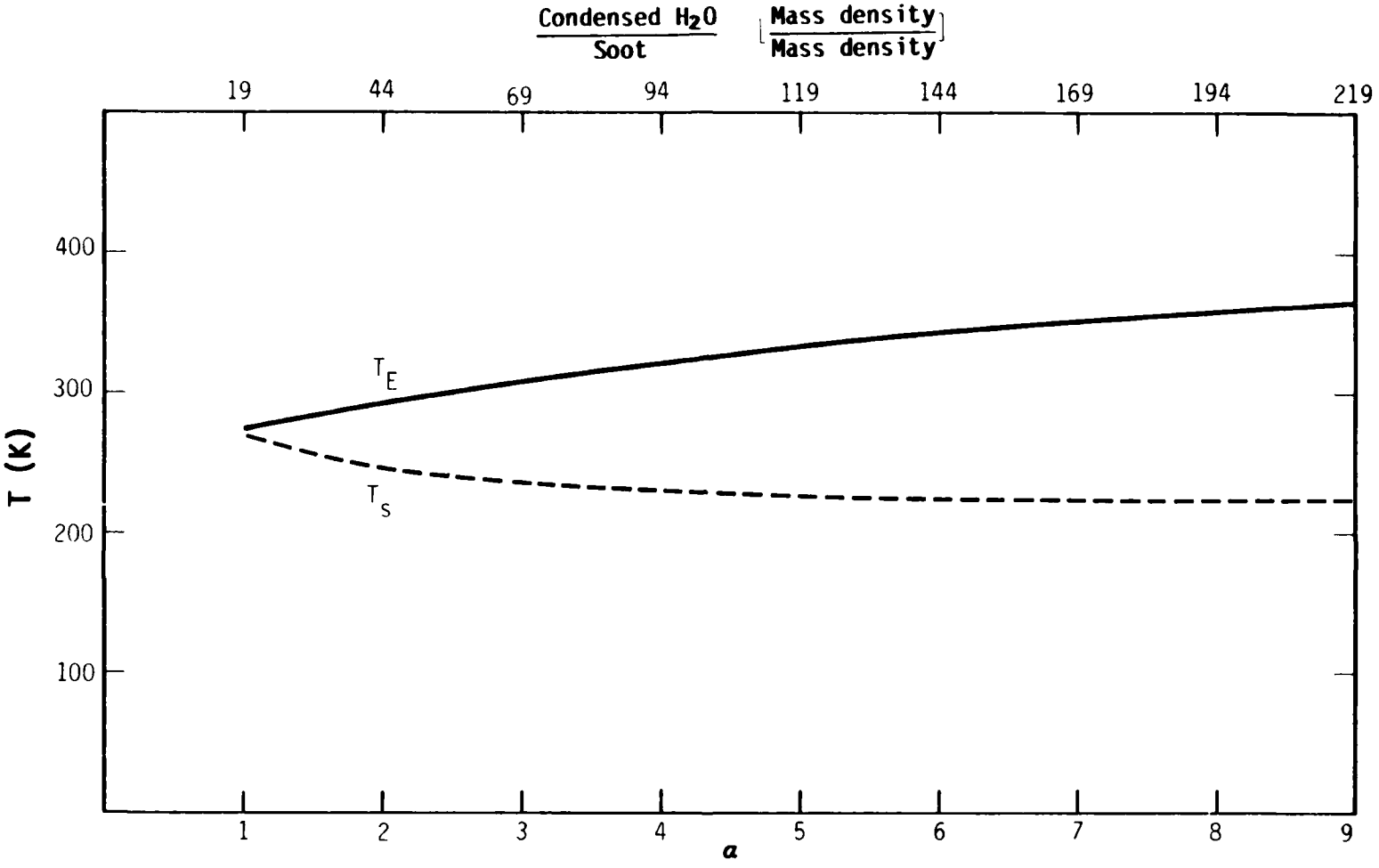

Figure 3-3. The temperature at the earth's surface, T_E, and the temperature at the top of the soot layer, T_s, plotted vs. α and vs. the ratio of cloud mass to soot mass. Convective instabilities are ignored in this calculation.

dry adiabatic lapse rate, and shall not in this report attempt to correct for condensation.

From the formula which gives the temperature in the cloud-soot layer (Equation D-2) we calculate the derivative of the temperature in that layer to be:

$$\frac{dT}{dz} = \left[\frac{(1-A_1)\ (1-A_2)\Sigma}{2\sigma}\right]^{1/4} \frac{.25\ \varepsilon_{s_2}\left(\alpha - \frac{1}{\alpha}\right)e^{-\varepsilon_{s_2} z}}{\left[\left(\frac{1}{\alpha} - \alpha\right)e^{-\varepsilon_{s_2} z} + 1+\alpha+\mu_{I_1}\right]^{3/4}} \qquad (3\text{-}11)$$

where z is zero at the top of the cloud-soot layer and increases as we proceed deeper into the layer. The maximum value of $\frac{dT}{dz}$ is at z=0 where the value is

$$\left.\frac{dT}{dz}\right|_{z=0} = \left[\frac{(1-A_1)\ (1-A_2)\Sigma}{2\sigma}\right]^{1/4} \frac{.25\ \varepsilon_{s_2}\left(\alpha - \frac{1}{\alpha}\right)}{\left[\frac{1}{\alpha} + 1 + \mu_{I_1}\right]^{3/4}} \qquad (3\text{-}12)$$

If we assume that the total optical depth in the solar of 2 is spread over 4 Km of altitude ε_{s_2} will be .5 Km^{-1}. For typical values of the other parameters we find that the temperature profile will be unstable for values of α greater than about 1.2. For a value of α of 4 the region z<3.2 Km has a gradient larger than 7K/Km.

The details of the way the unstable temperature profile is relieved by convection to become stable will depend on the way in which the instability develops and on the character of the atmosphere above the cloud-soot layer. Under the assumptions we have been making the temperature in layer 1 is nearly constant so that layer is quite stable.

If the cloud-soot layer mixes with the air above it the value of α would remain unchanged but the individual opacities, ε_{s_2} and ε_{I_2} would

be reduced; that would lead to a smaller gradient in the temperature and a more stable profile as can be seen by examination of Equation (3-12). If the convection is confined to occur entirely within the cloud-soot layer the values of α and the opacities will be unchanged. Since our goal here is to estimate the potential effects of the convection on the temperature profile, and the assumption that the convection takes place entirely within the layer will provide the maximum effect on that profile, we shall assume that the convection takes place within the layer.

We seek a solution of the form shown in Figure 3-4. At the top of the cloud-soot layer there is a convection zone in which the temperature gradient is 7K/Km. Below the convection region are stable layers of the type we have been studying. The solution to the problem will be determined such that the depth of the mixing layer is the smallest it can be and still allow us to satisfy the following requirements: the radiation transport equations are satisfied in all regions; energy conservation is produced by a physically realizable convective flux in the convection zone. This last requirement amounts to insisting that the convective flux necessary to conserve energy in the convection zone must vanish at the top and bottom of the zone.

In addition to the solutions already obtained we shall need the solution to Equations (3-2) except with the last of these replaced by the specification of the temperature gradient:

$$\frac{dS}{dz} = -\varepsilon_{S_2} S$$

$$\frac{dU}{dz} = \varepsilon_{I_2} U - \varepsilon_{I_2} \sigma T^4 \qquad (3\text{-}13)$$

$$\frac{dD}{dz} = -\varepsilon_{I2} D + \varepsilon_{I2} \sigma T^4$$

$$T = T_0 + \beta z$$

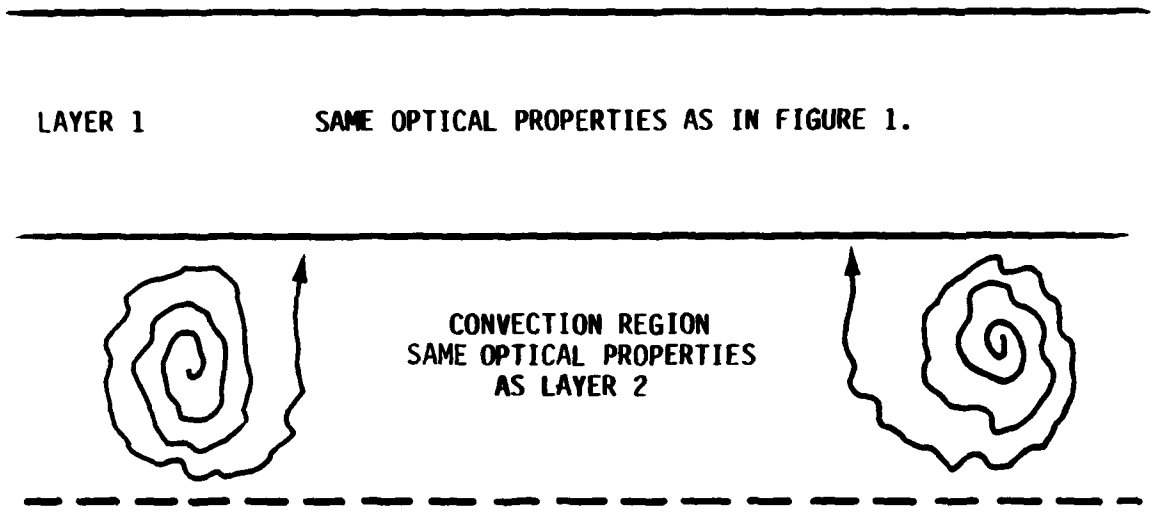

Figure 3-4. Schematic of the model nuclear winter with a convection region at the top of the cloud-soot layer.

where T_0 is the temperature at z=0 (the top of the cloud-soot layer) and we shall take β to be 7K/Km. We define a new independent variable to be

$$y = T_0 + \beta z \tag{3-14}$$

which is just the temperature. The equations become

$$\begin{aligned}
\frac{dS}{dy} &= -\frac{\varepsilon_{S_2}}{\beta} S \\
\frac{dU}{dy} &= \frac{\varepsilon_{I_2}}{\beta} U - \frac{\varepsilon_{I_2}}{\beta} \sigma y^4 \\
\frac{dD}{dy} &= -\frac{\varepsilon_{I_2}}{\beta} D + \frac{\varepsilon_{I_2}}{\beta} y^4
\end{aligned} \tag{3-15}$$

The general solution to these equations is

$$S = (1-A_1)(1-A_2)\,\Sigma\, e^{\frac{\varepsilon_{S_2} T_0}{\beta}} e^{-\frac{\varepsilon_{S_2}}{\beta} y} = (1-A_1)(1-A_2)\Sigma\, e^{-\varepsilon_{S_2} z}$$

$$\begin{aligned}
U &= \sigma \left[y^4 + 4\frac{\beta}{\varepsilon_{I_2}} y^3 + 12\left(\frac{\beta}{\varepsilon_{I_2}}\right)^2 y^2 + 24\left(\frac{\beta}{\varepsilon_{I_2}}\right)^3 y + 24\left(\frac{\beta}{\varepsilon_{I_2}}\right)^4 \right] + C_1\, e^{\varepsilon_{I_2} z} \\
D &= \sigma \left[y^4 - 4\frac{\beta}{\varepsilon_{I_2}} y^3 + 12\left(\frac{\beta}{\varepsilon_{I_2}}\right)^2 y^2 - 24\left(\frac{\beta}{\varepsilon_{I_2}}\right)^3 y + 24\left(\frac{\beta}{\varepsilon_{I_2}}\right)^4 \right] + C_2\, e^{-\varepsilon_{I_2} z}
\end{aligned} \tag{3-16}$$

Let F be the flux of convective energy in the convection zone. F must be zero at the top of the cloud-soot layer and at the bottom of the convection zone. The conservation of energy requires

$$\varepsilon_{S_2} S + \varepsilon_{I_2} (U+D) = 2\varepsilon_{I_2} \tau + \frac{dF}{dz} \tag{3-17}$$

F is negative throughout the convection zone and is approaching zero at the bottom of it. Therefore $\frac{dF}{dz}$ must be positive or zero at the bottom of the zone. The radiative fluxes are continuous at the bottom of the zone so if $\frac{dF}{dz}$ is not zero τ must be discontinuous there and must be colder at the bottom of the convection zone than at the top of the convection-free region beneath it; a situation which is unstable. To achieve a stable atmosphere we must therefore have $\frac{dF}{dz}$ equal to zero at the bottom of the convection zone which is equivalent to having the temperature be continuous there. We now have five conditions which must be satisfied in the convection zone: the continuity of the fluxes U and D at the top of the zone; the vanishing of F at the top and bottom of the zone; and the vanishing of $\frac{dF}{dz}$ at the bottom of the zone. The unknown parameters associated with the zone are the temperature at the top of the zone, T_0, the constants C_1 and C_2 in Equation (3-16), the constant of integration which appears when we integrate Equation (3-17) to solve for F, and the depth of the layer. The solution is therefore determined; we do not have the freedom to impose stability criteria on the layer under the convection zone and we must concern ourselves with whether or not our solution will have a stable temperature gradient in that region. We have shown above that the largest temperature gradient in the convection-free region will occur at the interface with the convection zone. Differentiating Equation (3-17) with respect to z we find:

$$\varepsilon_{S_2} \frac{dS}{dz} + \varepsilon_{I_2} \left(\frac{dU}{dz} + \frac{dD}{dz}\right) = 2\varepsilon_{I_2} \frac{d\tau}{dz} + \frac{d^2F}{dz^2} \qquad (3\text{-}18)$$

which we can use Equation (3-13) to rewrite (3-18) as:

$$\varepsilon^2_{S_2} S + \varepsilon^2_{I_2} (U - D) = 2\varepsilon_{I_2} \frac{d\tau}{dz} + \frac{d^2F}{dz^2} \qquad (3\text{-}19)$$

The left hand side of this equation is continuous across the interface. F is negative throughout the convection zone and both it and its first derivative vanish at the bottom of the convection zone; therefore the second derivative is either negative or zero at the interface. We thus conclude that the gradient of the temperature at the top of the convection-free region is less than or equal to that in the convection zone which is stable by construction so the entire cloud-soot layer is stable.

The radiative fluxes in the convection zone are given by Equation (3-16). We can use Equation (3-13) to rewrite Equation (3-17) as

$$\frac{dF}{dz} = \frac{d}{dz}\,(-S + U - D) \tag{3-20}$$

which gives

$$F = -S + U - D + C_3 \tag{3-21}$$

where C_3 is an integration constant. To simplify the notation we shall assume that ε_{I_1} is zero and shall include the albedo of layer 1 into that of layer 2 by defining $A = (1-A_1)(1-A_2)$. The boundary conditions at the top of the cloud-soot layer are then:

$$\sigma\left[T_0^4 + 4\frac{\beta}{\varepsilon_{I_2}}T_0^3 + 12\left(\frac{\beta}{\varepsilon_{I_2}}\right)^2 T_0^2 + 24\left(\frac{\beta}{\varepsilon_{I_2}}\right)^3 T_0 + 24\left(\frac{\beta}{\varepsilon_{I_2}}\right)^4\right] + C_1 = A\Sigma$$

$$\sigma\left[T_0^4 - 4\frac{\beta}{\varepsilon_{I_2}}T_0^3 + 12\left(\frac{\beta}{\varepsilon_{I_2}}\right)^2 T_0^2 - 24\left(\frac{\beta}{\varepsilon_{I_2}}\right)^3 T_0 + 24\left(\frac{\beta}{\varepsilon_{I_2}}\right)^4\right] + C_2 = 0 \tag{3-22}$$

$$-A\Sigma + 8\sigma\left[\frac{\beta}{\varepsilon_{I_2}}T_0^3 + 6\left(\frac{\beta}{\varepsilon_{I_2}}\right)^3 T_0\right] + C_1 - C_2 + C_3 = 0$$

These equations determine that $C_3 = 0$. The boundary conditions at the lower boundary are:

$$-A\Sigma e^{-\varepsilon_{S_2} d} + \sigma \left[8 \frac{\beta}{\varepsilon_{I_2}} (T_0 + \beta d)^3 + 24 \left(\frac{\beta}{\varepsilon_{I_2}}\right)^3 (T_0 + \beta d)\right]$$

$$+ C_1 e^{\varepsilon_{I_2} d} - C_2 e^{-\varepsilon_{I_2} d} = 0 \qquad (3\text{-}23)$$

$$\varepsilon_{S_2} A\Sigma e^{-\varepsilon_{S_2} d} + \varepsilon_{I_2} \sigma \left[24 \frac{\beta^2}{\varepsilon_{I_2}} (T_0 + \beta d)^2 + 48 \left(\frac{\beta}{\varepsilon_{I_2}}\right)^4\right]$$

$$+ \varepsilon_{I_2} + C_1 e^{\varepsilon_{I_2} d} + + \varepsilon_{I_2} C_2 e^{-\varepsilon_{I_2} d} = 0$$

In these equations d is the depth of the convection zone. By observing that T_0 will be large compared with $\frac{\beta}{\varepsilon_{I_2}}$ one can derive the following approximate solutions to these equations:

$$T_0 \approx T_B - \frac{\beta}{\varepsilon_{I_2}}$$

$$d \approx -\frac{1}{\varepsilon_{S_2}} \ln \frac{8\beta}{T_B(\varepsilon_{I_2} + \varepsilon_{S_2})} \qquad (3\text{-}24)$$

where we have defined

$$T_B = \left[\frac{A}{\sigma} \Sigma\right]^{1/4}$$

We have solved the transcendental Equations (3-22) and (3-23) numerically and find that the approximate solution (3-24) is adequate for our needs, using Equations (3-24) Equations (3-22) provide the values of C_1 and C_2.

The solution in the convective zone provides the boundary conditions which determine the solution in the layers below it; the full

solution is given in Appendix D. Here we shall focus our attention on the temperature at three points: the top of cloud-soot layer as given by Equation (3-24); the temperature at the bottom of the cloud-soot layer, which we call T_L and which is given by

$$\tau_L = \frac{1}{2}\left[2\sigma(T_0 + \beta d)^4 + A\Sigma\left(\frac{\varepsilon_{I_2}}{\varepsilon_{S_2}} - \frac{\varepsilon_{S_2}}{\varepsilon_{I_2}}\right)\left(e^{-\varepsilon_{S_2} d} - e^{\mu_{S_2}}\right)\right] \quad ; \tag{3-25}$$

and the temperature of the earth, T_E, given by

$$\tau_E = \frac{1}{2}\left[2\sigma(T_0 + \beta d)^4 + A\Sigma\left\{\left(\frac{\varepsilon_{I_2}}{\varepsilon_{S_2}} - \frac{\varepsilon_{S_2}}{\varepsilon_{I_2}}\right) e^{-\varepsilon_{S_2} d} + e^{-\mu_{S_2}}\left(1 + \mu_{I_3} - \frac{\varepsilon_{I_2}}{\varepsilon_{S_2}}\right)\right\}\right] \tag{3-26}$$

These three temperatures are shown as functions of α in Figure 3-5 with the assumption that the cloud-soot layer is distributed over 8 Km of altitude.

Comparing the results shown in Figures 3-3 and 3-5 we see that the effect of the convection has been to raise the temperature T_s and lower the temperature T_E. The reason we do not show results for values of α greater than about 5 is that for higher values the depth of the convection zone, d, becomes larger than the 8 Km we have assumed for the total depth of the cloud-soot layer. Calculations for these cases would require an extension of our methodology. The temperature profile from the top of the cloud-soot layer to the earth's surface is a stable one. The interface between the top of the cloud-soot layer and the air above it is probably unstable. The temperatures at the layer top are around 250K; the temperature just above it is probably somewhat less since the top of the layer is at an altitude of ≈9Km. If this instability is present it will cause the top of the layer to rise which in turn will cause the top of the layer to become colder and will increase the surface temperatures. Thus a

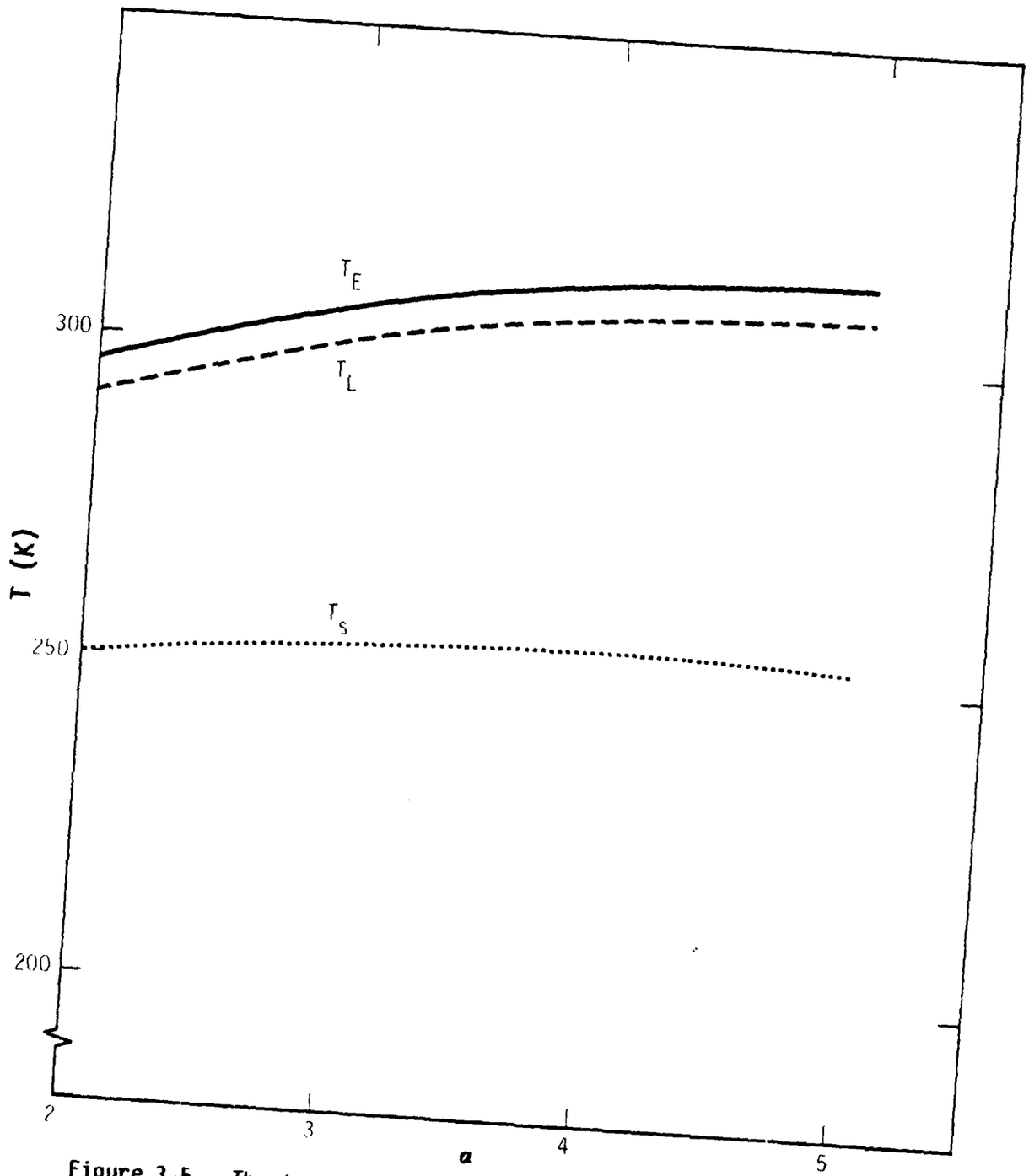

Figure 3-5. The temperature at the earth's surface, T_E, at the top of the cloud-soot layer, T_S, and at the bottom of the cloud-soot layer, T_L, plotted vs. α assuming convection within the cloud stabilizes the temperature profile.

temperature profile between that predicted by ignoring convective instabilities and that we have calculated by allowing convection only within the cloud-soot layer may be expected.

Another somewhat unrealistic feature of the present calculations is seen in the results for T_L, the temperature at the bottom of the cloud-soot layer. This quantity is seen, in Figure 3-5, to range from 290K to 310K; it is unlikely that there will be sufficient water to maintain a condensation cloud to such high temperatures and we should assume that the cloud disappears at some temperature which depends on the amount of water present. When the cloud disappears the value of α will change dramatically, probably falling below 1. Our present methodology can allow for such an effect but we shall postpone such calculations until a more realistic treatment of the interface at the top of cloud-soot layer has been developed.

We should perhaps remark on the comparison between the effects of the cloud-soot layers we have been studying and those of naturally occurring clouds. It may seem strange that either a soot cloud or a water cloud would cool the surface while a mixture of the two would warm the surface. The source of the effect is the difference in the albedos of water clouds and cloud-soot mixtures. Water clouds as heavy as those we have been studying would have albedos in the solar of .8 or more; the presence of the soot lowers this to about .2. Thus while the presence of naturally occurring water clouds leads to an increased IR opacity for the atmosphere, which tends to raise surface temperatures, the high albedo of the clouds tends to lower temperatures throughout the profile; the net effect is slightly lower surface temperatures. The presence of the soot mixed with the cloud allows for the presence of high IR opacity without a high solar albedo.

NUCLEAR WINTER OVER SNOWPACK

The nuclear winter phenomenon is always warming for the surface if it occurs over snowpack. By this we mean that the snow will ultimately absorb more of the solar energy directed at it if there exists a soot layer, with or without an accompanying water cloud, than it would under clear sky conditions. The reason for this is as follows: the absorption of solar energy by the soot ultimately results in a downwardly propagating IR flux. The magnitude of the IR flux at the surface depends on the opacity structure of the atmosphere but, as we shall see below, it is at least one half the value of the absorbed solar flux. The albedo of the snow in the visible is .8 or more while the snow is very nearly black in the IR. Thus more of the solar energy will be absorbed by the snow if it is first absorbed by the soot than if it propagates unimpeded to the surface.

To study the effect over snowpack we must allow for an upward as well as a downward solar flux. We call these respectively S_U and S_D. They satisfy the equations

$$\frac{dS_D}{dz} = -\varepsilon_s S_D$$

$$\frac{dS_U}{dz} = \varepsilon_s S_U \qquad (3\text{-}27)$$

All of Equations (3-2) remain valid except the last which becomes:

$$\varepsilon_s (S_U + S_D) + \varepsilon_I (U+D) - 2\varepsilon_I \tau = 0 \qquad (3\text{-}28)$$

the general solution to the system is

$$S_D = A\, e^{-\varepsilon_s z}$$

$$S_U = B\, e^{\varepsilon_s z} \qquad (3\text{-}29)$$

$$U = \frac{1}{2}(1-\alpha)A\, e^{-\varepsilon s^z} - \frac{1}{2}(1+\alpha)B\, e^{\varepsilon s^z} + C(z+1) + E$$

$$D = -\frac{1}{2}(1+\alpha)A\, e^{-\varepsilon s^z} + \frac{1}{2}(1-\alpha)B\, e^{\varepsilon s^z} + C(z-1) + E$$

$$\tau = \frac{1}{2}\left(\frac{1}{\alpha} - \alpha\right)\left(A\, e^{-\varepsilon s^z} + B\, e^{\varepsilon s^z}\right) + Cz + E$$

where A, B, C and E are constants. We shall consider the same model shown in Figure 1, with the same values for the parameters we used earlier, except that we shall assume that the earth has an albedo to solar radiation of .8. The solar fluxes can be solved for independently of the IR fluxes; the solution is given in Appendix D. Here we shall concentrate on the temperature at the surface. The temperature with all the layers present is given by:

$$\tau_E = \frac{1}{2}\left\{(1+\mu_{I_3})\left(S_{D_3}\, e^{-\mu s_2} - S_{U_3}\, e^{\mu s_2}\right) + \alpha\left[(1-e^{-\mu s_2})S_{D_3} + (1-e^{\mu s_2})S_{U_3}\right]\right.$$

$$\left. + S_N(1+\mu_{I_1})\right\} \qquad (3\text{-}30)$$

where
$$S_{D_3} = \Sigma\left\{(1-A_1)(1-A_2) + \frac{(1-A_1)(1-A_2)^2 A_1 A_e\, e^{-2\mu s_2}}{1 - A_2 A_e - A_1 A_e(1-A_2)\, e^{-2\mu s_2}}\right\}$$

$$S_{U_3} = \Sigma\left\{A_1 + A_2 - A_1A_2 + \frac{(1-A_1)(1-A_2)^2 A_e\, e^{-2\mu s_2}}{1 - A_2 A_e - A_1 A_e(1-A_2)\, e^{-2\mu s_2}}\right\} \qquad (3\text{-}31)$$

$$S_N = \Sigma\left\{1 - A_1 - A_2 + A_1A_2 - \frac{(1-A_1)^2(1-A_2)^2 A_e\, e^{-2\mu s_2}}{1 - A_2 A_e - A_1 A_e(1-A_2)\, e^{-2\mu s_2}}\right\}$$

where A_e is the albedo of the earth.

To render these expressions somewhat more transparent we shall assume that layer 1 is missing (it does little anyway) and that A_2 is zero (it is always small and is very small for a soot layer with no water cloud). We get

$$\tau_E = \frac{1}{2} \Sigma \left[1-A_e e^{-2\mu_{s_2}} + (1-A_e)(1+\mu_{I_3})e^{-\mu_{s_2}} + \alpha\,(1-e^{-\mu_{s_2}})(1+A_e e^{-\mu_{s_2}})\right] \quad (3\text{-}32)$$

For clear sky condition we get

$$\tau_{EC} = (1-A_e)\Sigma \quad (3\text{-}33)$$

The change is thus

$$\Delta\tau_E = \frac{1}{2} \Sigma \left[(1-e^{-2\mu_{s_2}}) \{(2A_e-1) + \alpha(1+A_e e^{-\mu_{s_2}})\} + \mu_{I_3}(1-A_e)e^{-2\mu_{s_2}}\right] \quad (3\text{-}34)$$

As long as $A_e > .5$ $\Delta\tau_E$ is always positive, even if α and μ_{I_3} are zero. Perhaps a better comparison is between the conditions with layers 2 and 3 present (the nuclear winter condition) with those for layer 3 alone (the normal troposphere). For that case it is not quite guaranteed that the soot cloud will lead to warming although it will be for most conditions expected to be encountered. If only layer 3 is present we get

$$\tau_{E_a} = \frac{1}{2} \Sigma\,(1-A_e)\left[2 + \mu_{I_3}\right] \quad (3\text{-}35)$$

Comparing this formula with Equation (3-32) we see that

$$\Delta\tau = \frac{1}{2} \Sigma \left[(1-e^{-2\mu_{s2}})\,(2A_e - 1 - \mu_{I3}(1-A_e) + \alpha(1 + A_e\, e^{-2\mu_{s2}}))\right] \quad (3\text{-}36)$$

This quantity is positive unless α is very small and μ_{I_3} is very large. The reason that $\Delta\tau$ can be negative is that the soot layer reduces the effectiveness of the tropospheric layer. In spite of this $\Delta\tau$ will be positive unless μ_{I_3} is very large (greater than 3) and α is near zero. If a water cloud is present along with the soot it will probably melt the snow; if we assume that the optical depth in the solar is 2, Equation (3-32) predicts melting of the snow if α is greater than .77. Thus even if the effective solar flux is considerably below our assumed value, which will probably be the case since we are presumably dealing with winter conditions or quite high latitudes, the values of α associated with soot-water cloud mixtures would in most cases be high enough to melt the snow.

The importance of the fact that the nuclear winter phenomenon is warming over snow pack is difficult to access. The fact that the regions of snowpack will be warmer than normal might alter normal circulation patterns. Whether that would occur and, if it did, what the consequences would be are questions beyond the scope of the present study.

SECTION 4
CONCLUSIONS

The principal conclusions of the present study pertain to the possible importance of various IR radiators on the nuclear winter phenomenon. We find that hydrocarbons, CO_2 and NO_2 will not have a major impact on the phenomenon. Water vapor will have at most a marginal effect on the temperature profile if convective instabilities are ignored; water vapor may be important to the development of the instability which will exist at the top of the soot layer if no condensation cloud is present. Condensed water has the potential to play a major, perhaps dominant role in the nuclear winter phenomenon.

If water clouds are present at late times they will probably alter the entire character of the temperature profile, changing it from one which is hot at the cloud top and cold at the earth's surface to one which is cold at the top and hot at the earth's surface. The amount of water needed to produce such clouds is well within the bounds of what might reasonably be expected to be entrained into the fire plumes. If a cloud exists at the top of the soot layer the temperature is cold there and the cloud tends to persist. If the top of the soot layer is cloud-free the temperature is hot there and clouds will form, if at all, only at lower altitudes where they have a much smaller effect on the temperature profile. This hysteresis effect greatly complicates the analysis as to whether or not a condensation cloud will be present. To analyze the problem one must calculate the development of the plumes, many of which will be cloud topped, some of which may not be, as they spread and merge to form the hemisphere-wide layer. The condensation clouds will probably

affect this merging process. If they survive to later times they may have a profound effect on the phenomenon. The models we have described in this report form a framework in which one may think about the problem and they provide a starting point from which to develop the much more detailed calculations which will be necessary. Performing sufficiently complete calculations in the necessary detail presents a challenge.

SECTION 5
LIST OF REFERENCES

1-1. The most complete study of which we are aware is: The Effects on the Atmosphere of a Nuclear Exchange, Committee on the Atmospheric Effects of Nuclear Explosions,National Research Council, National Academy Press, 1985; see also: Turco, R. P., O. B. Toon, T. P. Ackerman, J. B. Pollack and C. Sagan, Nuclear Winter: Global Consequences of Multiple Nuclear Explosions. Science 222:1283-1292.

1-2. Radke, L., private communication.

2-1. The Effects on the Atmosphere of a Nuclear Exchange, Draft Report, Committee on the Atmospheric Effects of Nuclear Explosions, National Research Council, December 1983.

2-2. Southern Forestry Smoke Management Guidebook, USDA Forest Service General Technical Report SE-10, December 1976.

2-3. Clements, H. B., and C. K. McMahon "Nitrogen Oxides from Burning Forest Fuels Examined by Thermogravimetry and Evolved Gas Analysis," Thermochimica Acta 35, 133, 1980.

2-4. Sandberg, D. V., et al., "Emission from Slash Burning and the Influence of Flame Retardant Chemicals," J. of the Air Pollution Control Association 25, 278, 1975.

2-5. Crutzen, P. J., and J. W. Birks, "The Atmosphere after a Nuclear War: Twilight at Noon," Ambio 11, 114, 1982.

2-6. U. S. Standard Atmosphere, 1976.

2-7. Oliver, R. C., et al., Aircraft Emissions: Potential Effects on Ozone and Climate, FAA-EQ-77-3, U.S. Dept. of Transportation, March 1977.

2-8. Broderick, A. J., and T. M. Hard (eds.), Proceedings of the Third Conference on the Climatic Impact Assessment Program, Department of Transport, DOT-TSC-OST-74-15, February 26 - March 1, 1974.

2-9. Pierluissi, J. H., and K. Tomiyama, "Validated Band Model for NO_2 Molecular Transmittance in the Infrared," Appl. Opt. 22, 1628, 1983.

2-10. Staley, D. O., and G. M. Jurica, "Flux Emissivity Tables for Water Vapor, Carbon Dioxide, and Ozone," J. Appl. Meterol. 9, 365, 1970.

2-11. Jarem, J. M., J. H. Pierluissi, and Wai-Lam Ng, "Validated Infrared Transmittance Band Model for Methane In the Atmosphere," Appl. Opt. 23, 3331, 1984.

2-12. Varanasi, P., et al., "The ν_9 Fundamental of Ethane: Integrated Intensity and Band Absorption Measurements with Application to the Atmospheres of the Major Planets," J. Quant. Spectr. Rad. Trans. 14, 1107, 1974.

2-13. Ludwig, C. B., et al., Handbook of Infrared Radiation from Combustion Gases, NASA, SP-3080, 1973.

2-14. Giver, L. P., et al., "Propane Absorption Band Intensities and Band Model Parameters from 680 to 1550 cm^{-1} at 296 and 200°K," J. Quant. Spectr. Rad. Trans. 31, 203, 1984.

2-15. Varanasi, P., and B. R. P. Bangaru, "Measurement of Integrated Intensities of Acetylene Bands at 3.04, 7.53 and 13.7 μm," J. Quant. Spectr. Rad. Trans. 14, 839, 1974.

2-16. Nakanaga, T., et al., "Infrared Intensities and Coriolis Interactions in Ethylene," J. Chem. Phys. 70, 2471, 1979.

2-17. Bartky, C. D., and E. Bauer, "Predicting the Emittance of a Homogeneous Plume Containing Alumina Particles," J. Spacecraft 3, 1523, 1966.

2-18. Thompson, J. H., Particulate Multiple Scattering Model, Appendix A, The ROSCOE Manuel (U), V. 31 - Sight Path Integration (U), DNA 3964F-31, General Electric Company - TEMPO, 15 June 1978 (C).

2-19. Dowling, J. M., and C. M. Randall, Infrared Emissivities of Micron-Sized Particles of C, MgO, Al_2O_3, and ZrO_2 at Elevated Temperatures, AFRPL-TR-77-14, Aerospace, 30 April 1977.

2-20. Hale, G. M., and M. R. Querry, "Optical Constants of Water in the 200-nm to 200-μm Wavelength Region," Appl. Optics, 12, 555, 1973.

2-21. Pollock, J. B., et al., "Optical Properties of Some Terrestrial Rocks and Glasses," Icarus 19, 372, 1973.

2-22. McCartney, E. J., Optics of the Atmosphere, p. 171, Wiley and Sons, 1976.

3-1. The Effects on the Atmosphere of a Nuclear Exchange, Committee on the Atmospheric Effects of Nuclear Explosions,National Research Council, National Academy Press, 1985.

3-2. The wording in the NRC document makes it appear that the value of α for pure soot could be as large as 5. Rich Turco, in private conversation, has explained to us that the wording is misleading and that α for pure soot can be assumed to be less than 1.

E-1. The Effects on the Atmosphere of a Nuclear Exchange, Draft Report, Committee on the Atmospheric Effects of Nuclear Explosions, National Research Council, December 1983.

E-2. Mihalas, D., Stellar Atmospheres, Second Edition, W. H. Freeman and Company, San Francisco, 1978.

APPENDIX A
BROAD-BAND EMISSIVITY FOR OPTICALLY-THIN BANDS

If a band model, or the spectral absorption coefficient for an infrared molecular band, ν_i, is unavailable, but the integrated band intensity, S_i, is known, then one can still obtain the broad-band infrared emissivity for the band in the optically-thin case. This is easily demonstrated as follows.

If $\varepsilon_i(\tilde{\nu})$ is the spectral emissivity of a layer at wavenumber $\tilde{\nu}$ within band ν_i, and $B(\tilde{\nu})$ is the Planck function, then the broad-band emissivity for the band is defined as

$$\bar{\varepsilon}_i = \frac{\int_{\text{band}} \varepsilon_i(\tilde{\nu})B(\tilde{\nu})d\tilde{\nu}}{\int_0^\infty B(\tilde{\nu})d\tilde{\nu}} \quad . \tag{A-1}$$

But $\varepsilon_i(\tilde{\nu})$ is related to the spectral transmissity, $T_i(\tilde{\nu})$, by the relation

$$\varepsilon_i(\tilde{\nu}) = 1 - T_i(\tilde{\nu}) \quad . \tag{A-2}$$

However, in the optically-thin case,

$$T_i(\tilde{\nu}) \approx e^{-k\tilde{\nu}U} \approx 1 - k_{\tilde{\nu}}U \tag{A-3}$$

where $k_{\tilde{\nu}}$ is the linear absorption coefficient (atm^{-1} cm^{-1}) for band ν_i and U is the path length (atm cm) through the absorber. Thus, in this case,

$$\varepsilon_i(\tilde{\nu}) \approx k_{\tilde{\nu}} U \quad . \tag{A-4}$$

Consequently, because the Planck function generally varies slowly over a molecular band, we can write

$$\int_{\text{band}} \varepsilon_i(\tilde{\nu}) B(\tilde{\nu}) d\tilde{\nu} \approx B(\tilde{\nu}_i) U \int_{\text{band}} k_{\tilde{\nu}} d\tilde{\nu} \tag{A-5}$$

where $\tilde{\nu}_i$ is the band-center wavenumber. Furthermore, by definition of the integrated band intensity,

$$S_i \equiv \int_{\text{band}} k_{\tilde{\nu}} d\tilde{\nu} \quad , \tag{A-6}$$

and we thus obtain, from Equations A-1, A-5, and A-6,

$$\bar{\varepsilon}_i \approx \frac{B'(\nu_i) S_i U}{\int_0^\infty B'(\tilde{\nu}) d\tilde{\nu}} \tag{A-7}$$

where

$$B'(\tilde{\nu}) = \frac{\tilde{\nu}^3}{e^{1.435\tilde{\nu}/T} - 1} \quad . \tag{A-8}$$

But, integration of A-8 yields

$$\int_0^\infty B'(\tilde{\nu}) d\tilde{\nu} = 1.53\ T^4 \quad , \tag{A-9}$$

and so

$$\bar{\varepsilon}_i \approx 1.53\ B'(\tilde{\nu}_i) S_i U / T^4 \quad . \tag{A-10}$$

APPENDIX B
BROAD-BAND EMISSIVITY FOR TWO SPECIES WITH OVERLAPPING BANDS

If we have a layer composed of two different species whose absorption bands partially overlap, then the broad-band emissivity of the layer is less than the sum of the broad-band emissivities for the individual species. This result is proved as follows.

Let $T_1(\tilde{\nu})$ and $T_2(\tilde{\nu})$ be the spectral transmissivities for species 1 and 2, respectively. Suppose that an absorption band for species 1 lies between wavenumbers 0 and $\tilde{\nu}_2$ and, for species 2, an absorption band lies beyond wavenumber $\tilde{\nu}_1$, where $\tilde{\nu}_1 < \tilde{\nu}_2$. Then, for $0 \leq \tilde{\nu} \leq \tilde{\nu}_1$, only species 1 absorbs; for $\tilde{\nu}_1 \leq \tilde{\nu} \leq \tilde{\nu}_2$, both species absorb; for $\tilde{\nu} \geq \tilde{\nu}_2$, only species 2 absorbs.

For simplicity, define a normalized Planck function, $B(\tilde{\nu})$, such that

$$\int_0^\infty B(\tilde{\nu})d\tilde{\nu} = 1 \quad . \tag{B-1}$$

Then the broad-band transmissivity of the layer, composed of the two species, is defined as

$$\overline{T} = \int_0^\infty T_1(\tilde{\nu})T_2(\tilde{\nu})B(\tilde{\nu})d\tilde{\nu} \quad . \tag{B-2}$$

But, considering the absorption regions described above, Equation B-2 can be written as

$$\overline{T} = \int_0^{\tilde{\nu}_1} T_1(\tilde{\nu})B(\tilde{\nu})d\tilde{\nu} + \int_{\tilde{\nu}_1}^{\tilde{\nu}_2} T_1(\tilde{\nu})T_2(\tilde{\nu})B(\tilde{\nu})d\tilde{\nu} + \int_{\tilde{\nu}_2}^{\infty} T_2(\tilde{\nu})B(\tilde{\nu})d\tilde{\nu} \quad . \qquad \text{(B-3)}$$

If $\overline{T}_1$ is the broad-band transmissivity of the layer if only species 1 were present, and $\overline{T}_2$ is the transmissivity if only species 2 were present, then

$$\overline{T}_1 = \int_0^{\infty} T_1(\tilde{\nu})B(\tilde{\nu})d\tilde{\nu}$$

$$= \int_0^{\tilde{\nu}_1} T_1(\tilde{\nu})B(\tilde{\nu})d\tilde{\nu} + \int_{\tilde{\nu}_1}^{\tilde{\nu}_2} T_1(\tilde{\nu})B(\tilde{\nu})d\tilde{\nu} + \int_{\tilde{\nu}_2}^{\infty} B(\tilde{\nu})d\tilde{\nu} \qquad \text{(B-4)}$$

and

$$\overline{T}_2 = \int_0^{\infty} T_2(\tilde{\nu})B(\tilde{\nu})d\tilde{\nu}$$

$$= \int_{\tilde{\nu}_1}^{\tilde{\nu}_2} T_2(\tilde{\nu})B(\tilde{\nu})d\tilde{\nu} + \int_{\tilde{\nu}_2}^{\infty} T_2(\tilde{\nu})B(\tilde{\nu})d\tilde{\nu} + \int_0^{\tilde{\nu}_1} B(\tilde{\nu})d\tilde{\nu} \qquad \text{(B-5)}$$

Equations B-3 to B-5 can now be combined to yield

$$\overline{T} = \overline{T}_1 + \overline{T}_2 + \int_{\tilde{\nu}_1}^{\tilde{\nu}_2} \{T_1(\tilde{\nu})T_2(\tilde{\nu}) - T_1(\tilde{\nu}) - T_2(\tilde{\nu})\} B(\tilde{\nu})d\tilde{\nu} - \int_0^{\tilde{\nu}_1} B(\tilde{\nu})d\tilde{\nu} - \int_{\tilde{\nu}_2}^{\infty} B(\tilde{\nu})d\tilde{\nu} \quad . \qquad \text{(B-6)}$$

But, since

$$T_1T_2 - T_1 - T_2 = (1-T_1)(1-T_2) - 1 \quad , \tag{B-7}$$

and, in view of the normalization B-1, Equation B-6 can be written as

$$\overline{T} = \overline{T1} + \overline{T2} - 1 + \int_{\tilde{\nu}}^{\tilde{\nu}_2} [1-T_1(\tilde{\nu})][1-T_2(\tilde{\nu})]B(\tilde{\nu})d\tilde{\nu} \quad . \tag{B-8}$$

Equation B-8 can be expressed, alternatively, in terms of the broad-band emissivities, by noting that both the spectral and broad-band emissivities, ε, are related to the spectral and broad-band transmissivities, T, through the relation

$$\varepsilon = 1 - T \quad . \tag{B-9}$$

We thus obtain the result

$$\overline{\varepsilon} = \overline{\varepsilon}_1 + \overline{\varepsilon}_2 - \int_{\tilde{\nu}_1}^{\tilde{\nu}_2} \varepsilon_1(\tilde{\nu})\varepsilon_2(\tilde{\nu})B(\tilde{\nu})d\tilde{\nu} \tag{B-10}$$

where $\overline{\varepsilon}_1$ and $\overline{\varepsilon}_2$ are the broad-band emissivities of the layer with only species 1 and 2, respectively, present.

This proves that the broad-band emissivity for the mixture is less than the sum of the individual emissivities by the average cross product of the two emissivities in the region of band overlap. Although we have made no attempt to prove that this result is valid for an arbitrary number of different species, we see no reason to doubt that when band overlap occurs, the broad-band emissivity is always less than the sum of the individual emissivities.

APPENDIX C
TABULATIONS OF OPTICAL PROPERTIES

Presented here are tabulations of the complex index of refraction, especially for the infrared (IR) region, used in the Mie-code calculations reported in Section 2. Detailed tabular results are also presented of the emissivity, transmissivity, and reflectivity of sooty water clouds, both for broad-band IR thermal radiation and for visible (λ = 0.55 μm) radiation.

Tables C-1 to C-3 give, respectively, the real and imaginary components of the complex index of refraction ($n = n_R - in_I$) for water, dust (basaltic glass), and soot (carbon). Table C-4 gives the broad-band IR properties of sooty water clouds for parametric values of the water-to-soot density ratio, ρ^W/ρ^S, and the cloud thickness U(gm cm^{-2}). Table C-5 gives corresponding results for radiation of wavelength 0.55 μm, and includes as well the optical depth, τ, of the cloud. The log-normal distribution parameters used for Tables C-4 and C-5 are those for water (1) and soot shown in Table 2-6 of Section 2. In all cases the temperature was taken to be 250 °K.

Table C-1. Complex index of refraction values for water (Reference 2-20).

λ (μm)	n_R	n_I	λ (μm)	n_R	n_I	λ (μm)	n_R	n_I
0.200	1.396	1.10^{-7}	2.85	1.149	0.185	6.6	1.334	3.56^{-2}
0.225	1.373	4.90^{-8}	2.90	1.201	0.268	7.0	1.317	3.20^{-2}
0.450	1.337	1.02^{-9}	2.95	1.292	0.298	9.0	1.262	3.99^{-2}
0.475	1.336	9.35^{-10}	3.00	1.371	0.272	10.0	1.218	5.08^{-2}
0.500	1.335	1.00^{-9}	3.10	1.467	0.192	11.5	1.126	0.142
0.725	1.330	9.15^{-8}	3.15	1.483	0.135	12.0	1.111	0.199
0.750	1.330	1.56^{-7}	3.2	1.478	9.24^{-2}	12.5	1.123	0.259
0.775	1.330	1.48^{-7}	3.7	1.374	3.60^{-3}	13.5	1.177	0.343
0.800	1.329	1.25^{-7}	3.8	1.364	3.40^{-3}	15.0	1.270	0.402
0.925	1.328	1.06^{-6}	3.9	1.357	3.80^{-3}	17.5	1.401	0.429
0.950	1.327	2.93^{-6}	4.6	1.330	1.47^{-2}	28	1.549	0.338
0.975	1.327	3.48^{-6}	4.7	1.330	1.57^{-2}	30	1.551	0.328
1.00	1.327	2.89^{-6}	4.8	1.330	1.50^{-2}	32	1.546	0.324
1.20	1.324	9.89^{-6}	5.2	1.317	1.01^{-2}	38	1.522	0.361
1.40	1.321	1.38^{-4}	5.3	1.312	9.80^{-3}	40	1.519	0.385
1.60	1.317	8.55^{-5}	5.4	1.305	1.03^{-2}	42	1.522	0.409
1.80	1.312	1.15^{-4}	5.8	1.262	3.30^{-2}	50	1.587	0.514
2.00	1.306	1.10^{-3}	5.9	1.248	6.22^{-2}	60	1.703	0.587
2.20	1.296	2.89^{-4}	6.0	1.265	0.107	100	1.957	0.532
2.40	1.279	9.56^{-4}	6.1	1.319	0.131	150	2.069	0.495
2.75	1.157	5.90^{-2}	6.2	1.363	8.80^{-2}	200	2.130	0.504
2.80	1.142	0.115	6.3	1.357	5.70^{-2}			

Table C-2. Complex index of refraction values for dust (basaltic glass) (Reference 2-21).

λ (μm)	n_R	$n_I \times 10^3$	λ (μm)	n_R	$n_I \times 10^3$	λ (μm)	n_R	$n_I \times 10^3$
3.0	1.52	0.47	11.0	2.2	570.	20.5	1.57	770.
3.1	1.52	0.44	11.5	2.11	340.	21.0	1.66	840.
3.15	1.52	0.42	12.0	2.01	230.	21.5	1.77	890.
3.2	1.52	0.41	12.5	1.93	180.	22.0	1.89	910.
3.3	1.52	0.35	13.0	1.87	160	22.5	2.00	890.
4.0	1.50	0.37	13.5	1.81	140.	23.0	2.10	850.
4.5	1.50	0.53	14.0	1.77	140.	23.5	2.18	790.
5.0	1.46	1.5	14.5	1.72	140.	24.0	2.24	730.
5.25	1.46	2.7	15.0	1.68	140.	25.0	2.31	590.
6.0	1.4	20.	15.5	1.65	160.	26.0	2.33	480.
6.5	1.36	32.	16.0	1.61	180.	27.0	2.32	390.
7.0	1.3	52.	16.5	1.57	210.	28.0	2.31	330.
7.5	1.21	89.	17.0	1.53	240.	29.0	2.29	280.
8.0	1.11	170.	17.5	1.50	290.	30.0	2.27	240.
8.5	0.98	340.	18.0	1.47	350.	35.0	2.20	140.
9.0	0.96	700.	18.5	1.45	420.	40.0	2.15	97.
9.5	1.26	1100.	19.0	1.45	500.	45.0	2.12	75.
10.0	1.69	1100.	19.5	1.46	590.	50.0	2.11	61.
10.5	2.04	940.	20.0	1.50	690.			

Table C-3. Complex index of refraction values for soot (carbon) (Reference 2-19).

λ (μm)	n_R	n_I	λ (μm)	n_R	n_I	λ (μm)	n_R	n_I
4.55	2.99	0.78	6.67	3.04	1.07	12.5	3.07	1.82
4.76	3.00	0.81	7.14	3.05	1.13	14.3	3.05	2.04
5.00	3.01	0.84	7.69	3.06	1.21	16.7	3.02	2.32
5.26	3.01	0.88	8.33	3.06	1.28	20.0	2.94	2.75
5.56	3.02	0.93	9.09	3.06	1.39	25.0	2.75	3.36
5.88	3.03	0.97	10.0	3.07	1.50	33.3	2.30	4.30
6.25	3.03	1.01	11.1	3.07	1.64	50.0	0.10	7.30

Table C-4. Broad-band IR properties of sooty water clouds.

ρ_{H_2O}/ρ_{soot}	U_{H_2O} (gm cm^{-2})	U_{soot_2} (gm cm^{-2})	Emissivity	Transmissivity	Reflectivity
1.000E-03	1.000E-06	1.000E-03	7.961E-01	1.791E-01	2.482E-02
1.000E-03	5.000E-06	5.000E-03	9.193E-01	5.416E-02	2.659E-02
1.000E-03	1.000E-05	1.000E-02	9.329E-01	3.967E-02	2.746E-02
1.000E-03	5.000E-05	5.000E-02	9.5[illegible]E-01	1.397E-02	2.940E-02
1.000E-03	1.000E-04	1.000E-01	9.636E-01	6.464E-03	2.[illegible]E-02
1.000E-03	5.000E-04	5.000E-01	9.698E-01	9.135E-05	3.011E-02
1.000E-03	1.000E-03	1.000E+00	9.699E-01	6.477E-07	3.011E-02
1.000E-03	2.000E-03	2.000E+00	9.699E-01	3.272E-11	3.011E-02
1.000E-03	4.000E-03	4.000E+00	9.699E-01	8.349E-20	3.011E-02
1.000E-03	6.000E-03	6.000E+00	9.699E-01	2.131E-28	3.011E-02
1.000E-03	1.000E-02	1.000E+01	9.699E-01	0.000E+00	3.011E-02
1.000E-03	5.000E-02	5.000E+01	9.699E-01	0.000E+00	3.011E-02
1.000E-03	1.000E-01	1.000E+02	9.699E-01	0.000E+00	3.011E-02
1.000E-03	5.000E-01	5.000E+02	9.699E-01	0.000E+00	3.011E-02
1.000E-03	1.000E+00	1.000E+03	9.699E-01	0.000E+00	3.011E-02
1.000E-02	1.000E-06	1.000E-04	2.261E-01	7.609E-01	1.303E-02
1.000E-02	5.000E-06	5.000E-04	6.416E-01	3.350E-01	2.337E-02
1.000E-02	1.000E-05	1.000E-03	7.976E-01	1.775E-01	2.486E-02
1.000E-02	5.000E-05	5.000E-03	9.214E-01	5.193E-02	2.668E-02
1.000E-02	1.000E-04	1.000E-02	9.360E-01	3.647E-02	2.755E-02
1.000E-02	5.000E-04	5.000E-02	9.618E-01	9.123E-03	2.909E-02
1.000E-02	1.000E-03	1.000E-01	9.680E-01	2.714E-03	2.928E-02
1.000E-02	2.000E-03	2.000E-01	9.703E-01	3.477E-04	2.930E-02
1.000E-02	4.000E-03	4.000E-01	9.707E-01	7.786E-06	2.930E-02
1.000E-02	6.000E-03	6.000E-01	9.707E-01	1.888E-07	2.930E-02
1.000E-02	1.000E-02	1.000E+00	9.707E-01	1.128E-10	2.930E-02
1.000E-02	5.000E-02	5.000E+00	9.707E-01	0.000E+00	2.930E-02
1.000E-02	1.000E-01	1.000E+01	9.707E-01	0.000E+00	2.930E-02
1.000E-02	5.000E-01	5.000E+01	9.707E-01	0.000E+00	2.930E-02
1.000E-02	1.000E+00	1.000E+02	9.707E-01	0.000E+00	2.930E-02
1.000E-01	1.000E-06	1.000E-05	2.735E-02	9.707E-01	1.964E-03
1.000E-01	5.000E-06	5.000E-05	1.270E-01	8.649E-01	9.131E-03
1.000E-01	1.000E-05	1.000E-04	2.323E-01	7.545E-01	1.321E-02
1.000E-01	5.000E-05	5.000E-04	6.569E-01	3.205E-01	2.369E-02
1.000E-01	1.000E-04	1.000E-03	8.123E-01	1.624E-01	2.530E-02
1.000E-01	5.000E-04	5.000E-03	9.386E-01	3.412E-02	2.729E-02
1.000E-01	1.000E-03	1.000E-02	9.565E-01	1.573E-02	2.782E-02
1.000E-01	2.000E-03	2.000E-02	9.677E-01	4.281E-03	2.800E-02
1.000E-01	4.000E-03	4.000E-02	9.716E-01	4.023E-04	2.802E-02
1.000E-01	6.000E-03	6.000E-02	9.719E-01	4.219E-05	2.802E-02
1.000E-01	1.000E-02	1.000E-01	9.720E-01	5.261E-07	2.802E-02
1.000E-01	5.000E-02	5.000E-01	9.720E-01	2.396E-25	2.802E-02
1.000E-01	1.000E-01	1.000E+00	9.720E-01	0.000E+00	2.802E-02
1.000E-01	5.000E-01	5.000E+00	9.720E-01	0.000E+00	2.802E-02
1.000E-01	1.000E+00	1.000E+01	9.720E-01	0.000E+00	2.802E-02

Table C-4. Broad-band IR properties of sooty water clouds (continued).

ρ_{H_2O}/ρ_{soot}	U_{H_2O} (gm cm^{-2})	U_{soot} (gm cm^{-2})	Emissivity	Transmissivity	Reflectivity
5.000E-01	1.000E-06	2.000E-06	6.254E-03	9.933E-01	4.361E-04
5.000E-01	5.000E-06	1.000E-05	3.078E-02	9.671E-01	2.092E-03
5.000E-01	1.000E-05	2.000E-05	6.035E-02	9.357E-01	3.977E-03
5.000E-01	5.000E-05	1.000E-04	2.594E-01	7.267E-01	1.394E-02
5.000E-01	1.000E-04	2.000E-04	4.363E-01	5.441E-01	1.966E-02
5.000E-01	5.000E-04	1.000E-03	8.641E-01	1.095E-01	2.640E-02
5.000E-01	1.000E-03	2.000E-03	9.362E-01	3.661E-02	2.721E-02
5.000E-01	2.000E-03	4.000E-03	9.631E-01	9.350E-03	2.751E-02
5.000E-01	4.000E-03	8.000E-03	9.714E-01	1.060E-03	2.755E-02
5.000E-01	6.000E-03	1.200E-02	9.723E-01	1.345E-04	2.755E-02
5.000E-01	1.000E-02	2.000E-02	9.724E-01	2.361E-06	2.755E-02
5.000E-01	5.000E-02	1.000E-01	9.724E-01	1.773E-23	2.755E-02
5.000E-01	1.000E-01	2.000E-01	9.724E-01	0.000E+00	2.755E-02
5.000E-01	5.000E-01	1.000E+00	9.724E-01	0.000E+00	2.755E-02
5.000E-01	1.000E+00	2.000E+00	9.724E-01	0.000E+00	2.755E-02
1.000E+00	1.000E-06	1.000E-06	3.572E-03	9.962E-01	2.361E-04
1.000E+00	5.000E-06	5.000E-06	1.771E-02	9.811E-01	1.155E-03
1.000E+00	1.000E-05	1.000E-05	3.504E-02	9.627E-01	2.249E-03
1.000E+00	5.000E-05	5.000E-05	1.612E-01	8.296E-01	9.201E-03
1.000E+00	1.000E-04	1.000E-04	2.918E-01	6.935E-01	1.477E-02
1.000E+00	5.000E-04	5.000E-04	7.688E-01	2.058E-01	2.541E-02
1.000E+00	1.000E-03	1.000E-03	9.062E-01	6.703E-02	2.675E-02
1.000E+00	2.000E-03	2.000E-03	9.587E-01	1.413E-02	2.714E-02
1.000E+00	4.000E-03	4.000E-03	9.714E-01	1.417E-03	2.719E-02
1.000E+00	6.000E-03	6.000E-03	9.726E-01	1.870E-04	2.720E-02
1.000E+00	1.000E-02	1.000E-02	9.728E-01	3.940E-06	2.720E-02
1.000E+00	5.000E-02	5.000E-02	9.728E-01	5.149E-23	2.720E-02
1.000E+00	1.000E-01	1.000E-01	9.728E-01	0.000E+00	2.720E-02
1.000E+00	5.000E-01	5.000E-01	9.728E-01	0.000E+00	2.720E-02
1.000E+00	1.000E+00	1.000E+00	9.728E-01	0.000E+00	2.720E-02
5.000E+00	1.000E-06	2.000E-07	1.419E-03	9.985E-01	1.487E-05
5.000E+00	5.000E-06	1.000E-06	7.073E-03	9.926E-01	5.719E-04
5.000E+00	1.000E-05	2.000E-06	1.409E-02	9.852E-01	1.460E-03
5.000E+00	5.000E-05	1.000E-05	6.845E-02	9.281E-01	3.956E-03
5.000E+00	1.000E-04	2.000E-05	1.321E-01	8.615E-01	6.107E-03
5.000E+00	5.000E-04	1.000E-04	5.027E-01	4.783E-01	1.892E-02
5.000E+00	1.000E-03	2.000E-04	7.437E-01	2.331E-01	2.319E-02
5.000E+00	2.000E-03	4.000E-04	9.171E-01	5.342E-02	2.403E-02
5.000E+00	4.000E-03	8.000E-04	9.708E-01	4.565E-03	2.465E-02
5.000E+00	6.000E-03	1.200E-03	9.749E-01	4.631E-04	2.466E-02
5.000E+00	1.000E-02	2.000E-03	9.753E-01	7.510E-06	2.466E-02
5.000E+00	5.000E-02	1.000E-02	9.753E-01	2.760E-22	2.466E-02
5.000E+00	1.000E-01	2.000E-02	9.753E-01	0.000E+00	2.466E-02
5.000E+00	5.000E-01	1.000E-01	9.753E-01	0.000E+00	2.466E-02
5.000E+00	1.000E+00	2.000E-01	9.753E-01	0.000E+00	2.466E-02

Table C-4. Broad-band IR properties of sooty water clouds (continued).

ρ_{H_2O}/ρ_{soot}	U_{H_2O} (gm cm^{-2})	U_{soot} (gm cm^{-2})	Emissivity	Transmissivity	Reflectivity
1.000E+01	1.000E-06	1.000E-07	1.149E-03	9.988E-01	5.439E-05
1.000E+01	5.000E-06	5.000E-07	5.733E-03	9.940E-01	2.707E-04
1.000E+01	1.000E-05	1.000E-06	1.143E-02	9.880E-01	5.381E-04
1.000E+01	5.000E-05	5.000E-06	5.584E-02	9.416E-01	2.565E-03
1.000E+01	1.000E-04	1.000E-05	1.085E-01	8.866E-01	4.840E-03
1.000E+01	5.000E-04	5.000E-05	4.349E-01	5.492E-01	1.588E-02
1.000E+01	1.000E-03	1.000E-04	6.760E-01	3.033E-01	2.075E-02
1.000E+01	2.000E-03	2.000E-04	8.833E-01	9.393E-02	2.279E-02
1.000E+01	4.000E-03	4.000E-04	9.674E-01	9.574E-03	2.302E-02
1.000E+01	6.000E-03	6.000E-04	9.759E-01	1.054E-03	2.303E-02
1.000E+01	1.000E-02	1.000E-03	9.770E-01	1.548E-05	2.303E-02
1.000E+01	5.000E-02	5.000E-03	9.770E-01	4.186E-22	2.303E-02
1.000E+01	1.000E-01	1.000E-02	9.770E-01	0.000E+00	2.303E-02
1.000E+01	5.000E-01	5.000E-02	9.770E-01	0.000E+00	2.303E-02
1.000E+01	1.000E+00	1.000E-01	9.770E-01	0.000E+00	2.303E-02
5.000E+01	1.000E-06	2.000E-08	9.335E-04	9.990E-01	3.816E-05
5.000E+01	5.000E-06	1.000E-07	4.658E-03	9.952E-01	1.900E-04
5.000E+01	1.000E-05	2.000E-07	9.294E-03	9.903E-01	3.782E-04
5.000E+01	5.000E-05	1.000E-06	[illegible]	9.526E-01	1.819E-03
5.000E+01	1.000E-04	2.000E-06	[illegible]	9.075E-01	3.169E-03
5.000E+01	5.000E-04	1.000E-05	[illegible]	[illegible]	1.222E-02
5.000E+01	1.000E-03	2.000E-05	[illegible]	3.845E-01	1.694E-02
5.000E+01	2.000E-03	4.000E-05	[illegible]	[illegible]	1.941E-02
5.000E+01	4.000E-03	8.000E-05	[illegible]	2.593E-02	2.019E-02
5.000E+01	6.000E-03	[illegible]	[illegible]	[illegible]	[illegible]
5.000E+01	1.000E-02	[illegible]	[illegible]	2.905E-04	2.022E-02
5.000E+01	5.000E-02	[illegible]	[illegible]	2.713E-15	[illegible]
5.000E+01	1.000E-01	[illegible]	[illegible]	[illegible]	2.022E-02
5.000E+01	5.000E-01	[illegible]	[illegible]	[illegible]	2.022E-02
5.000E+01	1.000E+00	[illegible]	[illegible]	[illegible]	2.022E-02
1.000E+02	1.000E-06	[illegible]	[illegible]	[illegible]	[illegible]
1.000E+02	5.000E-06	[illegible]	[illegible]	[illegible]	[illegible]
1.000E+02	1.000E-05	[illegible]	[illegible]	[illegible]	[illegible]
1.000E+02	5.000E-05	5.000E-07	1.129E-02	[illegible]	[illegible]
1.000E+02	1.000E-04	[illegible]	[illegible]	[illegible]	[illegible]
1.000E+02	5.000E-04	5.000E-06	[illegible]	[illegible]	[illegible]
1.000E+02	1.000E-03	[illegible]	[illegible]	[illegible]	[illegible]
1.000E+02	2.000E-03	2.000E-05	8.172E-01	1.633E-01	1.995E-02
1.000E+02	4.000E-03	[illegible]	[illegible]	[illegible]	[illegible]
1.000E+02	6.000E-03	6.000E-05	9.732E-01	[illegible]	[illegible]
1.000E+02	[illegible]	[illegible]	[illegible]	[illegible]	[illegible]
1.000E+02	[illegible]	[illegible]	[illegible]	[illegible]	[illegible]
1.000E+02	[illegible]	[illegible]	9.803E-01	[illegible]	[illegible]
1.000E+02	[illegible]	[illegible]	9.803E-01	[illegible]	[illegible]
[illegible]	[illegible]	[illegible]	[illegible]	[illegible]	[illegible]

Table C-4. Broad-band IR properties of sooty water clouds (continued).

ρ_{H_2O}/ρ_{soot}	U_{H_2O} (gm cm^{-2})	U_{soot} (gm cm^{-2})	Emissivity	Transmissivity	Reflectivity
2.000E+02	1.000E-06	5.000E-09	8.930E-04	9.991E-01	3.511E-05
2.000E+02	5.000E-06	2.500E-08	4.457E-03	9.954E-01	1.749E-04
2.000E+02	1.000E-05	5.000E-08	8.892E-03	9.908E-01	3.481E-04
2.000E+02	5.000E-05	2.500E-07	4.364E-02	9.547E-01	1.676E-03
2.000E+02	1.000E-04	5.000E-07	8.529E-02	9.115E-01	3.200E-03
2.000E+02	5.000E-04	2.500E-06	3.569E-01	6.317E-01	1.136E-02
2.000E+02	1.000E-03	5.000E-06	5.809E-01	4.032E-01	1.589E-02
2.000E+02	2.000E-03	1.000E-05	8.117E-01	1.847E-01	1.958E-02
2.000E+02	4.000E-03	2.000E-05	9.462E-01	3.447E-02	1.928E-02
2.000E+02	6.000E-03	3.000E-05	9.724E-01	8.275E-03	1.934E-02
2.000E+02	1.000E-02	5.000E-05	9.800E-01	6.592E-04	1.935E-02
2.000E+02	5.000E-02	2.500E-04	9.807E-01	5.657E-12	1.935E-02
2.000E+02	1.000E-01	5.000E-04	9.807E-01	4.363E-20	1.935E-02
2.000E+02	5.000E-01	2.500E-03	9.807E-01	0.000E+00	1.935E-02
2.000E+02	1.000E+00	5.000E-03	9.807E-01	0.000E+00	1.935E-02
5.000E+02	1.000E-06	2.000E-09	8.849E-04	9.991E-01	3.453E-05
5.000E+02	5.000E-06	1.000E-08	4.416E-03	9.954E-01	1.719E-04
5.000E+02	1.000E-05	2.000E-08	8.812E-03	9.908E-01	3.421E-04
5.000E+02	5.000E-05	1.000E-07	4.325E-02	9.551E-01	1.647E-03
5.000E+02	1.000E-04	2.000E-07	8.455E-02	9.123E-01	3.148E-03
5.000E+02	5.000E-04	1.000E-06	3.542E-01	6.346E-01	1.119E-02
5.000E+02	1.000E-03	2.000E-06	5.773E-01	4.071E-01	1.568E-02
5.000E+02	2.000E-03	4.000E-06	8.083E-01	1.933E-01	1.935E-02
5.000E+02	4.000E-03	8.000E-06	9.446E-01	3.830E-02	1.908E-02
5.000E+02	6.000E-03	1.200E-05	9.713E-01	9.048E-03	1.914E-02
5.000E+02	1.000E-02	2.000E-05	9.801E-01	2.855E-04	1.915E-02
5.000E+02	5.000E-02	1.000E-04	9.809E-01	4.087E-11	1.915E-02
5.000E+02	1.000E-01	2.000E-04	9.809E-01	1.667E-19	1.915E-02
5.000E+02	5.000E-01	1.000E-03	9.809E-01	0.000E+00	1.915E-02
5.000E+02	1.000E+00	2.000E-03	9.809E-01	0.000E+00	1.915E-02
1.000E+03	1.000E-06	1.000E-09	8.822E-04	9.991E-01	3.439E-05
1.000E+03	5.000E-06	5.000E-09	4.403E-03	9.954E-01	1.713E-04
1.000E+03	1.000E-05	1.000E-08	8.785E-03	9.909E-01	3.421E-04
1.000E+03	5.000E-05	5.000E-08	4.312E-02	9.552E-01	1.678E-03
1.000E+03	1.000E-04	1.000E-07	8.430E-02	9.126E-01	3.282E-03
1.000E+03	5.000E-04	5.000E-07	3.533E-01	6.360E-01	1.113E-02
1.000E+03	1.000E-03	1.000E-06	5.760E-01	4.084E-01	1.559E-02
1.000E+03	2.000E-03	2.000E-06	8.071E-01	1.944E-01	1.927E-02
1.000E+03	4.000E-03	4.000E-06	9.441E-01	3.893E-02	1.901E-02
1.000E+03	6.000E-03	6.000E-06	9.716E-01	9.324E-03	1.907E-02
1.000E+03	1.000E-02	1.000E-05	9.801E-01	2.933E-04	1.909E-02
1.000E+03	5.000E-02	5.000E-05	9.809E-01	3.111E-11	1.909E-02
1.000E+03	1.000E-01	1.000E-04	9.809E-01	1.901E-19	1.909E-02
1.000E+03	5.000E-01	5.000E-04	9.809E-01	0.000E+00	1.909E-02
1.000E+03	1.000E+00	1.000E-03	9.809E-01	0.000E+00	1.909E-02

Table C-4. Broad-band IR properties of sooty water clouds (continued).

ρ_{H_2O}/ρ_{soot}	U_{H_2O} (gm cm^{-2})	U_{soot} (gm cm^{-2})	Emissivity	Transmissivity	Reflectivity
1.000E+03	1.000E-06	1.000E-10	8.800E-04	9.991E-01	3.414E-05
5.000E+03	5.000E-06	1.000E-09	4.392E-03	9.954E-01	1.700E-04
1.000E+03	1.000E-05	2.000E-09	8.764E-03	9.909E-01	3.385E-04
5.000E+03	5.000E-05	1.000E-08	4.302E-02	9.553E-01	1.630E-03
1.000E+03	1.000E-04	2.000E-08	8.410E-02	9.128E-01	3.112E-03
5.000E+03	5.000E-04	1.000E-07	3.526E-01	6.364E-01	1.108E-02
1.000E+03	1.000E-03	2.000E-07	5.751E-01	4.094E-01	1.581E-02
5.000E+03	2.000E-03	4.000E-07	8.062E-01	1.756E-01	1.821E-02
5.000E+03	4.000E-03	8.000E-07	9.436E-01	3.745E-02	1.895E-02
5.000E+03	6.000E-03	1.200E-06	9.714E-01	9.953E-03	1.901E-02
5.000E+03	1.000E-02	2.000E-06	9.801E-01	8.745E-04	1.903E-02
5.000E+03	5.000E-02	1.000E-05	9.810E-01	1.422E-10	1.903E-02
1.000E+03	1.000E-01	2.000E-05	9.810E-01	5.964E-17	1.903E-02
5.000E+03	5.000E-01	1.000E-04	9.810E-01	0.000E+00	1.903E-02
5.000E+03	1.000E+00	2.000E-04	9.810E-01	0.000E+00	1.903E-02
1.000E+04	1.000E-06	1.000E-10	8.798E-04	9.991E-01	3.412E-05
1.000E+04	5.000E-06	5.000E-10	4.391E-03	9.954E-01	1.699E-04
1.000E+04	1.000E-05	1.000E-09	8.761E-03	9.909E-01	3.383E-04
1.000E+04	5.000E-05	5.000E-09	4.301E-02	9.554E-01	1.629E-03
1.000E+04	1.000E-04	1.000E-08	8.407E-02	9.128E-01	3.111E-03
1.000E+04	5.000E-04	5.000E-08	3.525E-01	6.365E-01	1.107E-02
1.000E+04	1.000E-03	1.000E-07	5.749E-01	4.096E-01	1.551E-02
1.000E+04	2.000E-03	2.000E-07	8.061E-01	1.757E-01	1.820E-02
1.000E+04	4.000E-03	4.000E-07	9.435E-01	3.751E-02	1.894E-02
1.000E+04	6.000E-03	6.000E-07	9.714E-01	9.582E-03	1.901E-02
1.000E+04	1.000E-02	1.000E-06	9.801E-01	8.798E-04	1.902E-02
1.000E+04	5.000E-02	5.000E-06	9.810E-01	1.525E-10	1.902E-02
1.000E+04	1.000E-01	1.000E-05	9.810E-01	6.930E-17	1.902E-02
1.000E+04	5.000E-01	5.000E-05	9.810E-01	0.000E+00	1.902E-02
1.000E+04	1.000E+00	1.000E-04	9.810E-01	0.000E+00	1.902E-02
1.000E+05	1.000E-06	1.000E-11	8.795E-04	9.991E-01	3.410E-05
1.000E+05	5.000E-06	5.000E-11	4.389E-03	9.954E-01	1.699E-04
1.000E+05	1.000E-05	1.000E-10	8.759E-03	9.909E-01	3.381E-04
1.000E+05	5.000E-05	5.000E-10	4.300E-02	9.554E-01	1.629E-03
1.000E+05	1.000E-04	1.000E-09	8.405E-02	9.128E-01	3.109E-03
1.000E+05	5.000E-04	5.000E-09	3.524E-01	6.365E-01	1.106E-02
1.000E+05	1.000E-03	1.000E-08	5.748E-01	4.097E-01	1.550E-02
1.000E+05	2.000E-03	2.000E-08	8.060E-01	1.758E-01	1.819E-02
1.000E+05	4.000E-03	4.000E-08	9.435E-01	3.757E-02	1.893E-02
1.000E+05	6.000E-03	6.000E-08	9.714E-01	9.608E-03	1.900E-02
1.000E+05	1.000E-02	1.000E-07	9.801E-01	8.815E-04	1.901E-02
1.000E+05	5.000E-02	5.000E-07	9.810E-01	1.525E-10	1.901E-02
1.000E+05	1.000E-01	1.000E-06	9.810E-01	7.942E-17	1.901E-02
1.000E+05	5.000E-01	5.000E-06	9.810E-01	0.000E+00	1.901E-02
1.000E+05	1.000E+00	1.000E-05	9.810E-01	0.000E+00	1.901E-02

Table C-4. Broad-band IR properties of sooty water clouds (Concluded).

ρ_{H_2O}/ρ_{soot}	U_{H_2O} (gm cm^{-2})	U_{soot} (gm cm^{-2})	Emissivity	Transmissivity	Reflectivity
1.000E+10	1.000E-06	1.000E-16	8.795E-04	9.991E-01	3.410E-05
1.000E+10	5.000E-06	5.000E-16	4.389E-03	9.954E-01	1.698E-04
1.000E+10	1.000E-05	1.000E-15	8.758E-03	9.909E-01	3.381E-04
1.000E+10	5.000E-05	5.000E-15	4.299E-02	9.554E-01	1.628E-03
1.000E+10	1.000E-04	1.000E-14	8.405E-02	9.128E-01	3.109E-03
1.000E+10	5.000E-04	5.000E-14	3.524E-01	6.365E-01	1.106E-02
1.000E+10	1.000E-03	1.000E-13	5.748E-01	4.097E-01	1.550E-02
1.000E+10	2.000E-03	2.000E-13	8.060E-01	1.758E-01	1.819E-02
1.000E+10	4.000E-03	4.000E-13	9.435E-01	3.758E-02	1.893E-02
1.000E+10	6.000E-03	6.000E-13	9.714E-01	9.611E-03	1.900E-02
1.000E+10	1.000E-02	1.000E-12	9.801E-01	8.851E-04	1.901E-02
1.000E+10	5.000E-02	5.000E-12	9.810E-01	1.637E-10	1.901E-02
1.000E+10	1.000E-01	1.000E-11	9.810E-01	8.052E-17	1.901E-02
1.000E+10	5.000E-01	5.000E-11	9.810E-01	0.000E+00	1.901E-02
1.000E+10	1.000E+00	1.000E-10	9.810E-01	0.000E+00	1.901E-02

Table C-5. Optical properties in the visible (λ=0.55 μm) of sooty water clouds.

ρ_{H_2O}/ρ_{soot}	τ^* (Optical Depth)	U_{soot} (gm cm^{-2})	U_{H_2O} (gm cm^{-2})	R (Reflectivity)	T (Transmissivity)	ε (Emissivity)
1.000E-03	4.422E+01	1.000E-03	1.000E-06	4.424E-02	3.986E-09	9.558E-01
1.000E-03	2.211E+02	5.000E-03	5.000E-06	4.424E-02	0.000E+00	9.558E-01
1.000E-03	4.422E+02	1.000E-02	1.000E-05	4.424E-02	0.000E+00	9.558E-01
1.000E-03	2.211E+03	5.000E-02	5.000E-05	4.424E-02	0.000E+00	9.558E-01
1.000E-03	4.422E+03	1.000E-01	1.000E-04	4.424E-02	0.000E+00	9.558E-01
1.000E-03	2.211E+04	5.000E-01	5.000E-04	4.424E-02	0.000E+00	9.558E-01
1.000E-03	4.422E+04	1.000E+00	1.000E-03	4.424E-02	0.000E+00	9.558E-01
1.000E-03	8.844E+04	2.000E+00	2.000E-03	4.424E-02	0.000E+00	9.558E-01
1.000E-03	1.769E+05	4.000E+00	4.000E-03	4.424E-02	0.000E+00	9.558E-01
1.000E-03	2.653E+05	6.000E+00	6.000E-03	4.424E-02	0.000E+00	9.558E-01
1.000E-03	4.422E+05	1.000E+01	1.000E-02	4.424E-02	0.000E+00	9.558E-01
1.000E-03	2.211E+06	5.000E+01	5.000E-02	4.424E-02	0.000E+00	9.558E-01
1.000E-03	4.422E+06	1.000E+02	1.000E-01	4.424E-02	0.000E+00	9.558E-01
1.000E-03	2.211E+07	5.000E+02	5.000E-01	4.424E-02	0.000E+00	9.558E-01
1.000E-03	4.422E+07	1.000E+03	1.000E+00	4.424E-02	0.000E+00	9.558E-01
1.000E-02	4.424E+00	1.000E-04	1.000E-06	4.333E-02	1.443E-01	8.124E-01
1.000E-02	2.212E+01	5.000E-04	5.000E-06	4.425E-02	6.305E-05	9.557E-01
1.000E-02	4.424E+01	1.000E-03	1.000E-05	4.425E-02	3.984E-09	9.557E-01
1.000E-02	2.212E+02	5.000E-03	5.000E-05	4.425E-02	0.000E+00	9.557E-01
1.000E-02	4.424E+02	1.000E-02	1.000E-04	4.425E-02	0.000E+00	9.557E-01
1.000E-02	2.212E+03	5.000E-02	5.000E-04	4.425E-02	0.000E+00	9.557E-01
1.000E-02	4.424E+03	1.000E-01	1.000E-03	4.425E-02	0.000E+00	9.557E-01
1.000E-02	8.847E+03	2.000E-01	2.000E-03	4.425E-02	0.000E+00	9.557E-01
1.000E-02	1.769E+04	4.000E-01	4.000E-03	4.425E-02	0.000E+00	9.557E-01
1.000E-02	2.654E+04	6.000E-01	6.000E-03	4.425E-02	0.000E+00	9.557E-01
1.000E-02	4.424E+04	1.000E+00	1.000E-02	4.425E-02	0.000E+00	9.557E-01
1.000E-02	2.212E+05	5.000E+00	5.000E-02	4.425E-02	0.000E+00	9.557E-01
1.000E-02	4.424E+05	1.000E+01	1.000E-01	4.425E-02	0.000E+00	9.557E-01
1.000E-02	2.212E+06	5.000E+01	5.000E-01	4.425E-02	0.000E+00	9.557E-01
1.000E-02	4.424E+06	1.000E+02	1.000E+00	4.425E-02	0.000E+00	9.557E-01
1.000E-01	4.439E-01	1.000E-05	1.000E-06	1.427E-02	8.236E-01	1.621E-01
1.000E-01	2.220E+00	5.000E-05	5.000E-06	3.802E-02	3.795E-01	5.825E-01
1.000E-01	4.439E+00	1.000E-04	1.000E-05	4.350E-02	1.442E-01	8.123E-01
1.000E-01	2.220E+01	5.000E-04	5.000E-05	4.442E-02	6.284E-05	9.555E-01
1.000E-01	4.439E+01	1.000E-03	1.000E-04	4.442E-02	3.957E-09	9.556E-01
1.000E-01	2.220E+02	5.000E-03	5.000E-04	4.442E-02	0.000E+00	9.556E-01
1.000E-01	4.439E+02	1.000E-02	1.000E-03	4.442E-02	0.000E+00	9.556E-01
1.000E-01	8.879E+02	2.000E-02	2.000E-03	4.442E-02	0.000E+00	9.556E-01
1.000E-01	1.776E+03	4.000E-02	4.000E-03	4.442E-02	0.000E+00	9.556E-01
1.000E-01	2.664E+03	6.000E-02	6.000E-03	4.442E-02	0.000E+00	9.556E-01
1.000E-01	4.439E+03	1.000E-01	1.000E-02	4.442E-02	0.000E+00	9.556E-01
1.000E-01	2.220E+04	5.000E-01	5.000E-02	4.442E-02	0.000E+00	9.556E-01
1.000E-01	4.439E+04	1.000E+00	1.000E-01	4.442E-02	0.000E+00	9.556E-01
1.000E-01	2.220E+05	5.000E+00	5.000E-01	4.442E-02	0.000E+00	9.556E-01
1.000E-01	4.439E+05	1.000E+01	1.000E+00	4.442E-02	0.000E+00	9.556E-01

Table C-5. Optical properties in the visible (λ=0.55 μm) of sooty water clouds (continued).

ρ_{H_2O}/ρ_{soot}	τ^* (Optical Depth)	U_{soot} (gm cm^{-2})	U_{H_2O} (gm cm^{-2})	R (Reflectivity)	T (Transmissivity)	ε (Emissivity)
5.000E-01	9.018E-02	2.000E-06	1.000E-06	3.376E-03	9.618E-01	3.478E-02
5.000E-01	4.509E-01	1.000E-05	5.000E-06	1.454E-02	8.233E-01	1.621E-01
5.000E-01	9.018E-01	2.000E-05	1.000E-05	2.439E-02	6.780E-01	2.976E-01
5.000E-01	4.509E+00	1.000E-04	5.000E-05	4.425E-02	1.438E-01	8.120E-01
5.000E-01	9.018E+00	2.000E-04	1.000E-04	4.517E-02	2.071E-02	9.341E-01
5.000E-01	4.509E+01	1.000E-03	5.000E-04	4.518E-02	3.842E-09	9.548E-01
5.000E-01	9.018E+01	2.000E-03	1.000E-03	4.518E-02	1.479E-17	9.548E-01
5.000E-01	1.804E+02	4.000E-03	2.000E-03	4.518E-02	2.192E-34	9.548E-01
5.000E-01	3.607E+02	8.000E-03	4.000E-03	4.518E-02	0.000E+00	9.548E-01
5.000E-01	5.411E+02	1.200E-02	6.000E-03	4.518E-02	0.000E+00	9.548E-01
5.000E-01	9.018E+02	2.000E-02	1.000E-02	4.518E-02	0.000E+00	9.548E-01
5.000E-01	4.509E+03	1.000E-01	5.000E-02	4.518E-02	0.000E+00	9.548E-01
5.000E-01	9.018E+03	2.000E-01	1.000E-01	4.518E-02	0.000E+00	9.548E-01
5.000E-01	4.509E+04	1.000E+00	5.000E-01	4.518E-02	0.000E+00	9.548E-01
5.000E-01	9.018E+04	2.000E+00	1.000E+00	4.518E-02	0.000E+00	9.548E-01
1.000E+00	4.596E-02	1.000E-06	1.000E-06	1.760E-03	9.807E-01	1.754E-02
1.000E+00	2.298E-01	5.000E-06	5.000E-06	8.154E-03	9.072E-01	8.469E-02
1.000E+00	4.596E-01	1.000E-05	1.000E-05	1.486E-02	8.230E-01	1.621E-01
1.000E+00	2.298E+00	5.000E-05	5.000E-05	3.952E-02	3.782E-01	5.823E-01
1.000E+00	4.596E+00	1.000E-04	1.000E-04	4.518E-02	1.432E-01	8.116E-01
1.000E+00	2.298E+01	5.000E-04	5.000E-04	4.613E-02	6.079E-05	9.538E-01
1.000E+00	4.596E+01	1.000E-03	1.000E-03	4.613E-02	3.703E-09	9.539E-01
1.000E+00	9.192E+01	2.000E-03	2.000E-03	4.613E-02	1.374E-17	9.539E-01
1.000E+00	1.838E+02	4.000E-03	4.000E-03	4.613E-02	1.892E-34	9.539E-01
1.000E+00	2.758E+02	6.000E-03	6.000E-03	4.613E-02	0.000E+00	9.539E-01
1.000E+00	4.596E+02	1.000E-02	1.000E-02	4.613E-02	0.000E+00	9.539E-01
1.000E+00	2.298E+03	5.000E-02	5.000E-02	4.613E-02	0.000E+00	9.539E-01
1.000E+00	4.596E+03	1.000E-01	1.000E-01	4.613E-02	0.000E+00	9.539E-01
1.000E+00	2.298E+04	5.000E-01	5.000E-01	4.613E-02	0.000E+00	9.539E-01
1.000E+00	4.596E+04	1.000E+00	1.000E+00	4.613E-02	0.000E+00	9.539E-01
5.000E+00	1.058E-02	2.000E-07	1.000E-06	4.217E-04	9.960E-01	3.534E-03
5.000E+00	5.292E-02	1.000E-06	5.000E-06	2.075E-03	9.804E-01	1.754E-02
5.000E+00	1.058E-01	2.000E-06	1.000E-05	4.070E-03	9.611E-01	3.478E-02
5.000E+00	5.292E-01	1.000E-05	5.000E-05	1.748E-02	8.204E-01	1.621E-01
5.000E+00	1.058E+00	2.000E-05	1.000E-04	2.925E-02	6.733E-01	2.975E-01
5.000E+00	5.293E+00	1.000E-04	5.000E-04	5.252E-02	1.390E-01	8.085E-01
5.000E+00	1.059E+01	2.000E-04	1.000E-03	5.354E-02	1.938E-02	9.271E-01
5.000E+00	2.117E+01	4.000E-04	2.000E-03	5.356E-02	3.766E-04	9.461E-01
5.000E+00	4.234E+01	8.000E-04	4.000E-03	5.356E-02	1.423E-07	9.464E-01
5.000E+00	6.351E+01	1.200E-03	6.000E-03	5.356E-02	5.374E-11	9.464E-01
5.000E+00	1.058E+02	2.000E-03	1.000E-02	5.356E-02	7.667E-18	9.464E-01
5.000E+00	5.293E+02	1.000E-02	5.000E-02	5.356E-02	0.000E+00	9.464E-01
5.000E+00	1.059E+03	2.000E-02	1.000E-01	5.356E-02	0.000E+00	9.464E-01
5.000E+00	5.293E+03	1.000E-01	5.000E-01	5.356E-02	0.000E+00	9.464E-01
5.000E+00	1.059E+04	2.000E-01	1.000E+00	5.356E-02	0.000E+00	9.464E-01

Table C-5. Optical properties in the visible (λ=0.55 μm) of sooty water clouds (continued).

ρ_{H_2O}/ρ_{soot}	τ^* (Optical Depth)	U_{soot} (gm cm^{-2})	U_{H_2O} (gm cm^{-2})	R (Reflectivity)	T (Transmissivity)	ϵ (Emissivity)
1.000E+01	6.163E-03	1.000E-07	1.000E-06	2.514E-04	9.980E-01	1.768E-03
1.000E+01	3.081E-02	5.000E-07	5.000E-06	1.247E-03	9.899E-01	8.811E-03
1.000E+01	6.163E-02	1.000E-06	1.000E-05	2.468E-03	9.800E-01	1.754E-02
1.000E+01	3.081E-01	5.000E-06	5.000E-05	1.140E-02	9.039E-01	8.468E-02
1.000E+01	6.163E-01	1.000E-05	1.000E-04	2.072E-02	8.172E-01	1.621E-01
1.000E+01	3.082E+00	5.000E-05	5.000E-04	5.415E-02	3.655E-01	5.803E-01
1.000E+01	6.163E+00	1.000E-04	1.000E-03	6.140E-02	1.340E-01	8.046E-01
1.000E+01	1.233E+01	2.000E-04	2.000E-03	6.251E-02	1.802E-02	9.195E-01
1.000E+01	2.465E+01	4.000E-04	4.000E-03	6.253E-02	3.261E-04	9.371E-01
1.000E+01	3.698E+01	6.000E-04	6.000E-03	6.253E-02	5.900E-06	9.375E-01
1.000E+01	6.163E+01	1.000E-03	1.000E-02	6.253E-02	1.931E-09	9.375E-01
1.000E+01	3.081E+02	5.000E-03	5.000E-02	6.253E-02	0.000E+00	9.375E-01
1.000E+01	6.163E+02	1.000E-02	1.000E-01	6.253E-02	0.000E+00	9.375E-01
1.000E+01	3.082E+03	5.000E-02	5.000E-01	6.253E-02	0.000E+00	9.375E-01
1.000E+01	6.163E+03	1.000E-01	1.000E+00	6.253E-02	0.000E+00	9.375E-01
5.000E+01	2.625E-03	2.000E-08	1.000E-06	1.145E-04	9.995E-01	3.539E-04
5.000E+01	1.313E-02	1.000E-07	5.000E-06	5.714E-04	9.977E-01	1.769E-03
5.000E+01	2.625E-02	2.000E-07	1.000E-05	1.140E-03	9.953E-01	3.534E-03
5.000E+01	1.313E-01	1.000E-06	5.000E-05	5.595E-03	9.769E-01	1.754E-02
5.000E+01	2.625E-01	2.000E-06	1.000E-04	1.093E-02	9.543E-01	3.478E-02
5.000E+01	1.313E+00	1.000E-05	5.000E-04	4.577E-02	7.923E-01	1.620E-01
5.000E+01	2.625E+00	2.000E-05	1.000E-03	7.455E-02	6.290E-01	2.964E-01
5.000E+01	5.251E+00	4.000E-05	2.000E-03	1.042E-01	3.979E-01	4.979E-01
5.000E+01	1.050E+01	8.000E-05	4.000E-03	1.209E-01	1.600E-01	7.191E-01
5.000E+01	1.575E+01	1.200E-04	6.000E-03	1.236E-01	6.448E-02	8.119E-01
5.000E+01	2.625E+01	2.000E-04	1.000E-02	1.241E-01	1.047E-02	8.654E-01
5.000E+01	1.313E+02	1.000E-03	5.000E-02	1.241E-01	1.342E-10	8.759E-01
5.000E+01	2.625E+02	2.000E-03	1.000E-01	1.241E-01	1.828E-20	8.759E-01
5.000E+01	1.313E+03	1.000E-02	5.000E-01	1.241E-01	0.000E+00	8.759E-01
5.000E+01	2.625E+03	2.000E-02	1.000E+00	1.241E-01	0.000E+00	8.759E-01
1.000E+02	2.183E-03	1.000E-08	1.000E-06	9.733E-05	9.997E-01	1.770E-04
1.000E+02	1.092E-02	5.000E-08	5.000E-06	4.861E-04	9.986E-01	8.847E-04
1.000E+02	2.183E-02	1.000E-07	1.000E-05	9.709E-04	9.973E-01	1.768E-03
1.000E+02	1.092E-01	5.000E-07	5.000E-05	4.802E-03	9.864E-01	8.811E-03
1.000E+02	2.183E-01	1.000E-06	1.000E-04	9.473E-03	9.730E-01	1.754E-02
1.000E+02	1.092E+00	5.000E-06	5.000E-04	4.260E-02	8.728E-01	8.464E-02
1.000E+02	2.183E+00	1.000E-05	1.000E-03	7.511E-02	7.631E-01	1.618E-01
1.000E+02	4.366E+00	2.000E-05	2.000E-03	1.191E-01	5.856E-01	2.953E-01
1.000E+02	8.733E+00	4.000E-05	4.000E-03	1.605E-01	3.479E-01	4.916E-01
1.000E+02	1.310E+01	6.000E-05	6.000E-03	1.752E-01	2.077E-01	6.171E-01
1.000E+02	2.183E+01	1.000E-04	1.000E-02	1.823E-01	7.435E-02	7.433E-01
1.000E+02	1.092E+02	5.000E-04	5.000E-02	1.834E-01	2.602E-06	8.166E-01
1.000E+02	2.183E+02	1.000E-03	1.000E-01	1.834E-01	7.006E-12	8.166E-01
1.000E+02	1.092E+03	5.000E-03	5.000E-01	1.834E-01	0.000E+00	8.166E-01
1.000E+02	2.183E+03	1.000E-02	1.000E+00	1.834E-01	0.000E+00	8.166E-01

AD-A168 717 INFRARED ISSUES FOR THE NUCLEAR WINTER PHENOMENON(U) 2/2
MISSION RESEARCH CORP SANTA BARBARA CA
G MCCARTOR ET AL. 03 OCT 85 MRC-R-955 DNA-TR-85-312
UNCLASSIFIED DNA001-84-C-0319 F/G 4/1 NL

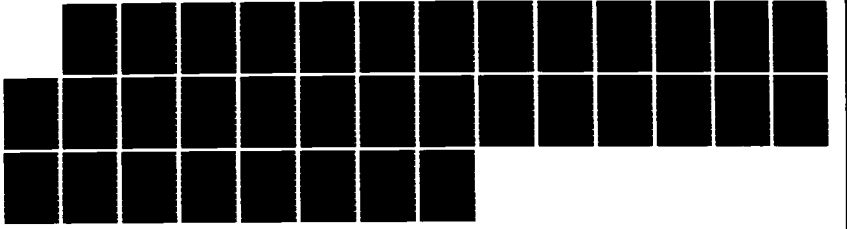

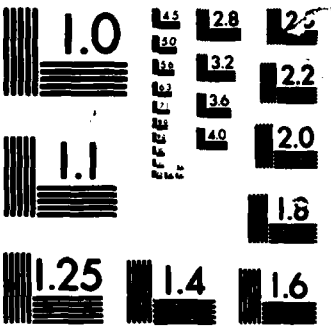

MICROCOPY CHART

Table C-5. Optical properties in the visible (λ=0.55 μm) of sooty water clouds (continued).

ρ_{H_2O}/ρ_{soot}	τ^* (Optical Depth)	U_{soot} (gm cm^{-2})	U_{H_2O} (gm cm^{-2})	R (Reflectivity)	T (Transmissivity)	ε (Emissivity)
2.000E+02	1.962E-03	5.000E-09	1.000E-06	8.874E-05	9.998E-01	8.851E-05
2.000E+02	9.810E-03	2.500E-08	5.000E-06	4.434E-04	9.991E-01	4.424E-04
2.000E+02	1.962E-02	5.000E-08	1.000E-05	8.860E-04	9.982E-01	8.846E-04
2.000E+02	9.810E-02	2.500E-07	5.000E-05	4.399E-03	9.912E-01	4.415E-03
2.000E+02	1.962E-01	5.000E-07	1.000E-04	8.720E-03	9.825E-01	8.811E-03
2.000E+02	9.811E-01	2.500E-06	5.000E-04	4.069E-02	9.160E-01	4.327E-02
2.000E+02	1.962E+00	5.000E-06	1.000E-03	7.489E-02	8.405E-01	8.459E-02
2.000E+02	3.924E+00	1.000E-05	2.000E-03	1.281E-01	7.105E-01	1.614E-01
2.000E+02	7.848E+00	2.000E-05	4.000E-03	1.938E-01	5.132E-01	2.930E-01
2.000E+02	1.177E+01	3.000E-05	6.000E-03	2.284E-01	3.739E-01	3.977E-01
2.000E+02	1.962E+01	5.000E-05	1.000E-02	2.568E-01	2.007E-01	5.425E-01
2.000E+02	9.811E+01	2.500E-04	5.000E-02	2.684E-01	4.323E-04	7.312E-01
2.000E+02	1.962E+02	5.000E-04	1.000E-01	2.684E-01	2.014E-07	7.316E-01
2.000E+02	9.810E+02	2.500E-03	5.000E-01	2.684E-01	4.468E-34	7.316E-01
2.000E+02	1.962E+03	5.000E-03	1.000E+00	2.684E-01	0.000E+00	7.316E-01
5.000E+02	1.829E-03	2.000E-09	1.000E-06	8.357E-05	9.999E-01	3.541E-05
5.000E+02	9.147E-03	1.000E-08	5.000E-06	4.177E-04	9.994E-01	1.769E-04
5.000E+02	1.829E-02	2.000E-08	1.000E-05	8.349E-04	9.988E-01	3.539E-04
5.000E+02	9.147E-02	1.000E-07	5.000E-05	4.155E-03	9.941E-01	1.768E-03
5.000E+02	1.829E-01	2.000E-07	1.000E-04	8.261E-03	9.882E-01	3.534E-03
5.000E+02	9.147E-01	1.000E-06	5.000E-04	3.943E-02	9.430E-01	1.754E-02
5.000E+02	1.829E+00	2.000E-06	1.000E-03	7.454E-02	8.907E-01	3.476E-02
5.000E+02	3.659E+00	4.000E-06	2.000E-03	1.340E-01	7.978E-01	6.822E-02
5.000E+02	7.318E+00	8.000E-06	4.000E-03	2.209E-01	6.481E-01	1.311E-01
5.000E+02	1.098E+01	1.200E-05	6.000E-03	2.789E-01	5.328E-01	1.884E-01
5.000E+02	1.829E+01	2.000E-05	1.000E-02	3.457E-01	3.679E-01	2.864E-01
5.000E+02	9.147E+01	1.000E-04	5.000E-02	4.103E-01	1.205E-02	5.776E-01
5.000E+02	1.829E+02	2.000E-04	1.000E-01	4.104E-01	1.746E-04	5.894E-01
5.000E+02	9.147E+02	1.000E-03	5.000E-01	4.104E-01	3.396E-19	5.896E-01
5.000E+02	1.829E+03	2.000E-03	1.000E+00	4.104E-01	0.000E+00	5.896E-01
1.000E+03	1.785E-03	1.000E-09	1.000E-06	8.184E-05	9.999E-01	1.772E-05
1.000E+03	8.926E-03	5.000E-09	5.000E-06	4.091E-04	9.995E-01	8.847E-05
1.000E+03	1.785E-02	1.000E-08	1.000E-05	8.179E-04	9.990E-01	1.770E-04
1.000E+03	8.926E-02	5.000E-08	5.000E-05	4.073E-03	9.950E-01	8.847E-04
1.000E+03	1.785E-01	1.000E-07	1.000E-04	8.106E-03	9.901E-01	1.768E-03
1.000E+03	8.926E-01	5.000E-07	5.000E-04	3.898E-02	9.522E-01	8.811E-03
1.000E+03	1.785E+00	1.000E-06	1.000E-03	7.438E-02	9.081E-01	1.754E-02
1.000E+03	3.570E+00	2.000E-06	2.000E-03	1.361E-01	8.292E-01	3.475E-02
1.000E+03	7.141E+00	4.000E-06	4.000E-03	2.314E-01	7.005E-01	6.810E-02
1.000E+03	1.071E+01	6.000E-06	6.000E-03	3.003E-01	5.998E-01	9.993E-02
1.000E+03	1.785E+01	1.000E-05	1.000E-02	3.898E-01	4.515E-01	1.587E-01
1.000E+03	8.926E+01	5.000E-05	5.000E-02	5.227E-01	4.270E-02	4.346E-01
1.000E+03	1.785E+02	1.000E-04	1.000E-01	5.240E-01	2.509E-03	4.735E-01
1.000E+03	8.926E+02	5.000E-04	5.000E-01	5.240E-01	3.588E-13	4.760E-01
1.000E+03	1.785E+03	1.000E-03	1.000E+00	5.240E-01	1.775E-25	4.760E-01

Table C-5. Optical properties in the visible (λ=0.55 μm) of sooty water clouds (continued).

ρ_{H_2O}/ρ_{soot}	τ^* (Optical Depth)	U_{soot} (gm cm^{-2})	U_{H_2O} (gm cm^{-2})	R (Reflectivity)	T (Transmissivity)	ε (Emissivity)
5.000E+03	1.750E-03	2.000E-10	1.000E-06	8.051E-05	9.999E-01	3.511E-06
5.000E+03	8.749E-03	1.000E-09	5.000E-06	4.023E-04	9.996E-01	1.769E-05
5.000E+03	1.750E-02	2.000E-09	1.000E-05	8.042E-04	9.992E-01	3.543E-05
5.000E+03	8.749E-02	1.000E-08	5.000E-05	4.008E-03	9.958E-01	1.771E-04
5.000E+03	1.750E-01	2.000E-08	1.000E-04	7.982E-03	9.917E-01	3.539E-04
5.000E+03	8.749E-01	1.000E-07	5.000E-04	3.862E-02	9.596E-01	1.769E-03
5.000E+03	1.750E+00	2.000E-07	1.000E-03	7.424E-02	9.222E-01	3.534E-03
5.000E+03	3.500E+00	4.000E-07	2.000E-03	1.377E-01	8.552E-01	7.054E-03
5.000E+03	6.999E+00	8.000E-07	4.000E-03	2.404E-01	7.455E-01	1.405E-02
5.000E+03	1.050E+01	1.200E-06	6.000E-03	3.196E-01	6.594E-01	2.098E-02
5.000E+03	1.750E+01	2.000E-06	1.000E-02	4.328E-01	5.325E-01	3.462E-02
5.000E+03	8.749E+01	1.000E-05	5.000E-02	7.129E-01	1.405E-01	1.467E-01
5.000E+03	1.750E+02	2.000E-05	1.000E-01	7.415E-01	4.012E-02	2.184E-01
5.000E+03	8.749E+02	1.000E-04	5.000E-01	7.441E-01	2.564E-06	2.558E-01
5.000E+03	1.750E+03	2.000E-04	1.000E+00	7.441E-01	1.473E-11	2.559E-01
1.000E+04	1.745E-03	1.000E-10	1.000E-06	8.032E-05	9.999E-01	1.821E-06
1.000E+04	8.727E-03	5.000E-10	5.000E-06	4.014E-04	9.996E-01	8.817E-06
1.000E+04	1.745E-02	1.000E-09	1.000E-05	8.026E-04	9.992E-01	1.763E-05
1.000E+04	8.727E-02	5.000E-09	5.000E-05	3.999E-03	9.959E-01	8.858E-05
1.000E+04	1.745E-01	1.000E-08	1.000E-04	7.966E-03	9.919E-01	1.770E-04
1.000E+04	8.727E-01	5.000E-08	5.000E-04	3.858E-02	9.605E-01	8.848E-04
1.000E+04	1.745E+00	1.000E-07	1.000E-03	7.422E-02	9.240E-01	1.769E-03
1.000E+04	3.491E+00	2.000E-07	2.000E-03	1.379E-01	8.585E-01	3.534E-03
1.000E+04	6.982E+00	4.000E-07	4.000E-03	2.416E-01	7.514E-01	7.053E-03
1.000E+04	1.047E+01	6.000E-07	6.000E-03	3.221E-01	6.673E-01	1.056E-02
1.000E+04	1.745E+01	1.000E-06	1.000E-02	4.388E-01	5.437E-01	1.751E-02
1.000E+04	8.727E+01	5.000E-06	5.000E-02	7.530E-01	1.668E-01	8.021E-02
1.000E+04	1.745E+02	1.000E-05	1.000E-01	8.014E-01	6.425E-02	1.344E-01
1.000E+04	8.727E+02	5.000E-05	5.000E-01	8.109E-01	7.122E-05	1.890E-01
1.000E+04	1.745E+03	1.000E-04	1.000E+00	8.109E-01	1.481E-08	1.891E-01
1.000E+05	1.741E-03	1.000E-11	1.000E-06	8.017E-05	9.999E-01	1.520E-07
1.000E+05	8.707E-03	5.000E-11	5.000E-06	4.007E-04	9.996E-01	8.359E-07
1.000E+05	1.741E-02	1.000E-10	1.000E-05	8.011E-04	9.992E-01	1.823E-06
1.000E+05	8.707E-02	5.000E-10	5.000E-05	3.992E-03	9.960E-01	8.861E-06
1.000E+05	1.741E-01	1.000E-09	1.000E-04	7.952E-03	9.920E-01	1.773E-05
1.000E+05	8.707E-01	5.000E-09	5.000E-04	3.853E-02	9.614E-01	8.866E-05
1.000E+05	1.741E+00	1.000E-08	1.000E-03	7.420E-02	9.256E-01	1.773E-04
1.000E+05	3.483E+00	2.000E-08	2.000E-03	1.381E-01	8.615E-01	3.544E-04
1.000E+05	6.966E+00	4.000E-08	4.000E-03	2.426E-01	7.566E-01	7.088E-04
1.000E+05	1.045E+01	6.000E-08	6.000E-03	3.245E-01	6.745E-01	1.063E-03
1.000E+05	1.741E+01	1.000E-07	1.000E-02	4.443E-01	5.539E-01	1.771E-03
1.000E+05	8.707E+01	5.000E-07	5.000E-02	7.952E-01	1.961E-01	8.772E-03
1.000E+05	1.741E+02	1.000E-06	1.000E-01	8.783E-01	1.045E-01	1.717E-02
1.000E+05	8.707E+02	5.000E-06	5.000E-01	9.351E-01	8.686E-03	5.620E-02
1.000E+05	1.741E+03	1.000E-05	1.000E+00	9.357E-01	6.009E-04	6.373E-02

Table C-5. Optical properties in the visible (λ=0.55 μm) of sooty water clouds (continued).

ρ_{H_2O}/ρ_{soot}	τ^* (Optical Depth)	U_{H_2O} (gm cm^{-2})	U_{soot} (gm cm^{-2})	R (Reflectivity)	T (Transmissivity)	ϵ (Emissivity)
1.000E+06	1.741E-03	1.000E-12	1.000E-06	8.024E-05	9.999E-01	0.000E+00
1.000E+06	8.705E-03	5.000E-12	5.000E-06	4.011E-04	9.996E-01	5.971E-08
1.000E+06	1.741E-02	1.000E-11	1.000E-05	8.001E-04	9.992E-01	1.790E-07
1.000E+06	8.705E-02	5.000E-11	5.000E-05	3.991E-03	9.960E-01	8.924E-07
1.000E+06	1.741E-01	1.000E-10	1.000E-04	7.951E-03	9.921E-01	1.778E-06
1.000E+06	8.705E-01	5.000E-10	5.000E-04	3.853E-02	9.615E-01	8.966E-06
1.000E+06	1.741E+00	1.000E-09	1.000E-03	7.420E-02	9.258E-01	1.800E-05
1.000E+06	3.482E+00	2.000E-09	2.000E-03	1.381E-01	8.618E-01	3.590E-05
1.000E+06	6.964E+00	4.000E-09	4.000E-03	2.427E-01	7.572E-01	7.181E-05
1.000E+06	1.045E+01	6.000E-09	6.000E-03	3.247E-01	6.752E-01	1.077E-04
1.000E+06	1.741E+01	1.000E-08	1.000E-02	4.448E-01	5.550E-01	1.796E-04
1.000E+06	8.705E+01	5.000E-08	5.000E-02	7.998E-01	1.993E-01	8.969E-04
1.000E+06	1.741E+02	1.000E-07	1.000E-01	8.880E-01	1.103E-01	1.790E-03
1.000E+06	8.705E+02	5.000E-07	5.000E-01	9.700E-01	2.153E-02	8.440E-03
1.000E+06	1.741E+03	1.000E-06	1.000E+00	9.776E-01	7.850E-03	1.450E-02
1.000E+07	1.741E-03	1.000E-13	1.000E-06	7.961E-05	9.999E-01	8.889E-08
1.000E+07	8.705E-03	5.000E-13	5.000E-06	4.021E-04	9.996E-01	0.000E+00
1.000E+07	1.741E-02	1.000E-12	1.000E-05	7.998E-04	9.992E-01	0.000E+00
1.000E+07	8.705E-02	5.000E-12	5.000E-05	3.990E-03	9.960E-01	8.854E-08
1.000E+07	1.741E-01	1.000E-11	1.000E-04	7.949E-03	9.921E-01	2.646E-07
1.000E+07	8.705E-01	5.000E-11	5.000E-04	3.853E-02	9.615E-01	1.111E-06
1.000E+07	1.741E+00	1.000E-10	1.000E-03	7.420E-02	9.258E-01	2.059E-06
1.000E+07	3.482E+00	2.000E-10	2.000E-03	1.382E-01	8.618E-01	4.142E-06
1.000E+07	6.964E+00	4.000E-10	4.000E-03	2.428E-01	7.572E-01	8.096E-06
1.000E+07	1.045E+01	6.000E-10	6.000E-03	3.247E-01	6.753E-01	1.217E-05
1.000E+07	1.741E+01	1.000E-09	1.000E-02	4.449E-01	5.551E-01	2.025E-05
1.000E+07	8.705E+01	5.000E-09	5.000E-02	8.002E-01	1.997E-01	1.013E-04
1.000E+07	1.741E+02	1.000E-08	1.000E-01	8.889E-01	1.109E-01	2.026E-04
1.000E+07	8.705E+02	5.000E-08	5.000E-01	9.750E-01	2.400E-02	1.006E-03
1.000E+07	1.741E+03	1.000E-07	1.000E+00	9.864E-01	1.166E-02	1.972E-03
1.000E+08	1.741E-03	1.000E-14	1.000E-06	8.151E-05	9.999E-01	9.607E-08
1.000E+08	8.705E-03	5.000E-14	5.000E-06	3.984E-04	9.996E-01	9.604E-08
1.000E+08	1.741E-02	1.000E-13	1.000E-05	7.965E-04	9.992E-01	0.000E+00
1.000E+08	8.705E-02	5.000E-13	5.000E-05	3.988E-03	9.960E-01	0.000E+00
1.000E+08	1.741E-01	1.000E-12	1.000E-04	7.953E-03	9.920E-01	0.000E+00
1.000E+08	8.705E-01	5.000E-12	5.000E-04	3.853E-02	9.615E-01	1.848E-07
1.000E+08	1.741E+00	1.000E-11	1.000E-03	7.420E-02	9.258E-01	5.338E-07
1.000E+08	3.482E+00	2.000E-11	2.000E-03	1.381E-01	8.618E-01	9.113E-07
1.000E+08	6.964E+00	4.000E-11	4.000E-03	2.428E-01	7.572E-01	1.748E-06
1.000E+08	1.045E+01	6.000E-11	6.000E-03	3.247E-01	6.753E-01	2.599E-06
1.000E+08	1.741E+01	1.000E-10	1.000E-02	4.449E-01	5.551E-01	4.385E-06
1.000E+08	8.705E+01	5.000E-10	5.000E-02	8.003E-01	1.997E-01	2.170E-05
1.000E+08	1.741E+02	1.000E-09	1.000E-01	8.890E-01	1.109E-01	4.338E-05
1.000E+08	8.705E+02	5.000E-09	5.000E-01	9.755E-01	2.427E-02	2.166E-04
1.000E+08	1.741E+03	1.000E-08	1.000E+00	9.874E-01	1.218E-02	4.312E-04

Table C-5. Optical properties in the visible (λ=0.55 μm) of sooty water clouds (Concluded).

ρ_{H_2O}/ρ_{soot}	τ^* (Optical Depth)	U_{soot} (gm cm^{-2})	U_{H_2O} (gm cm^{-2})	R (Reflectivity)	T (Transmissivity)	ε (Emissivity)
1.000E+09	1.741E-03	1.000E-15	1.000E-06	7.970E-05	9.999E-01	6.038E-08
1.000E+09	8.705E-03	5.000E-15	5.000E-06	3.984E-04	9.996E-01	6.036E-08
1.000E+09	1.741E-02	1.000E-14	1.000E-05	7.964E-04	9.992E-01	6.034E-08
1.000E+09	8.705E-02	5.000E-14	5.000E-05	3.992E-03	9.960E-01	6.015E-08
1.000E+09	1.741E-01	1.000E-13	1.000E-04	7.953E-03	9.920E-01	0.000E+00
1.000E+09	8.705E-01	5.000E-13	5.000E-04	3.853E-02	9.615E-01	1.742E-07
1.000E+09	1.741E+00	1.000E-12	1.000E-03	7.420E-02	9.258E-01	2.796E-07
1.000E+09	3.482E+00	2.000E-12	2.000E-03	1.381E-01	8.618E-01	5.727E-07
1.000E+09	6.964E+00	4.000E-12	4.000E-03	2.428E-01	7.572E-01	1.098E-06
1.000E+09	1.045E+01	6.000E-12	6.000E-03	3.247E-01	6.753E-01	1.633E-06
1.000E+09	1.741E+01	1.000E-11	1.000E-02	4.449E-01	5.551E-01	2.755E-06
1.000E+09	8.705E+01	5.000E-11	5.000E-02	8.003E-01	1.997E-01	1.373E-05
1.000E+09	1.741E+02	1.000E-10	1.000E-01	8.891E-01	1.109E-01	2.745E-05
1.000E+09	8.705E+02	5.000E-10	5.000E-01	9.756E-01	2.430E-02	1.371E-04
1.000E+09	1.741E+03	1.000E-09	1.000E+00	9.875E-01	1.223E-02	2.735E-04
1.000E+10	1.741E-03	1.000E-16	1.000E-06	8.212E-05	9.999E-01	0.000E+00
1.000E+10	8.705E-03	5.000E-16	5.000E-06	3.987E-04	9.996E-01	0.000E+00
1.000E+10	1.741E-02	1.000E-15	1.000E-05	7.972E-04	9.992E-01	6.217E-08
1.000E+10	8.705E-02	5.000E-15	5.000E-05	3.997E-03	9.960E-01	6.197E-08
1.000E+10	1.741E-01	1.000E-14	1.000E-04	7.950E-03	9.921E-01	1.235E-07
1.000E+10	8.705E-01	5.000E-14	5.000E-04	3.853E-02	9.615E-01	1.795E-07
1.000E+10	1.741E+00	1.000E-13	1.000E-03	7.420E-02	9.258E-01	2.305E-07
1.000E+10	3.482E+00	2.000E-13	2.000E-03	1.382E-01	8.619E-01	5.365E-07
1.000E+10	6.964E+00	4.000E-13	4.000E-03	2.428E-01	7.572E-01	1.095E-06
1.000E+10	1.045E+01	6.000E-13	6.000E-03	3.247E-01	6.753E-01	1.599E-06
1.000E+10	1.741E+01	1.000E-12	1.000E-02	4.449E-01	5.551E-01	2.596E-06
1.000E+10	8.705E+01	5.000E-12	5.000E-02	8.003E-01	1.997E-01	1.294E-05
1.000E+10	1.741E+02	1.000E-11	1.000E-01	8.891E-01	1.109E-01	2.586E-05
1.000E+10	8.705E+02	5.000E-11	5.000E-01	9.756E-01	2.430E-02	1.292E-04
1.000E+10	1.741E+03	1.000E-10	1.000E+00	9.875E-01	1.224E-02	2.576E-04

* Note that the optical depth is defined by Equation 2-36 and includes effects due to both scattering and absorption.

APPENDIX D
SOLUTIONS TO THE NUCLEAR WINTER MODELS

THE PROBLEM OF FIGURE 3-1

The solution to the problem of Figure 3-1 is as follows:

In layer 1:

$$\begin{aligned} S &= (1-A_1)\,\Sigma \\ U &= \tfrac{1}{2}(1-A_1)(1-A_2)\,\Sigma\,(2+\varepsilon_{I_1} z_1) \\ D &= \tfrac{1}{2}(1-A_1)(1-A_2)\,\Sigma\,\varepsilon_{I_1} z_1 \\ T &= \tfrac{1}{2}(1-A_1)(1-A_2)\,\Sigma\,(1+\varepsilon_{I_1} z_1) \end{aligned} \qquad \text{(D-1)}$$

where z_1 measures the distance from the top of layer 1.

In layer 2:

$$\begin{aligned} S &= (1-A_1)(1-A_2)\,\Sigma\, e^{-\varepsilon_{S_2} z_2} \\ U &= \tfrac{1}{2}(1-A_1)(1-A_2)\,\Sigma\,[1+\alpha+\mu_{I_1} + (1-\alpha)\, e^{-\varepsilon_{S_2} z_2}] \\ D &= \tfrac{1}{2}(1-A_1)(1-A_2)\,\Sigma\,[1+\alpha+\mu_{I_1} - (1+\alpha)\, e^{-\varepsilon_{S_2} z_2}] \\ T &= \tfrac{1}{2}(1-A_1)(1-A_2)\,\Sigma\,[1+\alpha+\mu_{I_1} + (\tfrac{1}{\alpha}-\alpha)\, e^{-\varepsilon_{S_2} z_2}] \end{aligned} \qquad \text{(D-2)}$$

where z_2 is the distance from the top of layer 2.

In layer 3:

$$S = (1-A_1)\ (1-A_2)\ \Sigma\ e^{-\mu s_2}$$

$$U = \frac{1}{2}\ (1-A_1)\ (1-A_2)\ \Sigma\ [1+\alpha+\mu_{I_1} +(1-\alpha)\ e^{-\mu s_2} + e^{-\mu s_2}\ \epsilon_{I_3} z_3] \tag{D-3}$$

$$D = \frac{1}{2}\ (1-A_1)\ (1-A_2)\ \Sigma\ [1 + \alpha + \mu_{I_1} -(1+\alpha)\ e^{-\mu s_2} + e^{-\mu s_2}\ \epsilon_{I_3} z_3]$$

$$\tau = \frac{1}{2}\ (1-A_1)\ (1-A_2)\ \Sigma\ [1 + \mu_{I_1} + \alpha(1-e^{-\mu s_2}) + e^{-\mu s_2}\ \epsilon_{I_3} z_3]$$

where z_3 is the distance from the top of layer 3.

For the earth:

$$\tau = \frac{1}{2}\ (1-A_1)\ (1-A_2)\ \Sigma\ [1+\mu_{I_1} + (1+\mu_{I_3})e^{-\mu s_2} + \alpha(1-e^{-\mu s_2})] \tag{D-4}$$

THE PROBLEM OF FIGURE 3-4

An approximate solution to the problem of Figure 3-4 in the case $\mu_{I_1}=0$ and defining $A \equiv (1-A_1)\ (1-A_2)$ is as follows:

In the convection zone:

$$S = A\ \Sigma\ e^{-\epsilon_{s_2} z_2}$$

$$U = \sigma\ [(T_0 + \beta z_2)^4 + 4\ \frac{\beta}{\epsilon_{I_2}}\ (T_0 + \beta z_2)^3 + 12\ (\frac{\beta}{\epsilon_{I_2}})^2 (T_0 + \beta z_2)^2 \tag{D-5}$$

$$+ 24\ (\frac{\beta}{\epsilon_{I_2}})^3\ (T_0 + \beta z_2) + 24\ (\frac{\beta}{\epsilon_{I_2}})^4] - \frac{\epsilon_{s_2}}{\epsilon_{I_2}}\ \Sigma\ A\ e^{-\epsilon_{s_2} d}$$

$$e^{-\epsilon_{I_2} d}\ e^{\epsilon_{I_2} z_2}$$

$$D = \sigma \left[(T_0 + \beta z_2)^4 - 4 \frac{\beta}{\varepsilon_{I_2}} (T_0 + \beta z_2)^3 + 12 \left(\frac{\beta}{\varepsilon_{I_2}}\right)^2 (T_0 + \beta z_2)^2 \right.$$

$$\left. - 24 \left(\frac{\beta}{\varepsilon_{I}}\right)^3 (T_0 + Bz_2) + 24 \left(\frac{\beta}{\varepsilon_{I_2}}\right)^4 \right] - \left[T_0^4 - \right.$$

$$\left. 4 \left(\frac{\beta}{\varepsilon_{I_2}}\right) T_0^3 + 12 \left(\frac{\beta}{\varepsilon_{I_2}}\right)^2 T_0^2 - 24 \left(\frac{\beta}{\varepsilon_{I_2}}\right)^3 T_0 + 24 \left(\frac{\beta}{\varepsilon_{I_2}}\right)^4 \right] e^{-\varepsilon_{S_2} z_2}$$

$$T = T_0 + \beta z_2$$

where z_2 is the distance from the top of the convection zone.

In the convection-free region of layer 2

$$S = A \Sigma e^{-\varepsilon_{S_2} z_2}$$

$$U = \frac{1}{2} \left[A\Sigma e^{-\varepsilon_{S_2} d} \left\{ (1-\alpha) e^{-\varepsilon_{S_2} z_2'} + \alpha - \frac{1}{\alpha} \right\} + 2\sigma (T_0 + \beta d)^4 \right] \qquad \text{(D-6)}$$

$$D = \frac{1}{2} \left[A\Sigma e^{-\varepsilon_{S_2} d} \left\{ -(1+\alpha) e^{-\varepsilon_{S_2} z_2'} + \alpha - \frac{1}{\alpha} \right\} + 2\sigma (T_0 + \beta d)^4 \right]$$

$$\tau = \frac{1}{2} \left[A\Sigma e^{-\varepsilon_{S_2} d} \left(\alpha - \frac{1}{\alpha}\right) \left(1 - e^{-\varepsilon_{S_2} z_2'}\right) + 2\sigma (T_0 + \beta d)^4 \right]$$

where z_2' is the distance from the top of the convection-free region of layer 2.

In layer 3:

$$S = A\,\Sigma\, e^{-\mu_{s_2}}$$

$$U = \frac{1}{2}\left[2\sigma(T_0 + \beta d)^4 + A\Sigma\left\{\left(\alpha + \frac{1}{\alpha}\right) e^{-\varepsilon_{s_2} d} - \alpha\, e^{-\mu_{s_2}} + e^{-\mu_{s_2}}(1 + \varepsilon_{I_3} z_3)\right\}\right]$$

$$D = \frac{1}{2}\left[2\sigma(T_0 + \beta d)^4 + A\Sigma\left\{\left(\alpha + \frac{1}{\alpha}\right) e^{-\varepsilon_{s_2} d} - \alpha\, e^{-\mu_{s_2}} + e^{-\mu_{s_2}}(-1 + \varepsilon_{I_3} z_3)\right\}\right] \qquad \text{(D-7)}$$

$$\tau = \frac{1}{2}\left[2\sigma(T_0 + \beta d)^4 + A\Sigma\left\{\left(\alpha - \frac{1}{\alpha}\right) e^{-\varepsilon_{s_2} d} - \alpha\, e^{-\mu_{s_2}} + e^{-\mu_{s_2}}\, \varepsilon_{I_3} z_3\right\}\right]$$

where z_3 is the distance from the top of layer 3.

For the earth:

$$\tau = \frac{1}{2}\left[2\sigma(T_0 + \beta d)^4 + A\Sigma\left\{\left(\alpha - \frac{1}{\alpha}\right) e^{-\varepsilon_{s_2} d} - \alpha\, e^{-\mu_{s_2}} + e^{-\mu_{s_2}}\,(1 + \mu_{I_3})\right\}\right] \qquad \text{(D-8)}$$

In the above equations:

$$T_0 = T_B - \frac{\beta}{\varepsilon_{I_2}}$$

$$D = -\frac{1}{\varepsilon_{s_2}} \ln \frac{8b}{T_B\left(\varepsilon_{I_2} + \varepsilon_{s_2}\right)}$$

where $T_B \equiv \left[\frac{A}{\sigma}\Sigma\right]^{1/4}$

THE CASE OF HIGH SURFACE ALBEDO

For the solar fluxes in the case where the earth has an albedo, A_e, in the solar we have:

Above layer 1:

$$S_D = \Sigma$$

$$S_U = \Sigma \left[A_1 + A_2 - A_1 A_2 + \frac{(1-A_1)^2 (1-A_2)^2 \, A_e \, e^{-2\mu s_2}}{1 - A_2 \, A_e - A_1 \, A_e (1-A_2) \, e^{-2\mu s_2}} \right] \qquad \text{(D-9)}$$

In layer 1:

$$S_D = (1-A_1) \, \Sigma$$

$$S_U = \Sigma \left[A_2 \, (1-A_1) + \frac{(1-A_1)^2 (1-A_2)^2 \, A_e \, e^{-2\mu s_2}}{1 - A_2 \, A_e - A_1 \, A_e (1-A_2) \, e^{-2\mu s_2}} \right] \qquad \text{(D-10)}$$

In layer 2:

$$S_D = \Sigma \left[(1-A_1) \, (1-A_2) + \frac{A_1 \, (1-A_1)^2 (1-A_2)^2 \, A_e \, e^{-2\mu s_2}}{1 - A_2 \, A_e - A_1 \, A_e (1-A_2) \, e^{-2\mu s_2}} \right] e^{-\epsilon s_2 z_2}$$

$$S_U = \Sigma \left[\frac{(1-A_1)(1-A_2)^2 \, A_e \, e^{-2\mu s_2}}{1 - A_2 \, A_e - A_1 \, A_e (1-A_2) \, e^{-2\mu s_2}} \right] e^{\epsilon s_2 z_2} \qquad \text{(D-11)}$$

where z_2 is the distance from the top of layer 2.

In layer 3:

$$S_D = \Sigma \frac{(1-A_1)\,(1-A_2)\,e^{-\mu s_2}}{1 - A_2\,A_e - A_1\,A_e(1-A_2)e^{-2\mu s_2}}$$

$$S_U = \Sigma \frac{(1-A_1)\,(1-A_2)\,A_e\,e^{-\mu s_2}}{1 - A_2\,A_e - A_1\,A_e(1-A_2)e^{-2\mu s_2}} \qquad \text{(D-12)}$$

APPENDIX E
CONVECTIVE EQUILIBRIUM WITH MULTIPLE IR GROUPS

In this appendix we shall demonstrate that a region as might be formed by the NRC baseline, soot and water-vapor layer (Reference E-1) can be represented by a set of IR groups with constant opacities such that the resulting temperature profile is significantly different from that for a single IR group. In particular, if the range of IR opacities needed to represent the water-vapor emissivity includes opacities both less than and greater than the solar opacity, the temperature profile will always have a peak at about one solar optical depth. The temperature gradient, in the absence of convection, on the top of the layer will normally exceed the critical lapse rate.

Without using a dynamical model for the profile changes which result from convection, it is difficult to be confident that a complete understanding has been gained. However, it is possible to include a convective flux component with transfer equations in order to find a new equilibrium condition which has a convective layer which holds the temperature gradient at the critical lapse rate through a modest mixing of the unstable region with the optically inert atmosphere above it. This results in a modified temperature profile including an altered asymptotic temperature at the base of the soot layer.

OPTICAL PROPERTIES OF THE LAYER

The NRC baseline, 30°-70° N case shows that after 25 days a minimum surface temperature is reached and at this time the optical depth

for solar extinction is 2.5 due to the presence of soot which is taken to be uniformly distributed from 0 to 9 km above the surface. The optical depth is the product of the physical depth, z, and the solar opacity, χ_s, so we can take $\chi_s \approx 0.25\ km^{-1}$. The broad-band infrared emissivity, $\bar{\varepsilon}$, is mainly from water vapor and its behavior with path length, U, is given by Figure E-1.

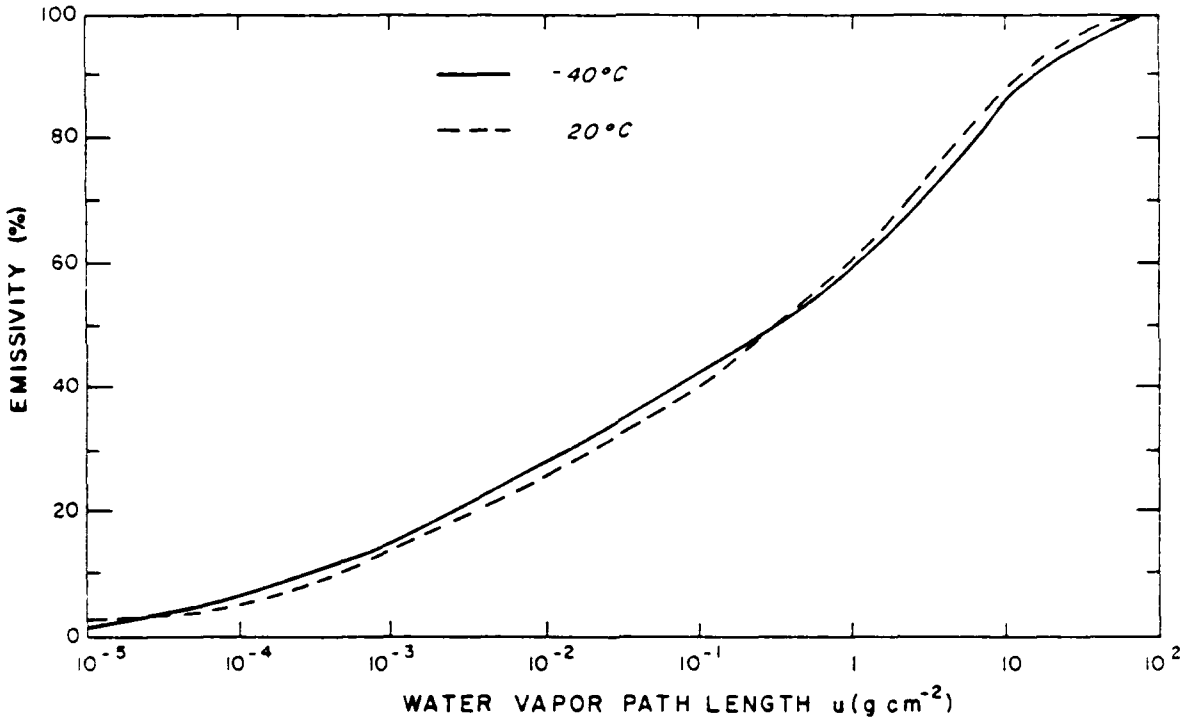

Figure E-1. Broad-band IR emissivity for water vapor (from Reference 2-10).

In the absence of scattering and for a parallel beam, the emissivity is related to the path length by

$$\bar{\varepsilon} = 1 - e^{-\bar{k}U} \qquad \text{(E-1)}$$

where $\bar{k}$ is a mean mass absorption coefficient with units of $cm^2\ g^{-1}$. Here $\bar{k}U$ is the optical depth.

The NRC baseline case provides for a water-vapor pathlength of 1.45 gm cm^{-2} giving an emissivity of 0.63 from Figure E-1. Thus, the optical depth for water vapor will be very nearly one for a mean opacity over a 9 km depth of $\bar{\chi}_{H_2O} \approx 0.1\ km^{-1}$.

Use of this mean value will give the correct emissivity at $U = 1.45\ gm/cm^2$ but it would provide a very poor representation for the $\bar{\varepsilon}(U)$ curve of Figure E-1. In fact, $\bar{\varepsilon}(U)$ results from an averaging over a complex absorption structure. It is possible to represent this curve as resulting from a set of IR groups with significantly different optical properties. For example, a reasonable fit to $\bar{\varepsilon}(U)$ is given by

$$\bar{\varepsilon} \approx .2(1 - e^{-1300U}) + .2(1 - e^{-50U}) + .3(1 - e^{-U}) + .3(1 - e^{-.12U}) \qquad \text{(E-2)}$$

over the range of U from 10^{-4} to 10^{2}. This form for $\bar{\varepsilon}$ would result if there were a set of four distinct IR frequency bands which contributed with uniform opacities within each band. The opacities $\chi = k\rho$ of the four groups in this fit correspond to, for this mean density if $\rho \sim 10^{-6}$ gm/cm^3, values of 130 km^{-1}, 5 km^{-1}, 0.1 km^{-1}, and 0.012 km^{-1}. Recall that the solar opacity was $\chi_s \approx 0.1\ km^{-1}$ so that there are IR groups with significant activities which are both more and less active than the solar absorption.

TRANSFER EQUATIONS

The equation for the steady state radiative transfer for a planar atmosphere can be written as (Reference E-?)

$$\mu \frac{\partial I}{\partial z} = \eta - \chi I \qquad \text{(E-3)}$$

where the specific intensity $I(z,\hat{n},\nu)$ is a function of position z, direction and frequency and has units of ergs cm^{-2} sec^{-1} Hz^{-1} sr^{-1}. Here μ is the cosine of the angle relative to vertical while η is the emission coefficient and χ is the opacity with units of cm^{-1}. Generally χ is the sum of absorption and scattering contributions but, for the present discussion, scattering will be ignored. Given η and χ, both possibly functions of frequency, direction, and position, it is possible to solve for I. However, in general, η and χ are functions of I, providing a nonlinear transfer equation. In a uniform medium at steady state there can be no net energy accumulation or loss so the emission coefficient and opacity are related by

$$\eta(\nu) = \chi(\nu)\ I(\hat{n},\nu) \qquad \text{(E-4)}$$

which is Kirchoff's law. For an enclosure in strict thermodynamic equilibrium the radiation field is given by the Planck function at temperature T so

$$\eta(\nu) = \chi(\nu)\ B_{\nu}(T) \quad . \qquad \text{(E-5)}$$

If a medium has only small gradient lengths relative to photon mean free paths the approximation of local thermodynamic equilibrium (LTE) is often useful and this implies

$$\eta(z,\nu) = \chi(z,\nu)\ B_{\nu}(T) \qquad \text{(E-6)}$$

so that the emissivity can be expressed in terms of the opacity and the known Planck function. Here $B_{\nu}(T)$ has the property that the flux from a blackbody is

$$\sigma T^4 = \pi \int_0^\infty B_\nu(T)\,d\nu \qquad \text{(E-7)}$$

which defines the Stefan-Boltzmann constant, σ.

Consider now an idealized atmospheric layer which has the properties that there are a finite number of infrared frequency ranges of importance and each of these has constant opacity. We assume that all thermal radiation takes place in these groups and that the solar spectrum does not significantly overlap the IR. Thus there is no emission into the solar spectrum. The layer then serves to absorb the solar radiation and convert the energy to thermal.

THREE GROUPS

In order to get an analytic handle on the problem, we will now develop a set of transfer equations appropriate for a three-group two-stream approximation where the three groups consist of two IR groups and one solar group. The transfer equation under LTE is

$$\mu \frac{\partial I}{\partial z} = \chi(\nu)(B_\nu(T) - I) \quad . \qquad \text{(E-8)}$$

Integrating over the frequency domains gives

$$\mu \frac{\partial I_1}{\partial z} = \chi_1\left(\alpha_1 \frac{\sigma T^4}{\pi} - I_1\right) \qquad \text{(E-9a)}$$

$$\mu \frac{\partial I_2}{\partial z} = \chi_2\left(\alpha_2 \frac{\sigma T^4}{\pi} - I_2\right) \qquad \text{(E-9b)}$$

and

$$\mu \frac{\partial I_S}{\partial z} = -\chi_S I_S \quad . \qquad \text{(E-9c)}$$

Here the χ_i are the opacities of IR groups and α_i is the fraction of the thermal emission which takes place into the i^{th} group. Both χ_i and α_i will be taken as known. (The opacities χ_i may be considered to be the product of the density and mass absorption coefficient.)

TWO STREAMS

The full solution to the transfer equations includes the angular dependence of the specific intensity. The details of this dependence are not expected to have a significant impact on the result and it is convenient to make an approximation which allows closure of the set of moment equations generated by Equation E-3. Eddington's approximation provides that the upward and downward components of I are each independent of μ but different from each other.

The flux associated with I is

$$\text{Flux} = \int \mu I(\mu)\, d\mu\, d\phi \qquad \text{(E-10)}$$

and defining $I^+ \equiv I(\mu > 0)$ and $I^- \equiv I(\mu < 0)$ the upward flux is

$$U = \int_0^1 \mu\, I^+ d\mu \int d\phi = \pi I^+ \qquad \text{(E-11)}$$

and the downward flux is

$$D = -\int_{-1}^{0} \mu\, I^- d\mu \int d\phi = \pi I^- \quad . \qquad \text{(E-12)}$$

Thus, from Equation E-7 upon integration over angle

$$\frac{\partial}{\partial z}(U_i) = 2\,\chi_1\alpha_1\sigma T^4 - 2\,\chi_i U_i \qquad \text{(E-13a)}$$

$$\frac{\partial}{\partial z}(-D_i) = 2\,\chi_i\alpha_i\sigma T^4 - 2\,\chi_i D_i \qquad \text{(E-13b)}$$

for i = 1,2. Since the solar flux is only down, $\pi I_s = S$ and

$$\frac{\partial(S)}{\partial z} = 2\,\chi_s S \quad . \tag{E-14}$$

Finally taking $\tau \equiv -2z$ as a convenient unit of depth and expressing the IR fluxes in terms of plus, P = U+D, and minus, M=U-D components, we arrive at

$$\frac{\partial}{\partial \tau}(P_i) = \chi_i M_i \tag{E-15a}$$

$$\frac{\partial}{\partial \tau}(M_i) = \chi_i P_i - 2\,\chi_i \alpha_i \sigma T^4 \tag{E-15b}$$

$$\frac{\partial}{\partial \tau}(S) = -\,\chi_s S \tag{E-15c}$$

which give the three-group, two-stream transfer equations. The steady state condition implies

$$\frac{\partial}{\partial \tau}(\Sigma M_i - S) = 0 \quad . \tag{E-16}$$

These results are correct for any number of IR groups. However, the essential features appear with two groups and this case can be solved analytically, providing a solution as follows:

$$S = S_0 \exp(-\chi_s \tau) \tag{E-17a}$$

$$M_1 = A \exp(\sqrt{\gamma}\,\tau) + B \exp(\sqrt{\gamma}\,\tau) + X \exp(\sqrt{\gamma}\,\tau) \tag{E-17b}$$

$$M_2 = S - M_1 \tag{E-17c}$$

$$P_1 = P_{10} + \chi_1\left[\frac{A}{\sqrt{\gamma}}\left(\exp(\sqrt{\gamma}\,\tau) - 1\right) - \frac{B}{\sqrt{\gamma}}\left(\exp(\sqrt{\gamma}\,\tau) - 1\right) + \frac{X}{\chi_s}\left(\exp(-\chi_s\,\tau) - 1\right)\right] \tag{E-17d}$$

$$P_2 = P_{20} + \chi_1\left[-\frac{A}{\sqrt{\gamma}}\left(\exp(\sqrt{\gamma}\,\tau) - 1\right) + \frac{B}{\sqrt{\gamma}}\left(\exp(\sqrt{\gamma}\,\tau) - 1\right)\right. \qquad \text{(E-17e)}$$

$$\left. - \frac{S_0 - X}{\chi_S}\left(\exp(-\chi_S\,\tau) - 1\right)\right]$$

where S_0 is the incident solar flux at the upper surface, τ=0,

$$\gamma = \frac{(\alpha_1\chi_2 + \alpha_2\chi_1)\chi_1\chi_2}{(\alpha_1\chi_1 + \alpha_2\chi_2)} \qquad \text{(E-18)}$$

and

$$X = S_0 \frac{\alpha_1\chi_1}{\alpha_1\chi_1 + \alpha_2\chi_2} \frac{\chi_2^2 - \chi_S^2}{\gamma - \chi_2^2} \quad . \qquad \text{(E-19)}$$

Finite fluxes in an infinitely deep layer requires A=0 so that

$$B = \frac{\frac{1}{\alpha_2}\left[(S_0 - X)\left(1 + \frac{\chi_S}{\chi_2}\right) + 2\,D_{20}\right] - \frac{1}{\alpha_1}\left[X\left(1 + \frac{\chi_S}{\chi_1}\right) + 2\,D_{10}\right]}{\sqrt{\gamma}\left(\frac{1}{\sigma_1\chi_1} + \frac{1}{\alpha_2\chi_2}\right) + \frac{1}{\alpha_1} + \frac{1}{\alpha_2}} \qquad \text{(E-20)}$$

where D_{i0} provides for possible non-zero downward fluxes at τ=0. The boundary conditions at τ=0 are

$$M_{10} = B + X = P_{10} - 2\,D_{10} \qquad \text{(E-21a)}$$

and

$$M_{20} = S_0 - M_{10} = P_{20} - 2\,D_{20} \quad . \qquad \text{(E-21b)}$$

These conditions provide the full solution for an infinitely deep region consisting of two IR groups and a solar group.

To illustrate the behavior exhibited by these conditions for a single layer, consider an example of equal strength IR groups (α_1= α_2=

0.5) with arbitrary normalization of $\chi_1 = 1$ and $\chi_2 = 10^{-2}$. The temperature profiles which result are shown for several values of χ_s in Figure E-2. If $\chi_s < \chi_2$ the temperature increases with depth to an asymptotic value. If $\chi_2 < \chi_s < \chi_1$ the temperature reaches a maximum at a depth comparable to χ_s^{-1}, or at a solar optical depth near 1. If $\chi_s > \chi_1$ the temperature monotonically decreases while if $\chi_s \gg \chi_1$ one sees structure at both of the depth scales of χ_s^{-1} and $(\sqrt{\chi_1\chi_2})^{-1/2}$ but the temperature still decreases monotonically.

As illustrated by the previous discussion of soot layer optical properties, the activities of the equivalent IR groups span that for the solar radiation. In order to demonstrate the basic features expected in a realistic temperature profile, let us approximate the water-vapor emissivity using just two IR groups. We will take

$$\bar{\varepsilon}(z) \approx .4\,(1 - e^{-12.5z}) + .3(1 - e^{-.0625z}) \qquad \text{(E-22)}$$

where z is in kilometers. Thus we are using $\alpha_1 = .4$, $\chi_1 = 12.5\ km^{-1}$, $\alpha_2 = .3$, and $\chi_2 = 1/16\ km^{-1}$, while taking $\chi_s = 1/4\ km^{-1}$. The above fit to $\bar{\varepsilon}(U)$ is not very good unless $U \sim 1$ but the essential feature is preserved--namely, there are IR groups both more and less active than the solar. The exact values for α_1 and χ_1 are not well determined by such a fit but it turns out that the essential features of solution remain largely independent of the selection of parameter values.

The temperature profile which results from the two IR groups plus one solar group approximation for two streams is shown in Figure E-3. Since $\chi_2 < \chi_s < \chi_1$, there is a maximum temperature which occurs and it is at a depth of $\tau = 2z = 2.2$ km, which corresponds to a solar optical depth of $\sim 1/2$. The temperature gradient at the top of the layer greatly exceeds the critical lapse rate of about 7 degrees per kilometer so that the profile will be unstable against convection. The resulting convection

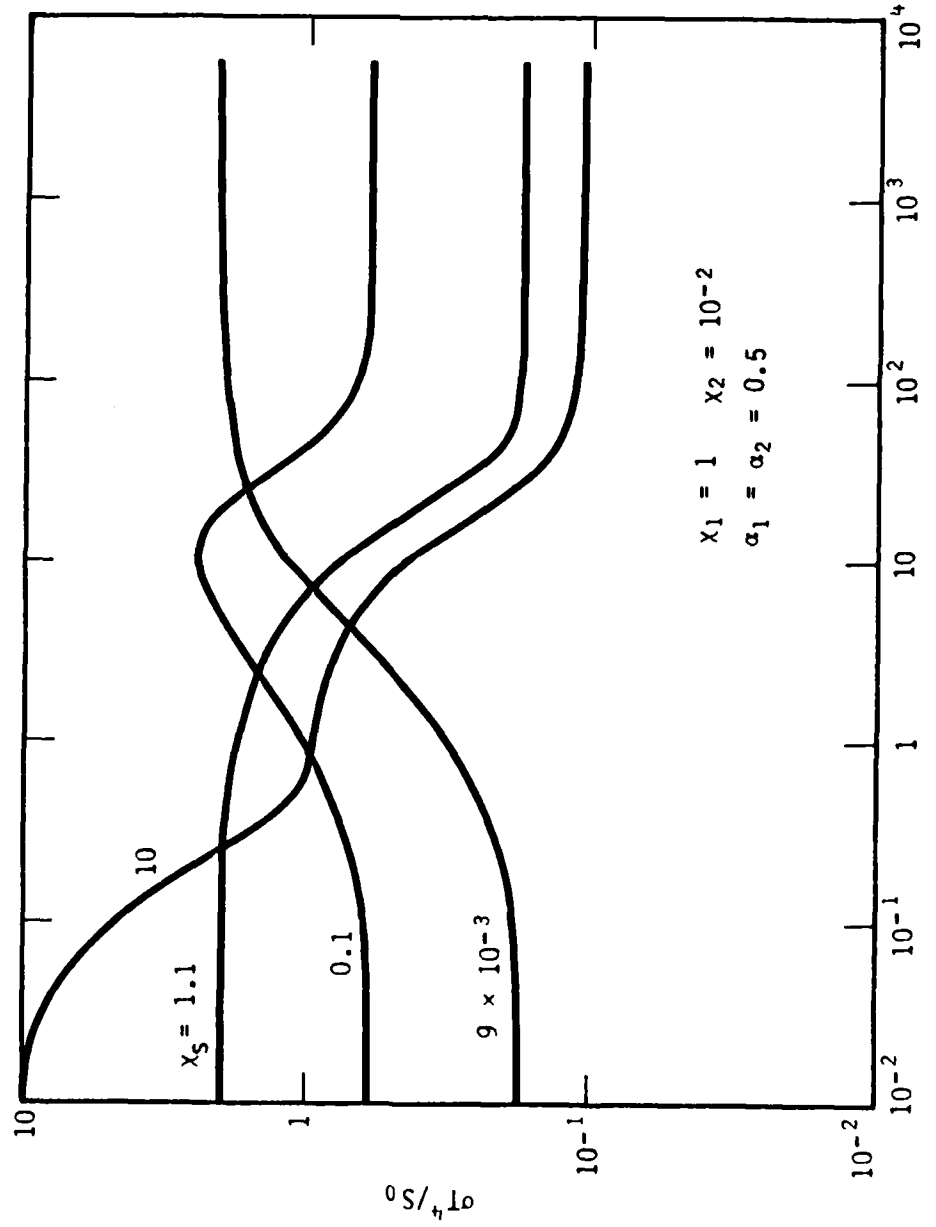

Figure E-2. Temperature profiles for two IR groups plus solar absorption.

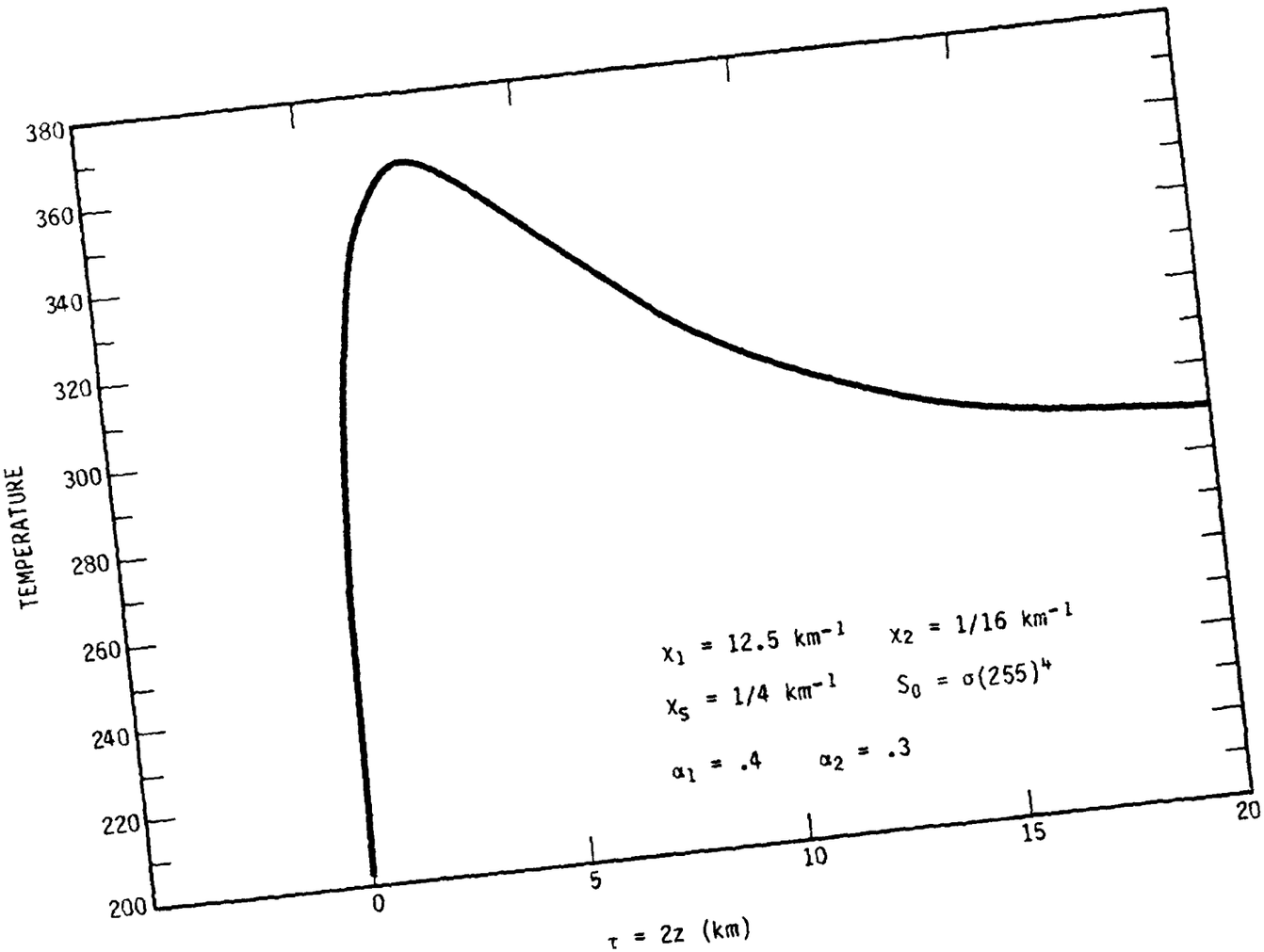

Figure E-3. Temperature profile for two IR group approximation in a soot layer.

will alter the profile so that the gradient will not exceed the critical lapse rate anywhere. It is not clear that there will exist a steady state profile maintained by convection. Without entering into a dynamical calculation we now want to consider the character of a possible steady state profile which is maintained by convection, allowing for the possibility that a portion of the layer may mix with air above to reduce the opacities and effectively expand the layer.

CONVECTIVE LIMIT

In a region in which convection enforces a maximum gradient equal to some critical lapse rate, β, our previous solution for 2 IR groups is inappropriate. In such a region the gradient will be constant at β and there will exist an additional flux from the convection.

The transfer equations for the IR and solar groups are the same as in the absence of convection. Namely,

$$\frac{\partial}{\partial \tau}(P_i) = \chi_i M_i \qquad \text{(E-23a)}$$

$$\frac{\partial}{\partial \tau}(M_i) = \chi_i P_i - 2\chi_i \alpha_i \sigma T^4 \qquad \text{(E-23b)}$$

$$S = S_0 e^{-\chi_s \tau} \qquad \text{(E-23c)}$$

but the steady state condition becomes

$$\frac{\partial}{\partial \tau}(\sum M_i - S + F) = 0 \qquad \text{(E-24)}$$

where F is the convective flux. Furthermore, the temperature now is restricted to the form

$$T = T_0 + \beta\,\tau \qquad \text{(E-25)}$$

where β is the critical gradient and T_0 is an unknown temperature at the top of the layer.

Eliminating M_i using Equations E-23a and b, while making use of Equation E-25, yields

$$-\frac{1}{\chi_i}\frac{\partial^2 P_i}{\partial \tau^2} + \chi_i P_i = 2\chi_i \alpha_i T_0^4 \left(1 + \left(\frac{\beta}{T_0}\right)\tau\right) \qquad \text{(E-26)}$$

which has a general solution of the form

$$P_i = A_i e^{-\chi_i \tau} + B_i e^{\chi_i \tau} + \sum_{j=0}^{4} a_{ij}\tau^j \quad . \qquad \text{(E-27)}$$

The coefficients a_{ij} can be expressed in terms of T_0 as

$$\begin{aligned}
a_{i4} &= 2\,\alpha_i \sigma\, T_0^4\, (\beta/T_0)^4 \\
a_{i3} &= 2\,\alpha_i \sigma\, T_0^4 (4(\beta/T_0)^3) \\
a_{i2} &= 2\,\alpha_i \sigma\, T_0^4 (6(\beta/T_0)^2) + 12\, a_{i4}/\chi_i^2 \qquad \text{(E-28)} \\
a_{i1} &= 2\,\alpha_i \sigma\, T_0^4 (4(\beta/T_0)) + 6\, a_{i3}/\chi_i^2 \\
a_{i0} &= 2\,\alpha_i \sigma\, T_0^4 + 2\, a_{i2}/\chi_i^2 \quad .
\end{aligned}$$

Using Equation (E-23a) the M_i can be written as

$$M_i = -A_i e^{-\chi_i \tau} + B_i e^{\chi_i \tau} + \sum_{j=1}^{4} j\, a_{ij}\tau^{j-1} \quad . \qquad \text{(E-29)}$$

For no downward flux at the boundary at $\tau=0$

$$P_{i0} = M_{i0} \tag{E-30}$$

and

$$A_i = (a_{i1}/x_i - a_{i0})/2 \quad . \tag{E-31}$$

Furthermore, fixing the convective flux to be zero at $\tau=0$ forces

$$\sum P_{i0} = \sum M_{i0} = S_0 \tag{E-32}$$

which requires

$$\sum B_i = S_0 - \sum_i (a_{i1}/x_i + a_{i0})/2 \quad . \tag{E-33}$$

Thus the remaining unknowns are T_0 and B_1. (From Equation E-33 $B_1 + B_2$ can be written in terms of T_0. So it is only the split between the B_i which is unknown.)

The convective flux can be found by integrating Equation E-24, giving

$$F = S_0(e^{-x_s\tau} - 1) - [\sum_i A_i(e^{-x_i\tau} - 1) + \sum_i B_i(e^{x_i\tau} - 1)$$

$$+ \sum_i \sum_{j=2}^{4} j\left(\frac{a_{ij}}{x_i}\right) \tau^{j-1}] \tag{E-34}$$

where the condition $F=0$ at $\tau=0$ is imposed giving no convective flux at the boundary.

Figure E-3 indicates that in the absence of convection there will be a finite region with a temperature gradient exceeding the critical lapse rate. Since this region is unstable to convection, it will be

altered through convection, perhaps including a mixing with the inactive region above and also perhaps dynamically changing the previously stable region below. Without exploring the dynamics of such processes, we shall now consider the possibility that there may exist a different steady state equilibrium in which convection holds the upper region at a gradient β while the semi-infinite lower region is unaltered except for possible changes in boundary conditions at the interface. This new configuration is to allow the possibility that, through mixing, the upper region is uniformly stretched, if necessary, to provide a solution which matches the boundary conditions at the interface. This stretching will be carried out by a uniform reduction of the χ's in the upper region such that their ratios are fixed.

The conditions to be met are as follows:

The convective flux, F, is to vanish at the top (τ=0) and at the interface, τ_0.

The gradient of the convective flux, $\partial F/\partial \tau$, is the vanish at the interface--this forces the temperature to be continuous.

All IR fluxes M_i and P_i are to be continuous at the interface--actually only one of the four conditions is independent.

The maximum temperature gradient in the lower non-convective region must be no greater than β.

In general, it is found that parameters τ_0, T_0, and B_1 (or, equivalently, the mix between B_1 and B_2) can be found which satisfy the above conditions without any stretching or mixing of the upper convective region.

It is further found that there exist solutions with a stretching up to some maximum value beyond which the temperature gradient at the top of the nonconvective lower region exceeds β. The maximum allowed stretching is generally no more than about 50 percent for typical parameters. Any degree of stretching less than this maximum results in a discontinuity in the temperature gradient at the interface. While there is no physical reason to rule out such a possibility, it seems likely that the dynamics of the change from an unstable profile to one maintained by convection would not leave such a discontinuity. This reasoning is further supported by the example in Figure E-4, which indicates that the final convective region is much larger than the original region for which $dT/d_\tau > \beta$.

Figure E-4 shows three temperature profiles which result from opacities which approximate those for a soot layer. The profiles are for a fully nonconvective equilibrium (ORIGINAL), for an unstretched convective layer above a stable layer (UNSTRETCHED), and for a stretched convective layer above a stable layer such that the temperature gradient is continuous across the interface (STRETCHED).

The effect of introduction of a convectively stabilized layer is generally a reduction in temperatures at the peak and at the bottom of the region with an attendant sharp increase in the temperature at the top of the layer. The temperature peak of the original region is at a solar optical depth, $\chi_S\tau$, of about 1/2 while the convection induced peak is at an optical depth of about 2.

REMARKS

The goal of the, currently incomplete, work described in this appendix is to understand the development of the instability at the top of the soot layer when no condensation cloud is present. The most obvious conclusion of the work so far is that it is necessary to resolve the IR

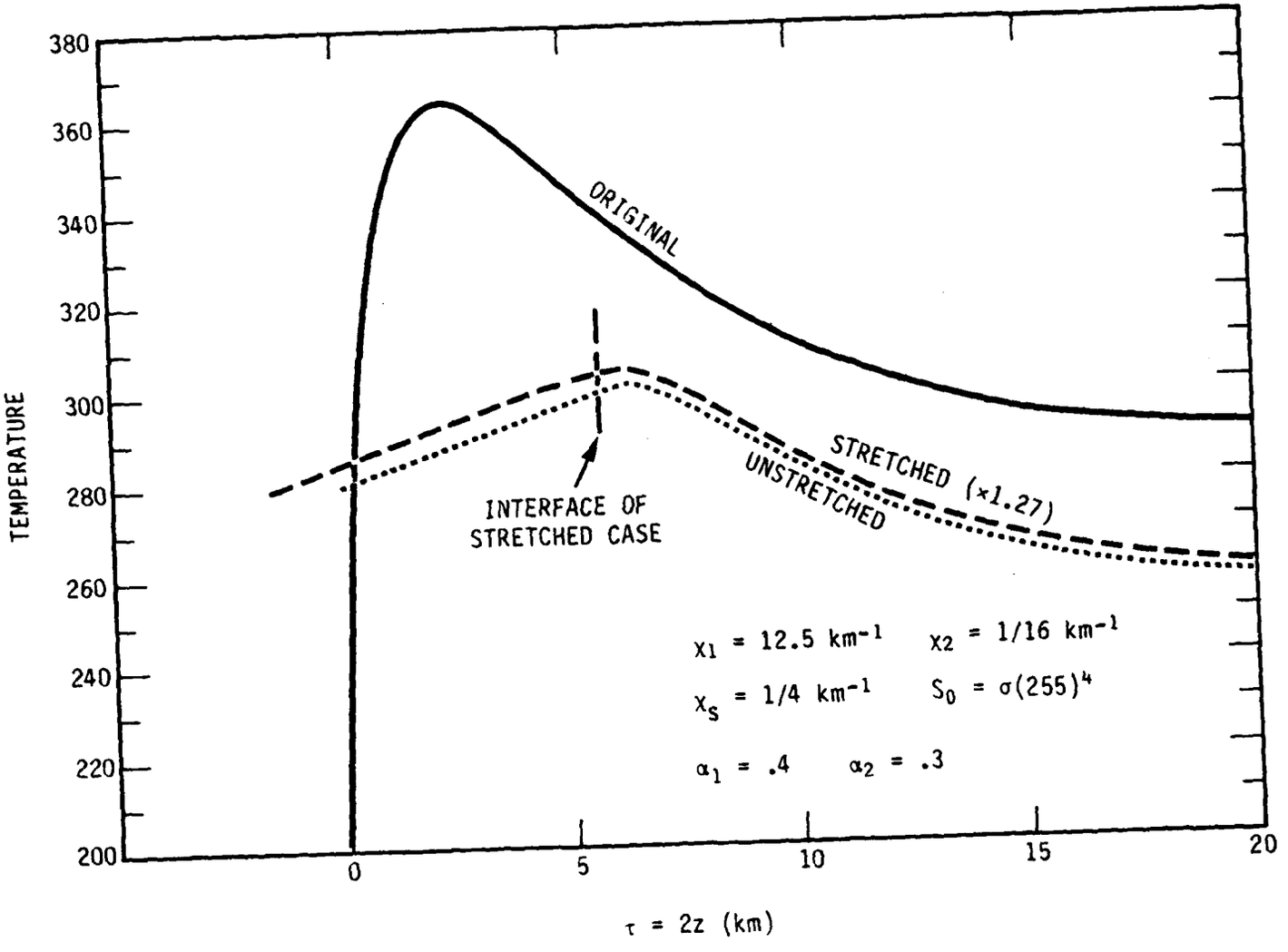

Figure E-4. Temperature profiles for two IR group approximation in a soot layer (ORIGINAL), under convective equilibrium (UNSTRETCHED) and following a mixing with the layer above (STRETCHED).

opacity of H_2O into more than one band unlike was done in Chapter 3. If there are portions of the IR band where the opacity is higher than is the solar opacity and portions where it is lower than the solar one obtains behavior--the details of which cannot be simulated by any single IR band. These details are not of great importance for estimating the maximum temperature or the temperature level in the cloud, such as at the earth's surface, but they are very important for understanding stability properties. The opacity of water-vapor is so high in the ten to twenty percent of the IR band which has the highest opacity and so low in the thirty percent which is lower that we believe there will always be substantial parts of the IR band when the opacity is on either side of the solar. For these reasons amounts of water-vapor which are too small to affect the main character of the temperature profile as calculated in Chapter 3 can be important to the development of the instability. Note that the IR opacity of condensed water is quite constant as a function of frequency so the problem under discussion here must affect the stability calculations of Chapter 3 which were for condensed water.

DISTRIBUTION LIST

DEPARTMENT OF DEFENSE

ASSIST SECY OF DEF CMD, CON, COMM & INTEL
ATTN: DADSD (I)
ATTN: DIR OF INTELL SYS

ASSIST TO THE SECY OF DEF ATOMIC ENERGY
ATTN: EXECUTIVE ASSISTANT

DEFENSE ADVANCED RSCH PROJ AGENCY
ATTN: GSD R ALEWINE
ATTN: T TETHER

DEFENSE COMMUNICATIONS AGENCY
ATTN: CODE 230
ATTN: J300 FOR YEN-SUN FU

DEFENSE COMMUNICATIONS AGENCY
ATTN: A200 R CRAWFORD
ATTN: A320 P BIRD
ATTN: A730 G JONES

DEFENSE COMMUNICATIONS ENGINEER CENTER
ATTN: CODE R123 TECH LIB
ATTN: CODE R410
ATTN: CODE R410 N JONES

DEFENSE INTELLIGENCE AGENCY
ATTN: DB A WISE
ATTN: DB-4C
ATTN: DC-7B
ATTN: DIR
ATTN: DT-1B
ATTN: RTS-2B

DEFENSE NUCLEAR AGENCY
ATTN: NATF
ATTN: NAWE
3 CYS ATTN: RAAE
ATTN: RAAE P LUNN
ATTN: RAEE
ATTN: RAEE K SCHWARTZ
ATTN: STNA
4 CYS ATTN: STTI-CA

DEFENSE TECHNICAL INFORMATION CENTER
2 CYS ATTN: DD

FIELD COMMAND DNA DET 2
LAWRENCE LIVERMORE NATIONAL LAB
ATTN: FC-1

FIELD COMMAND DEFENSE NUCLEAR AGENCY
ATTN: FCPR
ATTN: FCTT W SUMMA
ATTN: FCTXE

JOINT CHIEFS OF STAFF
ATTN: C3S
ATTN: C3S EVAL OFC (HDOO)

JOINT DATA SYSTEM SUPPORT CTR
ATTN: C-312 R MASON

JOINT STRAT TGT PLANNING STAFF
ATTN: JLAA
ATTN: JLK ATTN: DNA REP
ATTN: JLKS
ATTN: JPPFD
ATTN: JPSS
ATTN: JPTM

NATIONAL SECURITY AGENCY
ATTN: B432 C GOEDEKE

UNDER SECY OF DEF FOR RSCH & ENGRG
ATTN: STRAT & SPACE SYS (OS)

DEPARTMENT OF THE ARMY

ARMY LOGISTICS MANAGEMENT CTR
ATTN: DLSIE

ASSIST CH OF STAFF FOR AUTOMATION & COMM
ATTN: DAMO-C4 P KENNY

BMD ADVANCED TECHNOLOGY CENTER
ATTN: ATC-O W DAVIES
ATTN: ATC-R D RUSS
ATTN: ATC-R W DICKSON

DEP CH OF STAFF FOR OPS & PLANS
ATTN: DAMO-RQC C2 DIV

HARRY DIAMOND LABORATORIES
ATTN: DELHD-NW-R R WILLIAMS 22000
2 CYS ATTN: SCHLD-NW-P

U S ARMY ATMOSPHERIC SCIENCES LAB
ATTN: SLCAS-AE-E

U S ARMY COMM-ELEC ENGRG INSTAL AGENCY
ATTN: CC-CE-TP W NAIR

U S ARMY COMMUNICATIONS R&D COMMAND
ATTN: DRDCO-COM-RY W KESSELMAN

U S ARMY FOREIGN SCIENCE & TECH CTR
ATTN: DRXST-SD

U S ARMY MATERIAL COMMAND
ATTN: DRCLDC J BENDER

U S ARMY NUCLEAR & CHEMICAL AGENCY
ATTN: LIBRARY

U S ARMY SATELLITE COMM AGENCY
ATTN: DOCUMENT CONTROL

U S ARMY STRATEGIC DEFENSE CMD
ATTN: BMDSC-LEH R C WEBB
ATTN: DASD-H-SAV

DEPARTMENT OF THE ARMY (CONTINUED)

U S ARMY STRATEGIC DEFENSE COMMAND
ATTN: DASD-H-L M CAPPS
ATTN: DASD-H-S W DAVIES
ATTN: DASD-H-SA R C WEBB
ATTN: DASD-H-Y D RUSS

U S ARMY TRADOC SYS ANALYSIS ACTVY
ATTN: ATAA-PL
ATTN: ATAA-TCC F PAYAN JR
ATTN: ATAA-TDC

US ARMY WHITE SANDS MISSILE RANGE
ATTN: STEWS-TE-N K CUMMINGS

USA MISSILE COMMAND
ATTN: DRSMI-YSO J GAMBLE

DEPARTMENT OF THE NAVY

JOINT CRUISE MISSILES PROJECT OFC
ATTN: JCMG-707

LEAHY (CG 16)
ATTN: WPNS OFCR

NAVAL AIR SYSTEMS COMMAND
ATTN: PMA 271

NAVAL INTELLIGENCE SUPPORT CTR
ATTN: NISC-50

NAVAL OCEAN SYSTEMS CENTER
ATTN: CODE 532
ATTN: CODE 5322 M PAULSON
ATTN: CODE 5323 J FERGUSON

NAVAL RESEARCH LABORATORY
ATTN: CODE 4180 J GOODMAN
ATTN: CODE 4187
ATTN: CODE 4700 S OSSAKOW
ATTN: CODE 4706 P RODRIGUEZ
ATTN: CODE 4720 J DAVIS

NAVAL SPACE SURVEILLANCE SYSTEM
ATTN: J BURTON

NAVAL SURFACE WEAPONS CENTER
ATTN: CODE F31

NAVAL TELECOMMUNICATIONS COMMAND
ATTN: CODE 341

OFC OF THE DEPUTY CHIEF OF NAVAL OPS
ATTN: NOP 654 STRAT EVAL & ANAL BR
ATTN: NOP 941D
ATTN: NOP 981N

OFFICE OF NAVAL RESEARCH
ATTN: CODE 412, W CONDELL

SPACE & NAVAL WARFARE SYSTEMS CMD
ATTN: CODE 3101 T HUGHES
ATTN: CODE 501A
ATTN: PDE-110-X1 B KRUGER
ATTN: PDE-110-11021 G BRUNHART
ATTN: PME 106-4 S KEARNEY
ATTN: PME 117-20
ATTN: PME-106 F W DIEDERICH

STRATEGIC SYSTEMS PROGRAMS (PM-1)
ATTN: NSP-2141
ATTN: NSP-2722
ATTN: NSP-43 TECH LIB

THEATER NUCLEAR WARFARE PROGRAM OFC
ATTN: PMS-423 D SMITH

DEPARTMENT OF THE AIR FORCE

AIR FORCE CTR FOR STUDIES & ANALYSIS
ATTN: AF/SASC C RIGHTMEYER

AIR FORCE GEOPHYSICS LABORATORY
ATTN: CA/A STAIR
ATTN: LID/J RAMUSSEN
ATTN: LIS J BUCHAU
ATTN: LS
ATTN: LS/H GARDINER
ATTN: LS/R O'NIEL
ATTN: LYD/K CHAMPION

AIR FORCE SATELLITE CTRL FACILITY
ATTN: WE

AIR FORCE TECHNICAL APPLICATIONS CTR
ATTN: TN

AIR FORCE WEAPONS LABORATORY, AFSC
ATTN: NTN
ATTN: SUL

AIR FORCE WRIGHT AERONAUTICAL LAB/AAAD
ATTN: A JOHNSON
ATTN: W HUNT

AIR UNIVERSITY LIBRARY
ATTN: AUL-LSE

BALLISTIC MISSILE OFFICE/DAA
ATTN: ENSN
ATTN: ENSN W WILSON
ATTN: SYC D KWAN

DEP CH OF STAFF RSCH DEV & ACQ
ATTN: AF/RDQI

DEP CH OF STAFF RSCH DEV & ACQ
ATTN: AFRDS SPACE SYS & C3 DIR

ELECTRONIC SYSTEMS DIVISION
ATTN: SCS-1E
ATTN: SCS-2 LTC ALEXANDER

FOREIGN TECHNOLOGY DIVISION, AFSC
ATTN: NIIS LIBRARY
ATTN: TQTD B BALLARD

DEPARTMENT OF THE AIR FORCE (CONTINUED)

ROME AIR DEVELOPMENT CENTER, AFSC
ATTN: OCDS R SCHNEIBLE
ATTN: TSLD

SPACE COMMAND
ATTN: DC T LONG

STRATEGIC AIR COMMAND
ATTN: SAC/SIJ

STRATEGIC AIR COMMAND
ATTN: SAC/LGW

STRATEGIC AIR COMMAND
ATTN: NRI/STINFO

STRATEGIC AIR COMMAND
ATTN: XPFC

STRATEGIC AIR COMMAND
ATTN: XPFS

STRATEGIC AIR COMMAND
ATTN: XPQ

DEPARTMENT OF ENERGY

DEPT OF ENERGY OFC OF MIL APPL GTN
ATTN: DP-233

EG&G, INC
ATTN: D WRIGHT

LAWRENCE LIVERMORE NATIONAL LAB
ATTN: L-31 R HAGER
ATTN: L-53 TECH INFO DEPT LIB

LOS ALAMOS NATIONAL LABORATORY
ATTN: D SAPPENFIELD
ATTN: D SIMONS
ATTN: J WOLCOTT
ATTN: MS 664 J ZINN
ATTN: R JEFFRIES
ATTN: T KUNKLE, ESS-5

SANDIA NATIONAL LABORATORIES
ATTN: D HARTLEY 8300
ATTN: T COOK

SANDIA NATIONAL LABORATORIES
ATTN: D DAHLGREN
ATTN: D THORNBROUGH
ATTN: ORG 1231 R C BACKSTROM
ATTN: ORG 1250 W BROWN
ATTN: ORG 4231 T WRIGHT
ATTN: SPACE PROJECT DIV
ATTN: TECH LIB 3141

OTHER GOVERNMENT

BUREAU OF POLITICO MILITARY AFFAIRS
ATTN: PM/STM

CENTRAL INTELLIGENCE AGENCY
ATTN: OSWR/NED
ATTN: OSWR/SSD FOR K FEUERPFETL

NATIONAL OCEANIC & ATMOSPHERIC ADMIN
ATTN: R GRUBB

U S DEPARTMENT OF COMMERCE
ATTN: A JEAN
ATTN: W UTLAUT

DEPARTMENT OF DEFENSE CONTRACTORS

AEROSPACE CORP
ATTN: D OLSEN
ATTN: E RODRIGUEZ
ATTN: I GARFUNKEL
ATTN: J KLUCK
ATTN: J STRAUS
ATTN: K S CHO
ATTN: R SLAUGHTER
ATTN: T SALMI
ATTN: V JOSEPHSON

AEROSPACE CORP
ATTN: S MEWATERS

ANALYTICAL SYSTEMS ENGINEERING CORP
ATTN: RADIO SCIENCES

ANALYTICAL SYSTEMS ENGINEERING CORP
ATTN: SECURITY

AUSTIN RESEARCH ASSOCIATES
ATTN: J THOMPSON

AUTOMETRIC, INC
ATTN: C LUCAS

BDM CORP
ATTN: A VITELLO
ATTN: L JACOBS

BERKELEY RSCH ASSOCIATES, INC
ATTN: C PRETTIE
ATTN: J WORKMAN
ATTN: S BRECHT

BOEING CO
ATTN: M/S 1F-72 G HALL
ATTN: M/S 6K-92 D CLAUSON

BR COMMUNICATIONS
ATTN: J MCLAUGHLIN

CALIFORNIA RESEARCH & TECHNOLOGY, INC
ATTN: M ROSENBLATT

UNIVERSITY AT CALIFORNIA, SAN DIEGO
ATTN: H BOOKER

CHARLES STARK DRAPER LAB, INC
ATTN: A TETEWSKI

COMMUNICATIONS SATELLITE CORP
ATTN: G HYDE

COMPUTER SCIENCES CORP
ATTN: F EISENBARTH

DEPT OF DEFENSE CONTRACTORS (CONTINUED)

CORNELL UNIVERSITY
ATTN: D FARLEY JR
ATTN: M KELLY

ELECTROSPACE SYSTEMS, INC
ATTN: H LOGSTON
ATTN: P PHILLIPS

EOS TECHNOLOGIES, INC
ATTN: B GABBARD
ATTN: W LELEVIER

GENERAL ELECTRIC CO
ATTN: A STEINMAYER
ATTN: C ZIERDT

GENERAL RESEARCH CORP
ATTN: B BENNETT

GEO CENTERS, INC
ATTN: E MARRAM

GTE GOVERNMENT SYSTEMS CORPORATION
ATTN: A MURPHY

HARRIS CORP
ATTN: E KNICK

HSS, INC
ATTN: D HANSEN

IBM CORP
ATTN: H ULANDER

INSTITUTE FOR DEFENSE ANALYSES
ATTN: E BAUER
ATTN: H WOLFHARD

JAYCOR
ATTN: J SPERLING

JOHNS HOPKINS UNIVERSITY
ATTN: C MENG
ATTN: J D PHILLIPS
ATTN: J NEWLAND
ATTN: K POTOCKI
ATTN: R STOKES 1-W250
ATTN: T EVANS

KAMAN SCIENCES CORP
ATTN E CONRAD

KAMAN TEMPO
ATTN B GAMBILL
ATTN DASIAC
ATTN W MCNAMARA

KAMAN TEMPO
ATTN DASIAC

LOCKHEED MISSILES & SPACE CO, INC
ATTN J KUMER
ATTN R SEARS

LOCKHEED MISSILES & SPACE CO, INC
2 CYS ATTN: D CHURCHILL

M I T LINCOLN LAB
ATTN: D TOWLE L-230
ATTN: I KUPIEC L-100

M/A COM LINKABIT INC
ATTN: H VAN TREES

MAXIM TECHNOLOGIES, INC
ATTN: J LEHMAN
ATTN: J MARSHALL
ATTN: R MORGANSTERN

MCDONNELL DOUGLAS CORP
ATTN: R HALPRIN

METEOR COMMUNICATIONS CORP
ATTN: R LEADER

MISSION RESEARCH CORP
ATTN: C LAUER
2 CYS ATTN: D ARCHER
ATTN: D KNEPP
ATTN: F FAJEN
ATTN: F GUIGLIANO
2 CYS ATTN: G MCCARTOR
ATTN: R BIGONI
ATTN: R BOGUSCH
ATTN: R DANA
ATTN: R HENDRICK
ATTN: R KILB
ATTN: S GUTSCHE
2 CYS ATTN: T OLD
ATTN: TECH LIBRARY
2 CYS ATTN: W WORTMAN

MITRE CORP
ATTN: A KYMMEL
ATTN: C CALLAHAN
ATTN: MS J104/M R DRESP

MITRE CORP
ATTN: J WHEELER
ATTN: M HORROCKS
ATTN: R C PESCI
ATTN: W FOSTER

PACIFIC SIERRA RESEARCH CORP
ATTN: E FIELD JR
ATTN: F THOMAS
ATTN: H BRODE, CHAIRMAN SAGE

PHOTOMETRICS, INC
ATTN: I KOFSKY

PHYSICAL DYNAMICS, INC
ATTN: E FREMOUW

PHYSICAL RESEARCH, INC
ATTN R DELIBERIS
ATTN T STEPHENS

DEPT OF DEFENSE CONTRACTORS (CONTINUED)

PHYSICAL RESEARCH, INC
ATTN: J DEVORE
ATTN: J THOMPSON
ATTN: W SCHLUETER

R & D ASSOCIATES
ATTN: B MOLLER
ATTN: C GREIFINGER
ATTN: F GILMORE
ATTN: G STCYR
ATTN: H ORY
ATTN: M GANTSWEG
ATTN: M GROVER
ATTN: P HAAS
ATTN: R TURCO
ATTN: W KARZAS
ATTN: W WRIGHT

R & D ASSOCIATES
ATTN: B YOON

R & D ASSOCIATES
ATTN: G GANONG

RAND CORP
ATTN: C CRAIN
ATTN: E BEDROZIAN
ATTN: P DAVIS

RAND CORP
ATTN: B BENNETT

ROCKWELL INTERNATIONAL CORP
ATTN: R BUCKNER

ROCKWELL INTERNATIONAL CORP
ATTN: S QUILICI

SCIENCE APPLICATIONS INTL CORP
ATTN: C SMITH
ATTN: D HAMLIN
ATTN: E STRAKER
ATTN: L LINSON

SCIENCE APPLICATIONS INTL CORP
ATTN: J COCKAYNE

SCIENCE APPLICATIONS INTL CORP
ATTN: M CROSS

SRI INTERNATIONAL
ATTN: C RINO
ATTN: D MCDANIEL
ATTN: D NIELSON
ATTN: G PRICE
ATTN: G SMITH
ATTN: J VICKREY
ATTN: R LEADABRAND
ATTN: R LIVINGSTON
ATTN: R TSUNODA
ATTN: W CHESNUT
ATTN: W JAYE

STEWART RADIANCE LABORATORY
ATTN: R HUPPI

TECHNOLOGY INTERNATIONAL CORP
ATTN: W BOQUIST

TELECOMMUNICATIONS SCIENCES ASSOCIATES
ATTN: J BUCKNER

TOYON RESEARCH CORP
ATTN: J GARBARINO
ATTN: J ISE

TRW ELECTRONICS & DEFENSE SECTOR
ATTN: R PLEBUCH HARD & SURV LAB

UTAH STATE UNIVERSITY
ATTN: A STEED
ATTN: D BURT
ATTN: K BAKER, DIR ATMOS & SPACE SCI
ATTN: L JENSEN, ELEC ENG DEPT

VISIDYNE, INC
ATTN: J CARPENTER

END

DTIC

7-86